Development of a Non-invasive Water Flow Meter for a Smart Geyser

by

Nicol Oswald Pirow

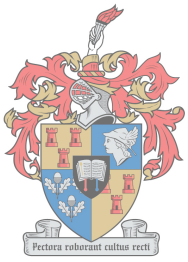

Thesis presented in partial fulfilment of the requirements for the degree of Master of Engineering (Electrical & Electronic) in the Faculty of Engineering at Stellenbosch University

Supervisor: Prof. M. Booysen
Co-supervisor: Dr. T. Louw

March 2018

Declaration

By submitting this thesis electronically, I declare that the entirety of the work contained therein is my own, original work, that I am the sole author thereof (save to the extent explicitly otherwise stated), that reproduction and publication thereof by Stellenbosch University will not infringe any third party rights and that I have not previously in its entirety or in part submitted it for obtaining any qualification.

Date: March 2018

Abstract

Development of a Non-invasive Water Flow Meter for a Smart Geyser

N. Pirow

Department of Electrical and Electronic Engineering,
University of Stellenbosch,
Private Bag X1, Matieland 7602, South Africa.

Thesis: MEng (E&E)

March 2018

South Africa has experienced electricity and water shortages in recent years. The use of smart geyser controller units has the potential to decrease the electricity and water consumption associated with the domestic sector. The installation of an in-line, invasive flow meter is the most expensive aspect of the costs associated with smart geyser controllers. The aim of the project is to develop a non-invasive, retrofit water flow meter which is intended to be used for smart geyser controllers in domestic applications. The successful design of such a non-invasive water flow meter would decrease the installation cost and installation inconvenience associated with smart geyser controllers. This means that more individuals can use smart geyser controllers which can result in a greater total decrease in resource consumption.

Several non-invasive fluid measurement methods were investigated in the context of domestic hot water flow. Many were found to be too expensive or require complex installation which meant that they would not provide the intended convenience to users. Thermal methods and vibration methods were investigated to design a non-invasive flow meter which required less expensive components and did not require a complex installation. The use of thermal methods only to measure domestic flow was investigated. It was determined to be impractical due to the small temperature differences associated with domestic conditions and the difficult installation required for accurate temperature measurements using inexpensive sensors. A non-invasive flow estimation algorithm was designed which used the fusion of thermal and vibration data provided using relatively inexpensive sensors which did not require complex installation. The algorithm was able to detect hot water usage events with over 90 % accuracy using thermal and vibration data. Event detection was successful for flow events spaced at least 2 minute apart.

Flow rate estimation was performed using vibration data. A quadratic relationship between higher industrial flow rates and vibration standard deviation was found in literature,

but a linear relationship was found for domestic conditions. Sufficiently accurate quantitative flow rate estimation was possible for flow rates above $5\,\mathrm{L\,min^{-1}}$.

The consumption patterns which occurred within these algorithm limitations were found to constitute 60 % of measured volumetric consumption for anonymous smart geyser controller units in a field dataset. The use of fixed flow rate approximations for low flow rates (which could be detected but not quantitatively estimated) increased the simulated performance of the system from the mentioned 60 % to 90 %. The volumetric flow estimation accuracy of the algorithm was sufficient and the same error margins of 10 % were achieved which matches the in-line flow meter currently used in installations.

The results of this study show a proof of concept that non-invasive flow measurement can be performed for domestic conditions using the combination of thermal and vibration methods. The required consumption data can be gathered with a system that does not require expensive components or a complex installation procedure.

Uittreksel

Ontwikkeling van 'n Nie-indringende Watervloeimeter vir Slim Waterverhitting-toestel

("Development of a Non-invasive Water Flow Meter for a Smart Geyser")

N. Pirow

Departement Elektries en Elektroniese Ingenieurswese,
Universiteit van Stellenbosch,
Privaatsak X1, Matieland 7602, Suid Afrika.

Tesis: MIng (E&E)

Maart 2018

Suid-Afrika het die afgelope paar jaar elektrisiteit en water tekorte ondervind. Die gebruik van slim waterverhitting-toestel beheerders het die potensiaal om die elektrisiteit en water verbruik van die huishoudelike sektor te verminder. Die installering van 'n interne en indringende vloeimeter is die duurste aspek van die kostes verbonde aan hierdie slim waterverhitting-toestel beheerders. Die doel van hierdie projek, is om 'n nie-indringende watervloeimeter vir slim waterverhitting-toestel beheerders te ontwikkel wat vir huishoudelike toepassing in die sisteem geintegreer kan word. Die suksesvolle ontwikkeling van so 'n nie-indringende watervloeimeter sal die installasiekoste en ongerief verbonde aan die instaleering van slim waterverhitting-toestel beheerders verminder. Dit sal meer individue in staat stel om hierdie slim waterverhitting-toestel beheerders te gebruik, wat kan lei tot 'n groter afname in hulpbron verbruik.

Verskeie nie-indringende vloeistofmetingsmetodes is ondersoek in die konteks van huishoudelike warmwatervloei. Baie is te duur bevind of vereis komplekse installasie wat beteken dat hulle nie die beoogde gerief aan verbruikers sal verskaf nie. Termiese metodes en vibrasie metodes is ondersoek om 'n nie-indringende vloeimeter te ontwerp wat goedkoper komponente bevat en nie ingewikkelde installasie vereis nie. Die gebruik van termiese metodes alleen vir huishoudelike gebruik, is ondersoek. Dit was vasgestel dat dit onpraktries sal wees weens die klein temperatuurverskille wat verband hou met huishoudelike toestande en die moeilike installasie wat benodig word vir akkurate temperatuurmetings deur goedkoop sensors te gebruik.

'n Nie-indringende vloeiskatting-algoritme is ontwerp wat gebruik maak van die samesmelting van termiese- en vibrasiedata en wat ook relatief goedkoop sensors verg met minder komplekse installasie. Die algoritme kon warm waterverbruik met meer as 90 % akkuraatheid bepaal. Gebeurlikheid opsporing was suksesvol vir vloeibewegings wat ten minste 2 min uit mekaar uit was.

Vloeitempo skatting is uitgevoer met behulp van vibrasie data. 'N Kwadratiese verhouding tussen hoër industriële vloeitempo's en vibrasie-standaardafwyking is in die literatuur aangetref, maar 'n lineêre verhouding is gevind vir huishoudelike toestande. Voldoende akkurate kwantitatiewe vloeitempo skatting was moontlik vir vloeitempo's bo $5\,\mathrm{L\,min^{-1}}$.

Die verbruikspatrone wat binne die algoritme-beperkings plaasgevind het, was 60 % van die gemete volumetriese verbruik vir onbekende slim waterverhitting-toestel beheerders in 'n veld datastelsel. Die gebruik van vaste vloeitempo-benaderings vir lae vloeitempo's (wat opgespoor kon word maar nie kwantitatief geskat was nie) het die gesimuleerde prestasie van die stelsel verhoog van die genoemde 60 % na 90 %. Die volumetriese vloeiberaming se akkuraatheid van die algoritme was voldoende en het dieselfde foutspeling van 10 % behaal, wat ooreenstem met die inlyn vloeimeters wat tans in installasies gebruik word.

Die resultate van hierdie studie toon 'n konseptuele bewys dat nie-indringende vloeimeting vir huishoudelike toestande uitgevoer kan word deur n kombinasie van termiese en vibrasiemetodes te gebruik. Die vereiste verbruiksdata kan ingesamel word met 'n stelsel wat nie duur komponente of 'n komplekse installasieprosedure benodig nie.

Acknowledgements

I would like to express my sincere gratitude to the following people and organisations for their invaluable support over the past two years:

- My supervisor, Prof. Thinus Booysen for his advice and guidance during the undertaking of this project.
- My co-supervisor, Dr Tobi Louw for his guidance and the assistance which he provided especially for the thermal, fluid and modelling aspects of this project.
- MTN for their continued support and funding through the MTN Mobile Intelligence Lab.
- The Department of Electrical and Electronic Engineering for their technical support especially in providing the necessary skills and labour during the installation of the experimental EWH unit.
- My colleagues and fellow students who contributed to this project. Specifically to Marcel Roux who provided the anonymous water consumption data which formed the Field Dataset and enabled the practicality of the algorithm limitations to be evaluated, and to Lowku Leewner who created the printed circuit board schematics according to my design specifications which allowed for the experimental unit to be installed in a shorter time frame at a critical time.
- My parents for their continued love and support.
- Friends and family for their emotional support and encouragement.

Contents

List of Figures

List of Tables

Nomenclature

Variables

A_c	Cross sectional area	$[\,\mathrm{m}^2\,]$
c_p	Specific heat capacity	$[\,\mathrm{kgm}^2/\mathrm{Ks}^2\,]$
D_i	Inner pipe diameter	$[\,\mathrm{m}\,]$
D_o	Outer pipe diameter	$[\,\mathrm{m}\,]$
h	Heat transfer coefficient	$[\,\mathrm{W/mK}^2\,]$
k	Thermal conductivity	$[\,\mathrm{W/mK}\,]$
L	Length	$[\,\mathrm{m}\,]$
L_h	Hydrodynamic entry length	$[\,\mathrm{m}\,]$
p	Pressure	$[\,\mathrm{N/m}^2\,]$
$\bar{p}$	Pressure (mean)	$[\,\mathrm{N/m}^2\,]$
p'	Pressure (fluctuating)	$[\,\mathrm{N/m}^2\,]$
$\dot{q}_A$	Surface heat flux	$[\,\mathrm{W/m}^2\,]$
$\dot{q}_V$	Volumetric heat flux	$[\,\mathrm{W/m}^3\,]$
R	Thermal resistance	$[\,\mathrm{m}^2\,\mathrm{K\,W}^{-1}\,]$
Re	Reynolds Number	[Unitless]
T	Temperature	$[\,^\circ\mathrm{C}\,]$
$\dot{T}$	Temperature gradient	$[\,^\circ\mathrm{C\,s}^{-1}\,]$
T_∞	Ambient temperature	$[\,^\circ\mathrm{C}\,]$
t	Time	$[\,\mathrm{s}\,]$
t_{cd}	Minimum cool down time between flow events	[min]
U	Thermal transmittance	$[\,\mathrm{W/m}^2\mathrm{K}\,]$
u	Longitudinal velocity (for two-dimensions)	$[\,\mathrm{m\,s}^{-1}\,]$
$\bar{u}$	Longitudinal velocity (mean)	$[\,\mathrm{m\,s}^{-1}\,]$
u'	Longitudinal velocity (fluctuating)	$[\,\mathrm{m\,s}^{-1}\,]$
V	Volume	[L]

$\dot{V}$	Volumetric flow rate	$[\mathrm{L\,min^{-1}}]$
$\bar{\dot{V}}_{(min)}$	Minimum flow rate for quantitative estimation	$[\mathrm{L\,min^{-1}}]$
v	Velocity	$[\mathrm{m\,s^{-1}}]$
$\bar{v}$	Velocity (mean)	$[\mathrm{m\,s^{-1}}]$
v'	Velocity (fluctuating)	$[\mathrm{m\,s^{-1}}]$
ρ	Density	$[\mathrm{kg\,m^{-3}}]$
σ	Accelerometer standard deviation	$[\mathrm{m\,s^{-2}}]$
σ_{min}	Accelerometer standard deviation minimum threshold	$[\mathrm{m\,s^{-2}}]$
τ	Shear Stress	$[\mathrm{Pa}]$
α	Thermal diffusivity	$[\mathrm{m^2\,s^{-1}}]$
μ	Dynamic viscosity of water	$[\mathrm{kg/ms}]$

Subscripts

air	Air
c	Copper
E	Estimated
$flag$	Variable used as a boolean flag
i	Discrete longitudinal coordinate
j	Discrete radial coordinate
k	Discrete time step
l	Discrete one-dimensional coordinate for flattened system
lam	Laminar
M	Measured
S	Simulated
$turb$	Turbulent
w	Water
x'	Accelerometer x-axis
y'	Accelerometer y-axis
z'	Accelerometer z-axis

Functions

f{ data }	Filtered data

Acronyms and Abbreviations

CCUF Cross-Correlation Ultra Sonic Flow Meter

CDM Central Difference Method

DUF Doppler Ultrasonic Flow Meter

EWH Electric Water Heater

FDM Finite Difference Method

GPIO General Purpose Input/Output

I^2C Inter-Integrated Circuit

MEMS Microelectromechanical Systems

ODE Ordinary Differential Equation

PVC Polyvinyl Chloride

RPi Raspberry Pi

SANS South African National Standard

SGC Smart Geyser Controller

TTUF Transit Time Ultrasonic Flow Meter

USFM Ultrasonic Flow Meter

Chapter 1

Introduction

1.1 Overview

South Africa has scarce energy and water resources. Domestic hot water consumption using Electric Water Heater (EWH) units, also referred to as geysers, contributes to both energy and water consumption. Widespread use of Smart Geyser Controller (SGC) units can decrease the resources consumed to provide domestic hot water. A way to increase the adoption of SGC use is to decrease the installation cost. Most geysers are already installed without a SGC and thus require a retrofit installation. The most expensive single aspect of a retrofit SGC installation is the non-trivial plumbing required to install an in-line flow meter. A non-invasive solution is proposed with the intention of providing the same flow rate accuracy as an in-line flow meter at a lower cost. The proposed non-invasive flow measurement system is split into research objectives which enables the evaluation of the success of the system.

1.2 Scarce Resources

South Africa has a history of struggling to meet energy generation requirements. In recent years the energy generation limitations have resulted in rolling blackouts to attempt to alleviate strain on the grid. The Western Cape is currently experiencing a serious water shortage [1]. The widespread implementation of SGC units can decrease both energy and water consumption. The most expensive single component of a retrofit installation of a SGC is the non-trivial plumbing required to install an in-line flow meter. South Africa has an economic divide, which means that many South Africans simply cannot afford to install a system which would save them money in the long term and assist the energy and water scarcity immediately. More users will be able to benefit from the electricity and water saving potential which a SGC provides if the installation costs are lower.

1.2.1 Electricity Consumption

Water heating contributes 34 % of residential electricity consumption in South Africa (uncontrolled: 26 %, controlled: 8 %) [2]. Widespread use of SGC units enables scheduling to be performed to ensure that the national electrical grid is not as strained and will reduce the energy consumed by uncontrolled residential water heating. Energy generation load strain can be reduced using demand side management by peak shaving [3]. This can be achieved by scheduling the time which each EWH heating element comes on to before

users consume hot water. An EWH can store energy in the form of hot water and demand side management of EWH units can decrease the peak energy demand associated with EWHs in the domestic sector [3].

1.2.2 Water Consumption

South Africa and specifically the Western Cape is currently experiencing a water crisis. Level 5 water restrictions were implemented in the City of Cape Town as of 3 September 2017 [1]. This means that domestic properties have a 87 L per person per day limit and a total monthly usage cap of 20 kL. Domestic users may face heavy fines if the water consumption limits are not met [1]. Reductions of municipal water pressure are to be implemented in an effort to curb the over-usage of water for domestic zones. The water shortage is not expected to improve in the near future. Water conservation is clearly a priority at the moment and in the foreseeable future for domestic and commercial users alike in South Africa [1].

It has been found that domestic users who make use of a SGC show trends of decreased water consumption after the installation of smart water meters as used in the SGC [4]. The SGC does not restrict ability of the user to consume water in any way. The noted decrease in water consumption is the result of water consumption feedback that users receive when using a SGC. Users obtain reports, which contain details of water consumption relating to times, durations and volumes of usage events. This data enables users to identify which activities consume more water than they were aware of. Users have generally been found to alter their water usage behaviour to decrease consumption after being made aware of their water usage statistics by the consumption feedback [5]. The consumption feedback coupled with other intervention methods reduced the water consumption of a primary school in Stellenbosch by 44 % [4].

SGC implementation has been observed to prompt users to decrease their hot water usage after being made aware of the impact which each usage event has on their total consumption. It is reasonable to assume that this behavioural change to consume less water when provided with usage feedback extends past the sample groups used in existing studies. Thus the more users who can obtain usage feedback from a SGC, the larger the total water usage reduction (for all users who use an EWH).

1.2.3 Installation Cost

The most expensive part of the installation of a SGC is the installation of an invasive, in-line flow meter. This is required to provide the user with hot water consumption data. Consumption data is also used calculate element scheduling to minimize energy wastage whilst maintaining user convenience by ensuring that usual consumption patterns have hot water available. The in-line flow meter used in the current SGC system has 0.5 L resolution and 10 % accuracy. The non-trivial installation of the in-line flow meter requires the cold inlet pipe to the EWH to be cut by a plumber. This increases the inconvenience to the user as two separate times must be available for the SGC to be fully installed; the first for the plumbing requirements and the second for the electrical requirements (the unit itself). In addition to the inconvenience of a complex installation procedure, there are high costs associated with the invasive flow meter installation as plumbers are skilled labourers. The plumbing costs vary from region to region. In Piet Retief, a lower income area where a large number of SGC units are in use, the plumbing installation

costs are R800. In Cape Town, a more affluent region, the plumbing installation costs are R1600. The cost of the approved in-line flow meters used is around $50. The rest of the installation can be performed without skilled labour. Thus the cost can be dramatically reduced if an alternative flow measurement system can be found which can be installed without cutting any water pipes.

The installation costs are most prevalent for retrofit solutions. The abrupt changes in water policy in the Western Cape and the severity of the drought mean that many people cannot wait to replace their geyser and simultaneously install a SGC. This means that retrofit solutions are the primary installation method due to the urgency of the water crisis. A non-invasive flow meter would reduce the retrofit installation cost, which could enable many more people to install a SGC.

1.3 Problem Statement

Many potential users cannot afford to install a SGC. A non-invasive flow meter which can be installed on existing EWHs as a retrofit solution, can decrease the installation cost by excluding expensive non-trivial plumbing associated with the installation of an in-line flow meter. A non-invasive flow meter is the most effective way to reduce the installation costs and make SGC units accessible to a larger portion of the public. A non-invasive water flow measurement system for domestic EWHs would be more convenient to users as the installation is simpler.

1.4 Proposed Solution

A non-invasive flow estimation system was required which took the form of an algorithm. The algorithm required sensor readings to provide non-invasive measurements. The sensors were required to be relatively inexpensive and easy to install.

Non-invasive flow measurement techniques were investigated in the domestic EWH context. The components cost and ease of installation were additionally considered. Thermal methods, using externally mounted temperature sensors, and vibration methods, using an externally mounted accelerometer, were determined to be the best non-invasive methods to implement. Both methods are used in industry but not as a stand alone measurement method for domestic conditions.

1.5 Research Question

Can non-invasive flow measurement reduce installation costs and user inconvenience, while providing the required flow estimation accuracy for domestic EWH applications?

1.6 Hypotheses

Hypothesis 1

It is not possible to design a non-invasive flow estimation algorithm using only thermal methods for a domestic EWH application.

Hypothesis 2

It is possible to design a non-invasive flow estimation algorithm using the combination of vibration and thermal methods to provide suitable flow esimation accuracy for domestic EWH application.

1.7 Objectives

Objective 1: Non-invasive Usage Event Detection

Develop a non-invasive system which can detect the temporal boundaries of water usage events, determine which events are caused by hot water flow and which events can receive reliable quantitative flow rate estimation.

1(a): Design an algorithm which can identify the temporal boundaries of potential usage events using non-invasive vibration methods.

1(b): Design an algorithm which can classify detected events as usage events (caused by hot water flow) or interference events using non-invasive methods.

1(c): Design an algorithm which can non-invasively determine whether detected usage events can receive reliable quantitative flow rate estimation or require approximated values.

Objective 2: Non-invasive Flow Estimation

Develop a non-invasive flow estimation algorithm using sensors which can be installed on an EWH without skilled labour as a retrofit solution, and is able to provide similar flow usage data as the invasive flow meter which is currently used.

2(a): Determine what level of instantaneous flow rate estimation accuracy can be obtained using considered non-invasive techniques.

2(b): Determine what level of mean flow rate estimation accuracy can be obtained using the non-invasive system.

2(c): Determine the volumetric estimation accuracy which can be obtained using non-invasive methods.

2(d): Determine the usage limitations of the limitations, and determine what portion of measured volumetric consumption could be estimated for anonymous Field Test Units when considering the algorithm limitations.

1.8 Scope

The aim of the project is to determine the feasibility of replacing the current invasive flow meters with a non-invasive solution which has a lower installation cost which does not require non-trivial plumbing. The non-invasive flow estimation algorithm is intended to work for a single Experimental EWH Unit which was mounted in a test location and

had controlled conditions. Normal use conditions were considered. The installation of the EWH was assumed to be according to the regulations and adhered to the common conditions experienced in most SGC installations. The designed non-invasive flow rate system is not meant to be universal or ready for implementation; it is intended to be a proof of concept.

1.9 Contribution

This paper makes the following contributions:

- Develops a thermal model based on first principles which was used to simulate the heat transfer taking place in the outlet pipe. The thermal pipe model was used to determine whether noted temperature measurement problems were due to unconsidered thermal behaviours or sensor mounting limitations.
- Generates a dataset containing measured flow rate and temperature data for an EWH with scheduled flow events sampled at one second intervals. The dataset, Dataset 1, was gathered over 5 days; with each day having a unique consistent flow rate, with each day containing 4 Test Sets (6 hours apart), and each test set containing 3 separate scheduled flow events. Vibration data is additionally available at higher sample rates for 500 burst samples (taken at one second intervals during times where flow tests were scheduled to occur and at one minute intervals during times where no flow was scheduled to occur). Dataset 1 was used to design the non-invasive flow estimation algorithm.
- Generates a dataset containing measured flow rate, temperature and vibration data for an EWH with manually controlled flow events sampled at one second intervals to test a real time data acquisition system. The dataset, Dataset 2, was gathered over one hour and emphasis was placed on gathering a large variety of flow rates in a short amount of time. Dataset 2 was used to assess the performance of the designed non-invasive flow estimation algorithm on a larger variety of flow rates.
- Generates a dataset containing measured flow rate, temperature and vibration data for an EWH with scheduled flow events sampled at one second intervals. The dataset, Dataset 3, was gathered over one hour. The time between scheduled events increased in 15 s increments to determine the minimum time between events to enable the designed system to be used.
- Presents a system to acquire required data, data cleaning and data processing to design a non-invasive flow estimation algorithm using sensor fusion.
- Develops a non-invasive flow estimation algorithm which is intended to be used for domestic EWHs as a more affordable retrofit solution to enable users to install a SGC at a lower cost. The system makes use of non-invasive techniques which are usually used for industrial pipe diameters and flow rates and combines these with an event detection method to create a system which is useful for domestic tests conducted on a test EWH.
- Assesses the expected performance of the developed non-invasive flow estimation algorithm if it were applied to a "Field Dataset" comprised of 34 anonymous SGC

users flow usage data over 28 days, sampled at 1 minute intervals. The measured limitations of the designed non-invasive flow estimation algorithm were applied to existing field units and the expected performance of the designed system was installed on the field units was assessed.

1.10 Layout of Report

The contents of the report are described below.

Chapter 2 summarises research that was done to achieve the objectives mentioned in Chapter 1. The research comprises non-invasive flow rate measurement techniques for clean water, fluid kinematics required to understand internal fluid flow, heat transfer principles required to understand thermal behaviour of the physical system and the link between fluid flow in pipes and measurable vibrations.

Chapter 3 details the development of a suitable thermal pipe model for the heat transfer within the EWH copper outlet pipe which is based on first principles. Steady-state and transient models were investigated. The simulation of the transient thermal pipe model in software is discussed, and the implications of the simulation results on the development of the experimental unit and non-invasive flow estimation algorithm are mentioned.

Chapter 4 details the design of the experimental EWH unit, the data acquisition system and the experiments conducted. The data acquired using the experimental unit was used to design the non-invasive flow algorithm and determine the usage conditions which are required for the algorithm to perform correctly.

Chapter 5 details the data processing which was performed to design the non-invasive flow estimation algorithm by post-processing Dataset 1. The empirical design of the non-invasive flow rate estimation algorithm is discussed.

Chapter 6 shows the performance of the non-invasive flow estimation algorithm to achieve the research objectives for the project.

Chapter 7 evaluates the hypotheses, evaluates the success of the designed non-invasive flow estimation algorithm to achieve the research objectives and gives recommendations for future work.

Chapter 2

Literature Review

In order to design a non-invasive water flow meter for domestic EWH application several topics required investigation. Water conditions which can be expected for domestic EWH conditions were determined and a study of the relevant fluid kinematic and thermodynamic properties was done. Several fluid measurement methods were investigated. Most non-invasive flow measurement methods are used in industry so suitable technologies for expected domestic conditions were researched further.

2.1 Electric Water Heater Context

There are 5.4 million EWH units in South Africa which contribute 2940 MW to the evening peak electricity consumption [6]. Most EWHs do not have a SGC unit installed. The use of SGC units for domestic EWH installations can decrease the peak energy consumption.

Water consumption can be decreased by using end-use feedback [4, 5, 7]. A case study was performed by Fielding, et al which considered 221 households in South East Queensland, Australia over a period of 5 months [5, 7]. The effectiveness to reduce domestic water consumption using 3 different intervention methods was investigated in the case study. One of the intervention methods was by providing users with water consumption feedback information. The case study found that household consumption decreased during times when end-use consumption feedback was provided to users [7]. It was reported that an estimated 5.72 kL was saved per household over 120 days [7].

A study was done on the effects of intervention methods, leakage detection and consumption feedback for a primary school in the Western Cape [4]. The effect of consumption feedback in isolation cannot be determined, but the combined effect was a 44 % reduction in water use [4]. This was in relation to a similar school which did not receive interventions during the test period.

Smart water meters were used in both mentioned studies to provide immediate consumption statistics and usage behaviour. This information (often in conjunction with other intervening methods) resulted in lower water consumption through altered user behaviour [4, 7].

The installation of a SGC unit to a domestic household allows for the same consumption information to be readily available and thus individuals are likely to decrease their total water consumption. A SGC unit has the additional benefit of being able to benefit the energy supply in South Africa using demand side management [6]. It can be seen that

widespread use of SGC units is advantageous in South Africa. The most expensive and inconvenient part of SGC installation is the in-line flow meter which provides the water consumption data. Non-trivial plumbing is required as the EWH inlet pipe must be cut so that the flow meter can be installed. Plumbing costs are expensive and the time required to install a unit is inconvenient for potential clients.

An immediate way to make SGC units more appealing to potential clients is to decrease the installation cost and installation time required to install a SGC. The in-line flow meter is the only component which requires invasive plumbing to install, the rest of the installation can be performed without skilled plumbing labour. The use of less expensive components and avoidance of invasive plumbing in the installation process thus makes the SGC more attractive to more potential users.

This means that more users can install SGC units and result in greater total water consumption reduction (using consumption feedback) and electricity supply grid relief (using demand side management).

2.2 Fluid Kinematics

The design of a water flow meter requires an in depth knowledge of fluid behaviour for the expected conditions.

The study of stationary fluids is known as fluid statics and the study of moving fluids is known as fluid kinematics [8]. Fluid kinematics knowledge is relevant to the design of a water flow meter as this measurement device is concerned with fluids in motion.

When a moving fluid comes into contact with a surface (e.g. the internal wall of a pipe) then the velocity of the fluid at that point is zero. This is called the "no-slip condition" [8]. This forms an important basis for many fluid kinematics assumptions.

In fluid kinematics there are two fundamental ways to describe a problem: Lagrangian and Eulerian descriptions [8]. The separate frames of reference provide different methods to describe flow.

The Lagrangian reference is used to describe the motion of selected fluid elements usually by concepts like path lines. The Lagrangian description can be likened to being in a boat which is travelling down a river and describing the path which the boat travelled on [8]. The Lagrangian reference is more useful to determine the paths of flow for applications like simulating water currents.

In Eulerian descriptions, a finite control volume is defined and fluid flows in and out of the specified control volume [8]. Field variables (functions of space and time) are defined which describe the properties of whichever fluid element occupies the space that a field variable encompasses for that certain time [8]. The Eulerian description can be likened to sitting at a fixed point on the bank of the river and describing the paths that separate boats travel on past that fixed point. The Eulerian reference is more beneficial to visualise fluid flow in the context of measurement using sensors as the sensors have a fixed location (which can have an associated control volume).

2.3 Expected Water Flow Conditions

The type of fluid kinematics to be considered can be classified based on common characteristics [8]. This allows the physical properties of the system to narrow the scope of required analysis to the water flow conditions expected for a domestic EWH. For the context of flow measurement of water in an enclosed pipe the fluid kinematic problem can be simplified using assumptions resulting in a more specific case. The fluid flow problem can then be categorised and more easily analysed.

2.3.1 Assumptions

Fluid flow in pipes is a very complex phenomenon to fully model for any conditions that deviate from ideal. The factors which affect the exact behaviour of fluid flow are numerous and are often interlinked. It is therefore necessary to set up restrictions on the scenario being investigated which simplifies the fluid kinematic model by only considering relevant conditions.

For the application of water flow measurement in domestic EWH units, several restrictions are present which allow limiting conditions to be imposed on the scope of the basic fluid dynamic model under consideration.

- Internal Flow. EWH units have fully enclosed pipes which transport the water meaning that only internal flow needs to be considered.
- Single Phase Flow. This means that only one fluid is contained within the pipes (i.e. water). South African National Standard (SANS) specify that vacuum breakers must be installed upstream and downstream of an EWH [9]. Freezing temperatures are not common in South Africa so water freezing in pipes does not need to be included in the problem. The water from South African municipal supply is required to contain fewer than $1200\,\mathrm{mg\,L^{-1}}$ of dissolved solids [10]. The only state of matter being considered is thus the liquid state. Thus no air bubbles, ice or significant dissolved solids can be present in the water flow.
- Constant Water Properties. The SANS standards specify the operating temperatures of EWH units. The temperature of water affects physical properties of water such as kinematic viscosity and density. For the specified temperature ranges these can be assumed to be constant at all temperatures [9].
- Incompressibility. The SANS standards specify the operating pressure ranges of domestic EWH units, and water can be considered to be incompressible for the expected conditions [8, 11].
- Standard Plumbing. A 22 mm nominal diameter copper pipe is assumed to be the pipe used for EWH units. These tend to be connected using non-threaded 90° elbow joints (which affect the flow regime of the fluid near a disturbance).

There are however many factors which affect fluid flow which are not controlled in the EWH context. The internal roughness of the pipe is a factor which is prone to change with time as the pipe erodes or sediment gathers on the internal surface (each individual roughness factor cannot be specified; but for copper pipes ranges between 0.003 mm

and 0.060 mm [9]). The upstream and downstream piping configuration is not constant and varies drastically between installations depending on the physical limitations of the location.

These factors, although not constant for all expected conditions, do not affect the fluid flow categorization. They do affect the physical conditions of each installation. The governing equations can be expected to be the same but with different variable values dependant on the physical installation meaning that calibration would be required if a specific flow scenario were to be considered.

2.3.2 Fluid Flow Problem Characterisation

The flow meter is to be designed to work on circular water pipes so only internal flow needs to be considered. Water is usually considered to be an incompressible fluid as it is a liquid [8]. This assumption holds true for the pressure and temperature range being considered meaning that the density of water can be considered constant for the expected conditions. Domestic water systems are pressurised which means that forced flow conditions must be considered.

The section of pipe used for the measurement location can be considered to be a 'control volume' or 'open system' because water can enter and leave the pipe section, but the pipe section boundaries (pipe walls and sensor locations) remain fixed [8].

Cavitation (vapour bubbles that can form in low pressure regions of a liquid depending on pressure and temperature conditions) will not occur in a domestic EWH. This is because the vapour pressure (pressure at which a liquid changes state at a given temperature) at the operating temperatures of an EWH are lower than 1 atm vapour pressure, but the water pressure is 600 kPa which is well above 1 atm pressure [8].

The low volumetric flow rate of water and the internal pipe diameter, D_i, in domestic installations results in fluid velocities which are much lower than the speed of sound in water; and thus only subsonic flow occurs. The maximum expected domestic fluid velocity is sufficiently less than 30 % of the speed of sound. This means that the assumption of incompressibility results in an error or less than 5 % [11].

2.4 Flow Regimes

The type of expected water flow in the EWH context has been narrowed to a more specific case by using simplifying assumptions. Internal flow of fluids, such as those occurring within the enclosed EWH pipes, have more specific properties which affect the fluid behaviour.

When a fluid flows in a pipe, the no-slip condition means that the velocity of the fluid is zero on the internal contact surface [8]. This means that the fluid velocity cannot be constant at all points on the cross-sectional area of the pipe. The viscous forces of the fluid mean that the slow moving fluid elements exert forces on the fast moving fluid elements to slow them down. This then leads to the development of a concept called the velocity profile which describes the velocity of fluid particles as a function of distance (from the internal boundary wall in the case of a circular pipe) [8]. The minimum fluid velocity is zero and this occurs at the pipe wall, while the maximum velocity occurs at the centre of the pipe where the velocity profile is greatest. The average velocity (which is the value

of interest for flow rate measurement) is the integral of the velocity profile over the cross sectional area [8].

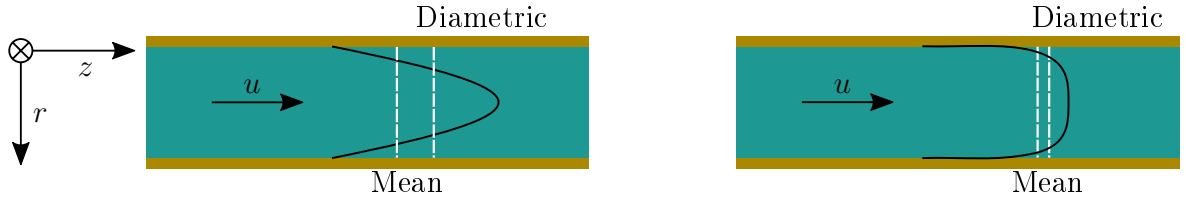

(a) Laminar velocity profile **(b) Turbulent velocity profile**

Figure 2.1: Velocity profiles for laminar and turbulent flow regimes. Representations showing the difference between the the average velocity determined using diametric paths and the actual mean velocity is shown using white dotted lines.

An illustration of the concept of the velocity profile and effect on different measures of flow rate is shown in Figure 2.1. It can be seen that the velocity of the fluid is not constant and is dependant on the radial position. It can be seen that there is a dramatic difference between fluid flow properties for different conditions which can affect the measured velocity.

The form of the velocity profile is dependant on the flow regime which occurs within the pipe. The flow regime is a categorisation of the 'type of flow' which occurs for specific conditions. The three flow regimes are laminar, transitional and turbulent flow. The transition between different flow regimes depends on "geometry, surface roughness, flow velocity, surface temperature, and type of fluid, among other things" [8]. Extensive testing provided a simplified representation of the factors that affect the flow regime and determined that the major factor is the "ratio of inertial forces to viscous forces within the fluid" [8]. This ratio is called the Reynolds Number, Re, and is defined as shown in Equation (2.1). Re is a dimensionless number as it describes a ratio.

$$\mathrm{Re} = \frac{\text{Inertial Forces}}{\text{Viscous Forces}} = \frac{\rho u}{\mu / D_i} \tag{2.1}$$

Where ρ is the density of water in $\mathrm{kg\,m^{-3}}$, u is the fluid velocity in $\mathrm{m\,s^{-1}}$, μ is the dynamic viscosity of water in kg/ms and D_i is the internal diameter of a circular pipe in m [8, 11].

The magnitude of the Reynolds number is an indication of which flow regime occurs. Table 2.1 shows the Reynolds number values which are generally associated with each flow regime for circular pipes [8]. Flow regime does not change abruptly at the exact listed values of Re.

Flow Regime	Reynolds Number Range
Laminar	$0 \leq \mathrm{Re} \leq 2300$
Transitional	$2300 \leq \mathrm{Re} \leq 4000$
Turbulent	$4000 \leq \mathrm{Re} \leq \infty$

Table 2.1: Flow regime and Reynolds number. The transitions between different flow regimes is not immediate but the listed values are used for internal flow in circular pipes [8].

The fluid takes a certain length of straight pipe to fully develop into the established regime. This is required because the fluid enters a pipe with a uniform (flat) velocity profile because there are no boundary conditions stopping flow or forces acting on the fluid. When the fluid first comes into contact with the internal pipe walls the fluid velocity at those points becomes zero, and the internal viscous effects mean that the interactions between slow moving and fast moving fluid elements eventually stabilises to a constant velocity profile. Flow which has a constant velocity profile is called fully developed flow. The required distance for fully developed flow to become established is called the "Hydrodynamic entrance length" or just "entry length", L_h [8].The shear stress, τ_w, which is exerted on the internal pipe walls is proportional to the gradient of the velocity profile [8]. Thus for fully developed flow the shear stress is constant and independent of the distance from the pipe entrance, whereas for developing flow the shear stress is largest nearest the pipe entrance and decreases until it reaches the fully developed flow value. The shear stress depends on the velocity profile, which depends on the flow regime which can be indicated by the magnitude of the Reynolds number.

2.4.1 Laminar Flow

Laminar flow occurs for small values of Re. Laminar flow is characterised by smooth streamlines and highly ordered motion [8]. Fully developed laminar flow has a parabolic velocity profile and can thus be accurately modelled. There is a thorough understanding of fully developed laminar flow in circular pipes and detailed models can accurately predict the behaviour of steady, incompressible fluid flows [8]. The relationship between entry length, L_h, and the internal diameter, D_i required for fully developed laminar flow is given by Equation (2.2).

$$\frac{L_{h,lam}}{D_i} \approx 0.05\text{Re} \tag{2.2}$$

The shear stress experienced by the pipe walls during laminar flow is expressed in Equation (2.3)

$$\tau_{lam} = \mu \frac{\partial u}{\partial r} \tag{2.3}$$

where u is the velocity of the fluid and r is the radial coordinate.

2.4.2 Transitional Flow

Transitional flow occurs when the Reynolds number lies between the lower laminar and higher turbulent values. It is very difficult to predict or model the behaviour of transitional flows. Transitional flow can either display characteristics from laminar and turbulent regimes simultaneously or can fluctuate between completely laminar and completely turbulent flow behaviour [8]. In the physical EWH system being considered, the only factors which can interact to result in expected transitional flow are certain combinations of low water temperature and low water velocity.

2.4.3 Turbulent Flow

Turbulent flow is characterised by velocity fluctuations and highly disorganised motion [8]. Rapidly fluctuating swirling regions of fluid known as eddies are a prominent feature of turbulent flow [8]. The intense mixing of fluid in turbulent flows as a result of the rapid fluctuations increases the momentum transfer occurring between fluid particles and thus increases the friction force on the pipe wall [8]. The longitudinal velocity (in the direction of flow) of fluid in turbulent flow, u, can be expressed as the sum of an average velocity, $\bar{u}$, and a fluctuating velocity, u' as in Equation (2.4).

$$\begin{aligned} u &= \bar{u} + u' \\ v &= \bar{v} + v' \\ p &= \bar{p} + p' \\ T &= \bar{T} + T' \end{aligned} \tag{2.4}$$

Other properties such as radial velocity v, pressure p, and temperature T, can be expressed as the sum of an average value and fluctuating value [8]. The time average of the fluctuating components of all properties is zero [8].

Although turbulent flow is not as consistent as laminar flow, turbulent flow still requires a given entry length to fully develop as shown in Equation (2.5). The turbulent entry length is derived experimentally and this approximation is usually considered sufficient [8].

$$\frac{L_{h,turb}}{D_i} \approx 10 \tag{2.5}$$

Where D_i is the internal diameter of the pipe. When fluid flow is disturbed (e.g. by a 90° bend in piping) then an upstream distance of $5\,D_i$ and downstream distance of $10\,D_i$ is usually considered sufficient to be sure that fully developed turbulent flow can be expected at those locations [8, 12].

Turbulent shear stress cannot be described as neatly as laminar shear stress shown in Equation (2.3) [8, 13]. The total shear stress consists of the sum of the laminar shear stress and the turbulent shear stress (which is larger due to eddies). The turbulent shear stress is given in Equation (2.6) as described in [8].

$$\tau_{turb} = -\rho\,\overline{u'\,v'} \tag{2.6}$$

where $\overline{u'\,v'}$ is the time average of the product of the fluctuating longitudinal and radial velocities, u' and v' respectively and ρ is the density of water. Although the individual time averages $\overline{u'}$ and $\overline{v'}$ are zero respectively, the time average of the product of the fluctuating components $\overline{u'\,v'}$ is usually a negative value according to experimental results [8].

2.5 Flow Meters

An important application of fluid mechanics is the determination of the flow rate of fluids. For industrial applications flow rate measurement is often required as it affect several process variables including pressure, temperature, chemical composition and fluid levels [11]. For domestic EWH contexts the flow rate is less important than the total volumetric consumption.

Flow rate can be measured in terms of fluid velocity, volumetric flow rate or mass flow rate [8]. Mass flow rate is generally used in "energy-giving fluids" (e.g. petrol, natural gas) whereas volumetric flow rate is more important for water meters [11].

Volumetric flow rate in pipes is defined as the volume of fluid which crosses the perpendicular cross sectional area of the pipe per unit time [11]. The relationship between the volumetric flow rate, $\frac{\mathrm{d}V}{\mathrm{d}t}$ (or $\dot{V}$) in $\mathrm{m^3\,s^{-1}}$, and average longitudinal velocity, $\bar{u}$ in $\mathrm{m\,s^{-1}}$, is given by Equation (2.7)

$$\dot{V} = \frac{\mathrm{d}V}{\mathrm{d}t} = \bar{u}\, A_c \tag{2.7}$$

where A_c is the cross sectional area of the pipe. From Equation (2.7) it can be seen that for a pipe of known cross sectional area the volumetric flow rate can easily be obtained from the fluid velocity.

Flow meters can be broadly categorised as being invasive or non-invasive as shown in Figure 2.2.

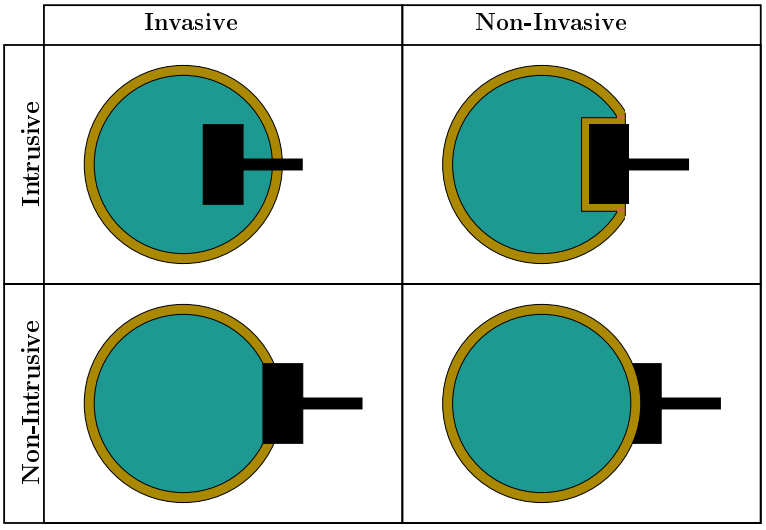

Figure 2.2: An illustration of intrusive and invasive sensors.

Invasive flow meters are known as 'wetted' meters as the transducers used come into contact with the fluid being measured [12]. Invasive transducers are thus unsuited for applications where any problematic fluids (e.g. radioactive, corrosive) are being measured. Non-invasive flow meters do not come in contact with the fluid and can thus be used for problematic fluids [14].

Flow meters can further be described by whether they are intrusive or not. Intrusive flow meters obstruct the flow of the fluid in some way without physically coming into

contact with the fluid [12]. A retrofit solution to an existing EWH system must thus be non-invasive and non-intrusive.

Certain flow measurement principles are more suited to certain applications (e.g. for clean water or slurries different technologies are required). The selection of flow measurement method is determined by the fluid to be measured to ensure reliable flow measurement [11]. The physical installation of the flow meter can also affect the measurement accuracy. For industrial flow measurement the typical accuracy of flow measurement can be between 0.2 % and 5 % of the full scale range [11]. Domestic flow measurement has less monetary incentive to be accurate so less expensive and less accurate flow meters are more likely to be used.

2.5.1 Invasive Flow Meters

Intrusive and invasive flow meters can directly measure the water flow rate in some way as they come in contact with the fluid and change the flow in some way to obtain a definite reading. Intrusive flow meters obstruct the flow of the fluid in some way by altering the shape of the fluid containing vessel. Invasive flow meters use sensors which come into contact with the fluid being measured and are thus often called 'wetted' sensors. Alterations in existing plumbing are required for the retrofit installation of invasive flow meters.

'Positive displacement' flow meters measuring fluid flow directly. These work by measuring the volume of fluid which passes through a surface area of a pipe over a fixed time period rather than measuring the instantaneous flow rate [8]. Positive displacement flow meters work by repeatedly filling and discharging a fixed, known volume (measuring chamber) and counting the number of discharges in a certain time frame [11]. A commonly used application for positive displacement flow meters is Municipal water meters. The existing in-line flow meter used in the SGC units is a positive displacement flow meter. The advantages of positive displacement flow meters are the high potential accuracy, no power supply requirements and no turbulence restrictions (no dependence on higher Re) to operate [11]. The disadvantages which relate to domestic EWH applications are a pressure reduction and the inability to install on an existing EWH without non-trivial plumbing.

Invasive flow meters tend to have the benefit of potentially being more accurate than non-invasive flow meters. This is because invasive flow meters can directly monitor the fluid [14]. A definite drawback to invasive flow meters in industry is that they can corrode as they are in contact with the fluid being measured. Invasive flow meters are often intrusive as well (changing the flow path) and can cause a pressure loss (as they generally also intrusively obstruct the flow) [11].

2.5.2 Non-invasive Flow Meters

Non-invasive flow meters do not come into contact with the fluid being measured. Non-invasive flow meters are generally non-intrusive as well meaning that the fluid flow path is not altered by the presence of the sensor. Non-invasive flow meters function by measuring a physical aspect which is caused or in some way affected by fluid flow. They are sometimes referred to as "inferential flow meters" because they infer the flow rate by measuring other physical properties related to fluid flow [11].

Because non-invasive flow meters cannot measure the fluid directly they are more prone to other factors which affect their accuracy. An example of a fluid property which can affect the performance of non-invasive flow meters is the velocity profile of the fluid [11]. The drastic which the velocity profile can have on measurable flow rate can be seen in Figure 2.1.

Flow meters which are both non-invasive and non-intrusive have the benefits of no fluid pressure loss, retrofit installation capability, no corrosion (because transducers are not wetted), no wear and tear as there are no moving parts, and the ability to operate using problematic fluids [8, 14].

2.5.3 Vibration Flow Meters

Vibrations can either be measured using an accelerometer to measure mechanical vibrations or using a microphone to measure acoustic vibrations (sounds). Vibration flow meters function by measuring some vibration which is caused by fluid flowing in a pipe and using the measured vibrations to estimate the fluid velocity.

2.5.3.1 Vibration Standard Deviation

Turbulent flow consists of average and fluctuating fluid as shown in Equation (2.4). Flow fluctuations result in a turbulent shear stress, τ_{turb} as shown in Equation (2.6). A derivation by Evans [13] further relates turbulent shear stress at the inner wall, τ_w, of an enclosed pipe with radius r to pressure fluctuations, p'.

$$\tau_w = -\frac{r}{2}\frac{dp}{dx} \tag{2.8}$$

Which can be rearranged as:

$$\frac{dp}{dx} = p' = -\frac{2\,\tau_w}{r} \tag{2.9}$$

Therefore from equations (2.6) and (2.9) it can be seen that the pressure fluctuations are proportional to the fluid velocity as shown in Equation (2.10). The importance of ensuring fully developed flow to obtain a constant shear stress is evident when considering the vibrations caused by flow. For flow that is not fully developed the shear stress is not constant and the proportionality between fluid velocity, shear stress and pressure fluctuations is not constant.

$$p' \,\alpha\, \overline{u'\,v'} \tag{2.10}$$

The derivation shows that pressure fluctuations are thus proportional to fluctuation of fluid velocity. It is then shown that the acceleration of the pipe is proportional to the fluid induced pressure fluctuations in a complex derivation [13].

The culmination of the derivation is that turbulent fluid flow in an enclosed pipe creates pressure fluctuations which are proportional to the pipe vibrations in the form of acceleration. Further, it is shown that that the standard deviation of the pipe vibrations

is proportional to the average longitudinal flow rate, $\bar{u}$. This relationship is shown in Equation (2.11)

$$\frac{1}{N-1}\sum_{i=1}^{N}[u_i(t)-\bar{u}]^2 = \frac{N\,C}{N-1}\,\bar{u^2} = K\,\bar{u^2} \tag{2.11}$$

Equation (2.11) shows the form of a sample standard deviation where N is the number of samples. The left hand side shows the sample standard deviation of the pipe vibrations in terms of fluid velocity. The pipe vibrations are related to pressure fluctuations which are proportional to the fluctuating fluid velocity (because from Equation (2.4): $u' = [u - \bar{u}]$). The centre expression is a simplification where C is a constant relating to the physical properties of the pipe related to the physical acceleration of the pipe. The right hand side shows a constant K multiplied by the square of the average fluid velocity, $\bar{u}$ [13].

A quadratic relationship between turbulent fluid velocity and transverse pipe vibrations for straight pipe sections with fully developed turbulent flow was determined in [15]. This relationship was determined using experimental and numeric methods. The numeric methods were performed using a super-computer. The simultaneous experimental methods confirmed the simulated behaviour which numerical methods provided. The results obtained from the experiments performed in [15] agree with the experimental results determined in [13]. The experimental conditions used in [13] considered 3 or 4 inch nominal diameter steel, aluminium or polyvinyl chloride (PVC) pipes. The flow rates tested were between $500\,\mathrm{L\,min^{-1}}$ and $1500\,\mathrm{L\,min^{-1}}$ [13]. This range equates to Reynolds number values between 100 000 and 1 000 000 and fluid velocities between $1.82\,\mathrm{m\,s^{-1}}$ and $5.48\,\mathrm{m\,s^{-1}}$.

The derivation of the relationship between measured pipe vibrations and mean fluid velocity performed by Evans, [13], culminated in Equation (2.11). It is reasonable to assume that the general mathematical relationship is true for the conditions of used in [13, 15, 16] and thus the relationship can expected to be valid when flow is sufficiently turbulent. This method requires fully developed turbulent flow and thus the tests were performed using a sufficiently long, straight pipe to limit the effect of flow disturbances [13].

The mounting location of the sensor was found to affect the proportionality. A linear relationship was found for a microphone based accelerometer mounted on a 90° bend but a quadratic relationship was found for straight sections for experiments performed in [17]. The complex nature of vibration propagation means that each investigated implementation of the vibration methods discussed required individual calibration. It was found that the pipe material as well as the pipe diameter contributed to the relationship between fluid velocity and pipe vibrations as discussed in [13].

2.5.3.2 Frequency Domain Analysis

A method to use the measured vibrations in the frequency domain to perform frequency spectral analysis is sometimes used in industry [13]. The working principle is that a frequency shift of the natural frequency of the pipe occurs when fluid flows in the pipe. For fluid velocities of less than 10 % of the speed of sound expected resonant frequency shift is less than 0.1 Hz [13]. The greatest expected fluid velocity for domestic EWH conditions is approximately 0.08 % of the speed of sound in water (for maximum expected domestic volumetric flow rates of $30\,\mathrm{L\,min^{-1}}$). Thus this is not possible for domestic applications

as the fluid velocity is too low for the principle to be applicable and the domestic water velocity range is too small to accurately measure a frequency shift.

The frequency domain analysis of vibrations is commonly used in non-destructive testing [14]. An example of this is the use of vibration sensors to identify faults in rotating machinery [18]. Expected frequencies are monitored which correspond to known failure types and thus failures can be identified. It is impossible to know what frequencies will correspond to fluid velocities for domestic EWH units. The plumbing system affects vibration propagation and intensive calibration would be required for each unique installation.

2.5.3.3 Transient Vibrations

In [19], vibration sensors were used to measure changes in hydraulic head (a measure of liquid pressure) to classify events or detect errors on large piping systems. Vibration sensors were placed on nodes (corners) and transient events were successfully detected. The hydraulic transients corresponded to sharp changes in measured acceleration at many points in a piping network. Damage detection was the primary implementation [19].

2.5.3.4 Acoustic Flow Meters

Acoustic flow meters use a microphone as the input source rather than an accelerometer. In [17], the vibration standard deviation method described in [13, 15] was used to develop a low-cost, non-intrusive water flow rate sensor using a microphone. The effect of the microphone location determined that the quadratic relationship between pipe vibrations and fluid flow rate occurred for transducers mounted on straight pipe sections. A linear relationship was found for sensors mounted on pipe bends [17]. Analysis of the amplitude of the frequency domain peaks at identified frequencies was used to derive an averaged value which was related to the fluid velocity. The accuracy of the system was limited by the need for extensive calibration. The results were sufficient to provide qualitative flow rate data such as categorising flow as low, medium, or high flow rates with little calibration [17].

Similar accuracy issues were experienced in [20] when using a piezo-electric transducer (which converts mechanical kinetic energy to electrical energy) to measure the pipe vibrations which occur on the valve of outside taps. An average error of 15 % was achieved in this study. Frequency domain and time domain analysis of the recorded signal was performed. A discontinuity between laminar and turbulent flow rates was observed for the estimation system [20]. A system was used which selected which of 3 frequency domain models was most accurate for different flow rate ranges and selected the relationship which resulted in the most accurate estimation. A trend of quadratic flow rate relationship was found for low flow rates and a linear relationship for higher flow rates was found to provide the most accurate results for the conditions tested [20]. It was found flow rate estimation was not possible for flow rates which corresponded to expected transitional flow regimes [20].

Fluids containing dissolved solids can me measured using vibration methods. When solid particles collide with the pipe they transfer kinetic energy to the pipe which results in vibrations [14]. A vibration sensor or microphone is used to record the rate of collisions of the dissolved solids against the pipe. Collisions occur most frequently at bends in the pipeline (where the flow is transient rather than fully developed) and thus vibration sensors which employ this method are typically installed on bends [14]. In industrial

scenarios where slurries are measured; if the flow rate is known then the slurry composition can be calculated, or else for a known composition the rate of collisions is an indicator of fluid velocity [14].

In [21], a vibration sensor based on a condenser microphone was developed. It was mounted a on tap outlet to measure water flow and a sample rate of 10 kHz was used. It was stated to somewhat accurately estimate flow rates of less than $0.2\,\mathrm{L\,min^{-1}}$ [21].

Acoustic emissions methods involve characteristic mechanical vibrations associated with a specific system [22]. Such a method was used to design a system which used piezo-electric transducers, cross-correlation, multi-sensor data fusion and artificial intelligence was used in systems where fluids contained dissolved particles. The system described in [22] was concerned with particle flows. It was seen that the velocity of particle flows could be determined using non-invasive acoustic emission methods in [22].

2.5.4 Ultrasonic Flow Meters

Ultrasonic flow meters (USFM) are non-invasive as they are mounted on the pipe exterior as well as non-intrusive as the pipe shape (and thus fluid flow) is unaffected by the presence or absent of the USFM. The most relevant benefit to the EWH application is the retrofit installation. On-line calibration calibration is required after installation [11].

USFMs operate using piezo-electric transducers which can convert electrical energy to mechanical energy and vice versa. Thus a set of 2 transducers can function as a transmit-receive pair or as a receive-transmit pair depending on which transducer is driven as the transmitter [12, 14].

The basis of all USFMs is an electronic excitation source which drives a transmitter transducer, a medium through which ultrasonic signals can propagate, a receiver transducer for the altered ultrasonic signal, reception electronics, signal processing section and an output. The excitation source can be a pulse, tone (sinusoidal) burst or a coded (digital) burst depending on the application [12].

The specific ultrasonic methods which are most prominently used in USFMs are transit time, Doppler shift and cross-correlation methods [12, 14, 8, 11].

2.5.4.1 Transit Time

Transit time ultrasonic flow meters (TTUFs) operate by transmitting an ultrasonic signal at an angle along the length of the pipe and recording the time taken to reach the receiver transducer when the signal path is known. The transmission angle is important because the ultrasonic signal refracts when passing through different media according to Snell's Law and thus affects the required distance between the two transducers [12]. The different media are the transducer mounting wedge, the pipe wall and the fluid.

Figure 2.3 shows the transmission paths for TTUFs. Direct transmission (Z), 2.3a, is preferred for large diameter pipes. Smaller diameter pipes require Single (V) or Multiple (W) reflections, 2.3b and 2.3c respectively, to increase the length of the transmission path to ensure that a large enough time delay can be measured [14, 23]. Single reflection configurations are preferred over multiple reflection configurations. Each reflection attenuates the signal and adds complexity to the system [23].

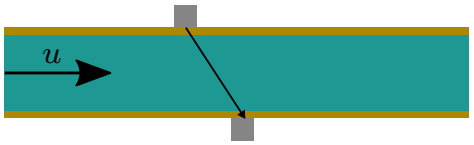

(a) Direct transmission: Z configuration.

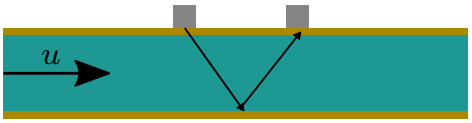

(b) Single reflection: V configuration.

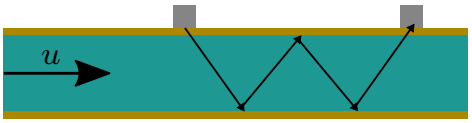

(c) Multiple reflection: W configuration.

Figure 2.3: Transit time ultrasonic transducer configurations. The direction of longitudinal fluid velocity, u, is indicated. The transmission paths of the ultrasonic signals and reflections are also shown. The Ultrasonic transducer and receiver pairs are shown.

The principle used for all configurations is the same but the path length differs. A downstream (in the direction of flow) ultrasonic signal is transmitted and the downstream transit time is recorded, then the process is repeated for an upstream transit time. The fluid velocity means that the downstream delay time is shorter than the static case and the upstream delay time is longer than the static case. The transit time is used to calculate the velocity of the fluid [14]. When using upstream and downstream transmissions then the speed of sound in the fluid is not required to calculate the volumetric flow rate [14].

Flow measurement accuracy of 1 % can be achieved for ideal conditions (when a flow conditioner is installed to ensure flat turbulent fluid velocity profiles). In practice 5 % accuracy can be expected due to the physical aspects such as imprecise pipe thickness, dissolved particles and upstream and downstream disturbances (pipe bends, etc) which affect the measurement [14].

TTUFs are best suited to clean, single phase fluids where the beam path lengths are known [14]. Reynolds number based flow profile correction is required to compensate for the velocity profile. This is necessary because for velocity profiles that are not flat the sensor configuration only uses the diametric path and excludes slower moving regions which results in an overestimation of average velocity [23]. Figure 2.1 showed an illustration of the effect of velocity profile and velocity measurement. On site calibration is often required [23].

For pipes diameters between 100 mm and 10 mm it is advised to use 2 MHz transducers [23]. Larger pipe diameters can use lower frequency ultrasonic transmissions.

2.5.4.2 Doppler Shift

Doppler shift or Doppler ultrasonic flow meters (DUFs) can have a lower accuracy than transit time ultrasonic flow meters [23]. DUFs require dissolved particles (gases or solids) to be present in the liquid of at least 30 micron in size and 25 parts per million in concentration for 1 MHz transmitter signals [14]. They are typically used for liquids in paper making industry or to for slurries [14]. DUFs can achieve a maximum of 2 % accuracy under ideal conditions but typically have an uncertainty of about 10 % [14, 23].

DUFs emit a signal at a specific frequency which is scattered by the gas or solid particles in the fluid and the received reflected signal is analysed [23].

For stationary fluids the transmitted and received signals have the same frequency, but for fluids in motion a frequency shift occurs due to the Doppler effect [12, 14]. The frequency shift from the known transmitted frequency is used to calculate the fluid velocity [23].

The requirement that dissolved particles be present means that traditional DUFs can not be used in clean water scenarios. High frequency units (8MHz) which use eddie currents to reflect the signal [14]. In addition to measurement inaccuracy caused by many unknowns when using DUFs, DUFs can also produce errors due to vibrations indicating that DUFs are not reliable enough for permanent installation [14].

2.5.4.3 Cross-correlation

Cross-correlation is a well known signal processing tool and is not limited to use in USFMs. Cross-correlation can be used in any system with multiple sensors to enhance the measuring precision of a signal [18]. Using cross-correlation of ultrasonic signals leads to the term cross-correlation ultrasonic flow meters (CCUFs). The general structure of a CCUF is shown in Figure 2.4.

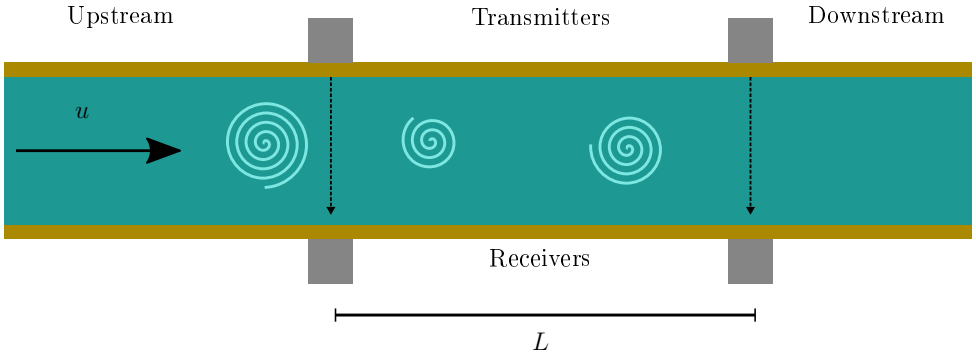

Figure 2.4: Cross-correlation ultrasonic flow meter representation. The turbulent eddies, shown as spirals, travel at a velocity of u. The time of the peak cross-correlation value is the time which the eddie took to pass a distance of L between the upstream and downstream sensor pairs.

In a CCUF there are two pairs of transducers a distance L apart. Both the upstream and downstream sensor pairs have a dedicated transmitter with a dedicated receiver. The pairs are positioned so that the ultrasonic signals are transmitted parallel to each other and perpendicular to the direction of flow [23].

For a pipe with an internal diameter of D_i, the distance L is typically between $0.5\,D_i$ and D_i. Turbulent eddies (swirls in fluids) do not decay enough to become sufficiently dissimilar at short distances, so a strong cross-correlation can be measured [23, 14].

The turbulent eddies affect the transmitter signal and which is recorded using the received signal. Flow turbulence causes slight perturbations in the propagation speed of the ultrasonic carrier signal through the fluid, so the received signal is a "randomly phase-modulated version" of the transmitted signal [24]. Demodulation removes the carrier signal which leaves only the low frequency signal which was caused by the turbulent eddy [24]. The disturbance passes by the upstream and downstream sensor pairs at different times in the upstream and downstream received waveforms.

Similar upstream and downstream waveforms result in a strong correlation occurring for a specific time shift which is shown by a peak in the cross-correlation representation.

The time value at which the peak occurs can be considered to be the transit time. The time taken for a specific disturbance to pass a known distance L from the upstream to downstream sensor pairs can be used to determine average fluid velocity [25, 26].

The accuracy of CCUF can be considered to be 5 % but calibration under similar conditions can improve this to 1 % [23].

2.5.5 Thermal Flow Meters

The measurement of fluids in industry often require different operating conditions. Invasive hot wire anemometer mass-flow meters are used as a reliable gas measurement method for industrial applications [11]. Thermal flow measurement is usually performed on gases [11]. Non-invasive thermal mass flow meters (or thermal dispersion flow meters) can also be used to measure fluid flow rate [27].

Thermal mass flow meters work by measuring the temperature difference between two points which are longitudinally spaced on a pipe containing fluid (thus separated by a distance, L, in the direction of fluid flow). Traditionally a heating element is required to be present between to two sensors to uniformally heat the fluid [27]. The power required to heat the upstream fluid to the higher downstream temperature is measured in addition to the temperature increase to determine the mass flow rate of a known fluid [27]. Mass flow meters are generally used for liquids with low flow rates or gases due to the lower power input required to result in a measurable temperature difference.

Another mass flow rate method uses invasively inserted copper heat exchangers to promote uniform fluid temperature dispersion. Such a system was developed to measure vehicle fuel consumption [27]. In this system a constant temperature different is maintained between an upstream and warmer downstream location and the required power to achieve the constant temperature difference is measured. A third measurement point is located further downstream to measure the error (the temperature at the furthest downstream location is supposed to be the same as at the middle location due to the mixing caused by invasive heat exchangers) [27]. It was found that higher flow rate measurement was possible when using the invasive heat exchangers and using external temperature measurement. The maximum measurable flow rate was found to be $10\,\mathrm{mL\,s^{-1}}$ or $0.6\,\mathrm{L\,min^{-1}}$ [27].

Another non-invasive thermal solution is the one implemented successfully on a SGC project by Nel in [28]. A temperature sensor was mounted on the outlet pipe of an EWH. A one or two node thermal model of the water contained in the EWH cylinder was developed. The thermal data was used to detect the start and duration of water flows with 1 min resolution. Detection of short events using thermal data was not possible using the described algorithm. Volumetric estimation was also performed using the measured enegy input into the system by the EWH heating element. The energy input was used to calculate the volume of cold water must have entered the EWH which needed to be heated by the element. Volumetric errors between 1 % and 44 % were recorded based on consumption patterns. Volumetric estimation of longer duration flow events (7 to 10 min) were significantly more accurate than short duration flow events. The minimum duration of a water flow event detected using the described algorithm was 3 min [28].

2.5.6 Electromagnetic Flow Meters

Non-invasive fluid velocity measurement using electromagnetic flow meters is often used in industry for single phase flow (pure fluids which are not mixed with other fluids) [29]. Electromagnetic flow meters use electromagnetic induction as the working principle [11]. The transverse field electromagnetic meter is an example of an electromagnetic technique which can be used to determine fluid velocity for enclosed flow [29]. Low conductivity fluids are preferred to implement electromagnetic velocity measurement as they affect the magnetic fields to a lesser extent [30].

For transverse field electromagnetic flow measurement to be implemented coils generating a nominally uniform magnetic field surround a fluid containing pipe. The magnetic field is generated perpendicular to the direction of flow for pipes which have electrically insulated interiors [29] . Varying fluid flow rates result in an electric potential difference appearing across two electrodes placed perpendicularly to the magnetic field and direction of flow. This phenomenon only occurs when the interior of the pipe (which interfaces with the flowing fluid) is electrically insulated. For certain fluid compositions, electromagnetic flow measurement perform well for unsteady flows [29].

Alternating current implementations of electromagnetic flow meters are possible which eliminate polarization [30]. Electrical insulation between the somewhat electrically conductive fluid and the surrounding pipe is required, otherwise most of the desired signal is lost in short circuits between the fluid and the encasing material [30].

2.5.7 Smart Flow Meters

Smart flow meters can be considered to be the next development of flow meters. Smart flow meters can account for several factors which can affect the accuracy of measurements in an adaptive way, which normal flow meters cannot do as they are calibrated once and left to function. Some of the factors which smart flow meters can consider include: "temperature, pressure, viscosity, dissolved particles", fluid velocity profile and errors due to incorrect installation of sensors [11].

The smart system developed in [16] provided accurate and spatially fine grained water consumption information using vibration sensors at the appliance-level . The system was designed to disaggregate total measured water usage to determine consumption per appliance. The system consists of an accurate in-line flow rate meter (from the existing infrastructure) to provide a trusted total flow rate value (accurate value), the further information tier consisting of vibration sensors installed on individual appliances to provide appliance-level water usage. The magnitude of the vibrations at each individual appliance pipeline provided an indication of the relative water division of the total measured water flow value. The system is self calibrating (which is possible because of the constant reference value of the total measured water flow) and sensor fusion considers the interaction between pipes to further increase accuracy. The results indicated that vibration based flow rate measurement is possible and accuracies of 7 % were achieved [16]. The related project described in [31] used an ultrasonic flow meter on the main water pipe to provide more accurate total reference values. The study also assessed the location of vibration sensors, method of securing vibration sensors and the material of the pipe and provided a real world application of the concept of tiered water flow measurement [31].

Smart meters which make use of sensor fusion can obtain more information using the fused readings than from individual sources in isolation. An example of non-flow related

sensor fusion (relating to vibration measurement) was presented in [18]. Several vibration sensors were used and the system described required no knowledge of sensor performance to calibrate. This was done by weighting sensors with higher correlations more heavily, effectively disregarding sensors that are outliers [18]. This is possible with cross-correlation due to the periodic nature of rotating machinery for the application of fault diagnosis. The cross-correlation based weighting of distributed sensors also enables the reduction of unrelated noise, as done in [18], for more broad applications than just rotating machinery.

The SGC system provides users with water consumption data as well as enables scheduling of the heating element. The availability of water consumption data was found to alter user behaviour and result in reduced total monthly consumption [4, 5].

2.6 Calibration

The calibration of a sensor is very important to ensure that the most accurate results can be obtained. In many cases calibration is required to be done for the specific scenario where measurements are to be made [14]. Because of the large numbers of parameters which affect the behaviour of domestic water installations, on-site calibration is likely required for a non-invasive flow meter for an EWH.

A simple calibration technique involves using an accurate sensor to give reference and to use these readings in the calibration of another sensor [14]. Offsets and scaling factors can be considered to be simple calibration methods.

Some sensors can self calibrate using machine learning. An example of this is the system described in [16]. The system was designed to "solve a two phase linear programming and mixed linear geometric programming problem" to adaptively calibrate [16]. The calibration system proved to be successful, but a measured total flow rate was required to calibrate the multiple vibrations sensors used (which enabled appliance-level water consumption statistics) [16]. The presence of a trusted water flow rate value is not possible for a stand alone water flow rate meter (which is intended to provide the 'reference value').

Cross-correlation was used to identify which sensors received the highest weighting factor in [18].

Calibration of ultrasonic flow meters requires the compensation for the flow velocity profile which is dependant on the location of the sensors and the geometry of the flow path (both of which determine the flow profile) [12]. Thus if the sensors remain stationary and the flow conditions are within the range which the calibration was performed then recalibration should not be necessary. The installation procedure is important to ensure the correct operation of USFMs [12]. The location of the sensors must be such that fully developed flow is present for accurate results. If the flow profile is disturbed (not fully developed, e.g. asymmetric) then the flow calculations will be based on a cross section of flow that misrepresents the average flow rate in a way that Reynolds number calibrations cannot account for [12].

Accelerometers measure absolute g-force values but when used to detect vibration then additional calibration steps are required. Vibration propagation is complex and the any vibrations in a system can affect the measurement at all points in the system. Multiple tests are often required for relevant patterns to be distinguished which makes off-site calibration unlikely. In [20] the identification of frequency bands which were experimentally

found to correspond with flow rates was required for the specific scenario of a tap valve. In [17] a calibration process was required which differed for vibration sensors placed in different locations along the pipe (straight section or elbow).

Chapter 3

Thermal Modelling

Two thermal models of different complexity were developed with the intention of quantitatively estimating fluid velocity using thermal data only.

The motivation for investigating thermal methods is given in Section 3.1. The most simplified steady-state thermal difference model is discussed in Section 3.2. The preliminary thermal tests which were performed are mentioned in Secion 3.3. The expected relationship between measured temperature difference and measured flow rate were not observed in preliminary thermal tests and a more complex thermal model was developed and simulated as discussed in Sections 3.5, 3.6 and 3.7. The difficulties encountered in using the described thermal methods to attempt to measure EWH hot water flow rates is described in Section 3.8. Indications of the practicality and requirements of thermal methods for domestic EWH conditions is given in Section 3.9.

3.1 Thermal Method Motivation

Non-invasive thermal mass flow meters are often used to measure gas and low flow rate liquid flows [11, 27]. Thermal mass flow rate measurement traditionally requires the measurement of two or more temperatures along the longitudinal axis of a pipe and a heating element to provide a temperature increase which can be measured [27]. Liquid measurement of low flow rates ($\leq 0.6\,\mathrm{L\,min^{-1}}$) was seen to be possible for the mass flow measurement system used in [27] as described in Section 2.5.5.

For the EWH application it was roughly calculated that to use an external heating element to increase the temperature of the 22 mm copper piping and contained water volume would be impractical. The required power would be similar to the heating element contained in the EWH. The requirement for non-invasive installation meant that invasive heat exchangers was not possible but were found to improve the performance of thermal mass measurement for liquids in [27].

For the EWH application it was noted that an existing heating device was already present in the form of the EWH element. The element heats the water within the EWH tank until it reaches the desired temperature (setpoint temperature). The water within the tank is assumed to at a uniform temperature, meaning that the water which flows in the outlet pipe should also be at a uniform temperature as well. An enclosed volume of water which is well mixed and at uniform temperature can be called a plug. The possibility of using the existing EWH element to act as a heating element for mass flow measurement purposes was investigated.

The energy input using the element can be measured using a SGC and if a relationship was found between longitudinal temperature drop during flow and measured flow rate then a thermal method similar to thermal mass flow meter could be created to estimate the flow rate of water flowing out of the EWH unit. An empirical system which used a one or two node model of the EWH tank was used by Nel to estimate volumetric consumption in an EWH, but the success was limited to long duration flow events [28]. The alternative of modelling the outlet pipe behaviour is investigated in this chapter.

3.2 Steady-State Thermal Difference Equation

Energy losses can theoretically be used to non-invasively estimate the velocity of gases moving within sealed pipes. An investigation was done into the feasibility of using the energy losses of water moving within a sealed pipe to estimate the fluid velocity using measured temperature difference in the longitudinal direction (direction of flow). Liquids have a higher thermal mass than gases and thus the measurable temperature difference is expected to be smaller for liquids. A greater longitudinal temperature loss can be created by increasing the heat transfer coefficient, h, on the pipe outer surface. This can be achieved by mounting a heat sink on the outlet pipe to increase the heat losses in the pipe when water is flowing to make the effect as pronounced as possible to facilitate measurement opportunities. This can be thought of as passive variation of the traditional thermal mass flow measurement technology.

A theoretical steady-state fluid velocity measurement equation was derived from first principles. The steady-state thermal equation makes the most simplifying assumption and is thus the most simple to develop and test. The steady-state thermal difference equation should be able to equate the fluid velocity to the measured longitudinal temperature difference for conditions where flow has occurred so that the copper pipe reaches a steady-state temperature. An energy balance was performed on a fluid element enclosed within a pipe. The assumption was made that the water behaved as a well-mixed plug meaning that the radial temperature of the water was constant (due to the expected turbulent flow regime). The heat transfer occurring in the radial direction into the copper wall was then considered. Copper has a high thermal conductivity so the common assumption was made that the convection losses within the copper were negligible. The copper pipe wall used is 1 mm thick, so to simplify the derivation the heat loss profile was assumed to be linear rather than logarithmic for such a thin wall. The convective heat transfer which occurs between the copper wall and the ambient air was also considered. The ambient temperature sensor was required to be placed far enough away from the copper pipe that convective heat transfer within the air did not affect the measurements.

The simplified model which results from the energy balance is:

$$\frac{\partial T}{\partial z} = \frac{4U}{\rho_w c_p D_i v}\left(T_\infty - T_{(z)}\right) \tag{3.1}$$

where T is the temperature of the external pipe surface, U is the combined heat transfer coefficient (thermal transmittance) of the copper pipe wall and the air layer, ρ_w is the density of water, c_p is the specific heat capacity of water, D_i is the internal diameter of the pipe, v is the velocity of the water and T_∞ is the ambient temperature.

Rearranging the ordinary differential Equation (3.1) to solve for v yields:

$$v = \frac{-4z \ln\left(\frac{T-T_\infty}{T_{(z)}-T_\infty}\right)}{\rho c_p R D_i} \tag{3.2}$$

Equation (3.2) was derived using first principles. R is the combined thermal resistance of the pipe wall and air layer ($R = 1/U$). Preliminary tests were performed to evaluate whether the steady-state thermal difference equation could be used to estimate water velocity in an EWH.

3.3 Preliminary Thermal Tests

Preliminary thermal tests were performed using an existing EWH in a 4th floor test location. The vertical height resulted in lower water pressure and thus lower flow rates available during preliminary experimentation. The data obtained from the preliminary tests did not correlate with the expected behaviour as indicated by the steady-state thermal difference equation. It was observed that the sensors had a time delay between when hot water flowed through the pipe and when the recorded temperature of each sensor increased. This indicated that the radial conduction of the copper had a more marked effect on the behaviour of the system than expected or that the thermal resistance of the sensors contributed heavily to the thermal mass of the system. The noticeable time delay which was observed indicated that the steady-state assumption could not be used in practice and the steady-state equation was suspected to be inadequate.

Thermal behaviour which is not physically possible was also recorded. It was noted that certain sensors located further away from the EWH reported higher steady-state temperatures than certain sensors located closer to the EWH. The EWH is the only heat source in the system and the water temperature must decrease in the longitudinal direction of water flow as radial heat losses through the copper wall and into the air occur. Thus it was suspected that the preliminary thermal experiment sensor mountings were not ideal and that the thermal mass of the sensors was not negligible as was previously assumed. It was also suspected that the sensors were not as reliable as the manufacturer claimed, especially when mounted on printed circuit boards (PCBs) or breakout boards due to a large discrepancy during calibration tests.

Additional thermal data was generated during the development of the experimental unit (Chapter 4). Different conditions were used than were present in the completed experimental unit, so thermal data generated during development stages is also considered to be preliminary thermal testing. This secondary preliminary thermal testing took place during the development of the more complex thermal pipe model. The second model was required to simulate the thermal behaviour of the copper pipe wall during water flow and determine if a more complex model was able to account for the discrepancy observed during preliminary thermal testing.

3.4 Thermal Pipe Model

A more complex thermal model was developed to simulate the transient heat transfer from the flowing hot water contained within the outlet pipe, through the copper pipe wall, to the external surface of the pipe where the temperature sensors are mounted. The measured results of preliminary testing showed a time delay between when events occurred and when a change of temperature was detected. It was suspected the time delay was caused by an unaccounted thermal inertia of the copper pipe or as a result of sensor problems. Thermal behaviour of a sensor is difficult to measure and evaluate. The thermal pipe model was therefore derived to determine the cause of the thermal anomalies noted in the preliminary tests. If it was determined a more complex model could be used to simulate the system in a way that corresponded with the noted thermal delay then this means that thermal methods can be used to estimate water velocity in an EWH. If it was determined that the copper pipe does indeed behave ideally, as assumed in the steady-state thermal difference equation, then the error must be due to the inability of inexpensive temperature sensors to measure pipe temperatures adequately and this means that thermal methods are impractical to use to estimate water velocity in an EWH.

Thermal and fluid kinematic models are often very complex. It is not uncommon for models of this nature to require super-computers to enable simulation. The thermal pipe model was designed to use fewer assumptions than the steady-state thermal model but still be simple enough to execute without a super-computer.

3.5 Continuous Thermal Pipe Model

The governing thermal equations were derived from first principles to create the continuous thermal pipe model. A continuous model was first derived before the complex task of semi-discretising the model as described in Section 3.6.

The continuous thermal pipe model was derived from first principles and used to describe the temperatures at points through the lateral or radial section of a pipe wall. The internal copper points were assumed to adhere to a two-dimensional conduction equation. Where the copper material interfaces with other materials (e.g. water or air) then other thermal equations are required to describe the thermal flux which occurs at these points. boundary conditions are required to equate the differing thermal behaviours between different materials at an interface. Boundary conditions are required for any isolated system to account for energy transfer through the section to be simulated and the interaction with the conditions outside the isolated system.

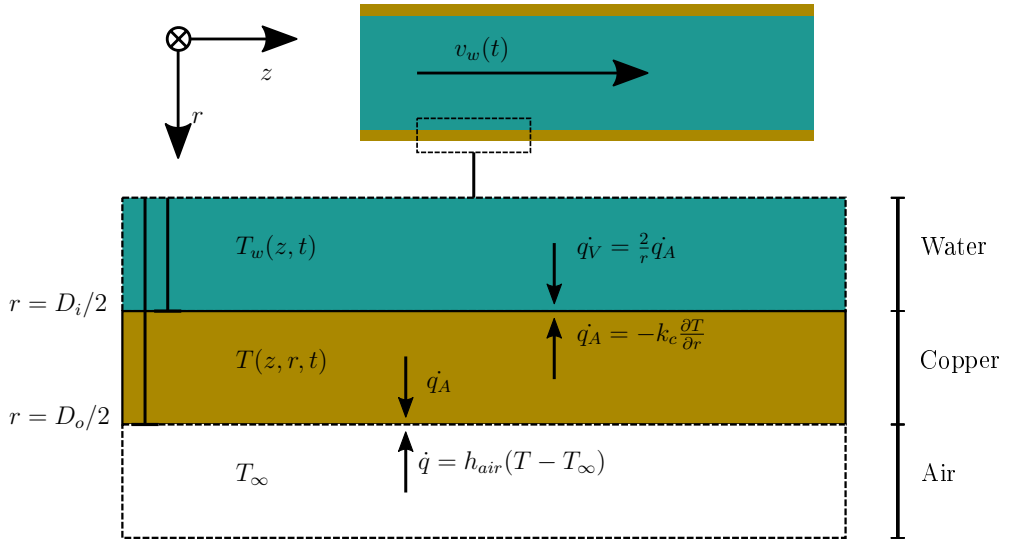

Figure 3.1: Continuous thermal pipe model diagram. It can be seen that the model describes the copper which forms the pipe wall (shown in the magnified section of the pipe wall to illustrate the energy transfers which occur). The inner and outer pipe diameters, D_i and D_o, show interfaces between materials. The heat flux, $\dot{q}$, which occurs at each interface is shown as well as the temperature, T, of each material.

Figure 3.1 shows the notation used for the continuous thermal pipe model. It can be seen that the governing equations to describe the spatially continuous temperature can be represented separately for each material (water, copper and air).

3.5.1 Copper

The copper pipe was modelled as having a wall thickness of 1 mm and length of 1 m (minimum expected length of copper pipe in installations). The copper was assumed to only conduct heat for internal points for the normal case. This assumption is generally considered a valid because the copper is a solid.

The general heat conduction equation (which described the thermal behaviour of the copper for no external energy input) was derived

$$\frac{\partial T}{\partial t} = \alpha \nabla^2 T, \qquad \alpha = \frac{k_c}{\rho_c c_{pc}} \tag{3.3}$$

where α, k_c, ρ_c and c_{pc} are the thermal diffusivity, thermal conductivity, density and specific heat capacity of copper respectively. Equation (3.3) can be expanded to cylindrical coordinates in two-dimensions to more specifically describe the outlet pipe geometry to form Equation (3.4).

$$\frac{\partial T}{\partial t} = \alpha \frac{\partial^2 T}{\partial z^2} + \alpha \frac{1}{r}\frac{\partial}{\partial r}\left(r\frac{\partial T}{\partial r}\right) \tag{3.4}$$

Equation (3.4) can be simplified because the curvature of the pipe changes insignificantly over the width of the pipe. This simplification was to facilitate computational efficiency in later stages. The computationally inexpensive form of Equation (3.4) is:

$$\frac{\partial T}{\partial t} = \alpha \frac{\partial^2 T}{\partial z^2} + \alpha \frac{\partial^2 T}{\partial r^2} \tag{3.5}$$

Equation (3.5) forms the continuous equation which describes all internal (copper) points of the thermal pipe model. The section of pipe which is being modelled is not infinitely large, and pipe section interacts with external conditions which have different thermal properties. Where the outermost copper pipe points interface with external conditions (e.g. ambient air, or water interfaces) then energy exchanges with the external points occur which do not strictly follow the thermal behaviour dictated by Equation (3.5). Boundary conditions must be established at these interfacing surfaces to describe the energy exchanges which occur.

3.5.2 Boundary Conditions

Boundary conditions are necessary to account for the physical exchanges which occur between the interior points (which are described by Equation (3.5)) and the surrounding environment (which are not described by (3.5)). Boundary conditions enable a section of a system to be simulated without having to simulate the entire system.

3.5.2.1 Inner Pipe Boundary

The hot water interfaces with the internal copper wall on the inner pipe boundary. Several assumptions were made regarding the simulated behaviour of the water. This was done to avoid the complexities associated with the simulation of turbulent fluids which is required to simulate the heat of a moving fluid. The water is simulated as a one-dimensional convection equation with heat flux into the internal wall of the copper pipe wall. The water assumptions are:

- Constant radial temperature ($T_w(z, r, t) = T_w(z, t)$)
- Incompressibility ($v_w(z, t) = v_w(t)$, ρ_w and c_{pw} constant)
- Sufficient and constant turbulence for considered velocities (fully developed turbulent flow)

The continuous form of the energy balance in the water medium is shown in Equation (3.6) where v is the velocity of water and ρ_w, c_{pw} are the density and specific heat capacity of water respectively. The volumetric heat flux out of the water (into the internal pipe wall), $\dot{q_V}$, must be equal to the radial conduction into the copper pipe wall to avoid energy accumulation at the interface.

$$\rho_w c_{pw} \frac{\partial T_w}{\partial t} = -v \rho_w c_{pw} \frac{\partial T_w}{\partial z} - \dot{q_V} \tag{3.6}$$

Performing an energy balance equating the volumetric heat flux $\dot{q_V}$ (from Equation (3.6)) to the surface heat flux $\dot{q_A}$ allows for a conversion between the different measures of heat flux.

$$\begin{aligned} \dot{q_V}\,\mathrm{d}z\,\pi r^2 &= \dot{q_A}\,\mathrm{d}z\,2\pi r \\ \therefore \dot{q_V} &= \frac{2}{r}\dot{q_A} \end{aligned} \tag{3.7}$$

Equation (3.7) shows the relationship between volume and surface heat flux where dz is the longitudinal differential element. Equation (3.6) can be rewritten using Equation (3.7) to represent the water convection equation with surface heat flux energy input:

$$\begin{aligned} \rho_w c_{pw}\frac{\partial T_w}{\partial t} &= -v\rho_w c_{pw}\frac{\partial T_w}{\partial z} - \frac{2}{r}\dot{q_A} \\ \therefore \frac{\partial T_w}{\partial t} &= -v\frac{\partial T_w}{\partial z} - \frac{1}{\rho_w c_{pw}}\frac{2}{r}\dot{q_A} \end{aligned} \tag{3.8}$$

The heat flux occurring at the water-copper interface must be equal to avoid energy accumulation at the interface. The surface heat flux between the water at the interface must be equal to the conduction heat flux between the interface and the internal copper wall. Thus the water surface heat flux, $\dot{q_A}$, can be equated to copper thermal conduction as they must be equal.

$$\dot{q_A} = -k_c\frac{\partial T}{\partial r} \tag{3.9}$$

Equation (3.9) shows the heat flux which occurs at the copper-water interface, where k_c is the thermal conductivity of copper. Equation (3.8) can be rewritten using Equation (3.9) into a convenient form to implement boundary conditions.

$$\begin{aligned} \frac{\partial T_w}{\partial t} &= -v\frac{\partial T_w}{\partial z} - \frac{1}{\rho_w c_{pw}}\frac{2}{r}(-k_c\frac{\partial T}{\partial r}) \\ &= -v\frac{\partial T_w}{\partial z} + \frac{1}{\rho_w c_{pw}}\frac{2}{r}k_c\frac{\partial T}{\partial r} \end{aligned} \tag{3.10}$$

Equation (3.10) was used to equate the one-dimensional water convection to the internal copper points at the water-copper interface because the temperatures and flux at any interface must be equal.

3.5.2.2 Outer Pipe Boundary

The outer pipe boundary is generally exposed to air, but several conditions can occur which need to be described by specific equations. The options for outer boundary conditions are commonly air convection, insulated, heat source or heat sink. The general convection equation is given by Equation (3.11) where $\dot{q}$ is the heat flux, h is the heat transfer coefficient and T_∞ the temperature of ambient air:

$$\dot{q} = h(T - T_\infty) \tag{3.11}$$

All outer boundary conditions must occur at the air interface with conductive copper surface, therefore each scenario must somehow be equivalent to the temperature and heat flux at the conductive copper interface. An approximation can be made to represent all outer boundary conditions using the convection equation by changing the heat transfer coefficient in the general convection Equation (3.11) to the relevant coefficient for different media for certain sections of pipe (i.e. h_{air}, $h_{heatsink}$). This approximation is not precise, but the simulation of convection of fluids is complex enough to justify making such a broad assumption which allows the behaviour of turbulent fluids to be avoided. This simplification to a single convective case allows the heat flux due to conduction in the copper at the interface to be equated to the heat flux due to convection in the air at the interface. It also enables for different lengths of the pipe to have different convective interfaces applied.

The convection equation in air is the most common condition for the system, and shown in Equation (3.12).

$$\dot{q} = h_{air}(T - T_{\infty}) \tag{3.12}$$

The heat flux occurring in the copper at the copper-air interface is shown in Equation (3.13).

$$-k_c \frac{\partial T}{\partial r} = \dot{q} \tag{3.13}$$

To avoid energy accumulation at the interface both heat flux values must again be equal. The heat flux found in equations (3.12) and (3.13) must be equal.

$$\dot{q} = -k_c \frac{\partial T}{\partial r} = h_{air}(T - T_{\infty}) \tag{3.14}$$

Equation (3.14) accounts for the external copper wall-air interface.

3.5.2.3 Fixed Temperature

When points on an interface are assumed to be maintained at a fixed temperature (e.g. if a control system is in place to achieve this using a heating element and sensor) then these points are no longer represented as variables in the system. The specific points are instead replaced with a constant temperature value and treated accordingly. This fixed temperature condition was useful to simulate the pipe boundary nearest the EWH when the EWH was assumed to be at a fixed temperature (because always-on setpoint control was implemented).

3.6 Semi-Discrete Thermal Pipe Model

In order for the physics based continuous thermal pipe model described in Section 3.5 to be coded for simulation, the continuous model was required to be be partially discretised. It was chosen to perform spatial discretisation on the thermal model using the Finite Difference Method (FDM). The time derivative thus remained continuous but the spatial derivative is discretised into two dimensions (z and r). This provides the benefit that

the system can be separated into a finite number of discrete spatial points which can be simulated. Each discrete spatial point has an Ordinary Differential Equation (ODE) which describes the thermal behaviour of the point. Reshaping the two-dimensional spatial system of ODEs into a column vector enables the use of a numerical integrator to solve the system. Existing ODE solvers can be used because the model still has a continuous time derivative because FDM was used to discretise the spatial component of the thermal model.

3.6.1 '*j*,*i*' Notation

The nature of the semi-discrete pipe model means that clear notation is important to be able to interpret the simulation data which must be displayed in two dimensions (z and r axis), but for computational efficiency the data must be restructured into a one-dimensional system and computed in time.

The notation denotes coordinates the longitudinal z direction using i and the radial r direction using j. Each coordinate point is the temperature, T, at the spatially discretised location. A section of the system can be represented by a grid of N longitudinal and M radial discrete coordinate locations.

A basic illustration of i in [0;N-1], j in [0,M-1] for N =4, M =3 section is shown in Figure 3.2 and then as a matrix in (3.15) to show the coordinate notation.

Figure 3.2 shows where the internal temperature points are physically located in the system. The illustration should show that the copper points which form the pipe wall are the only internal points.

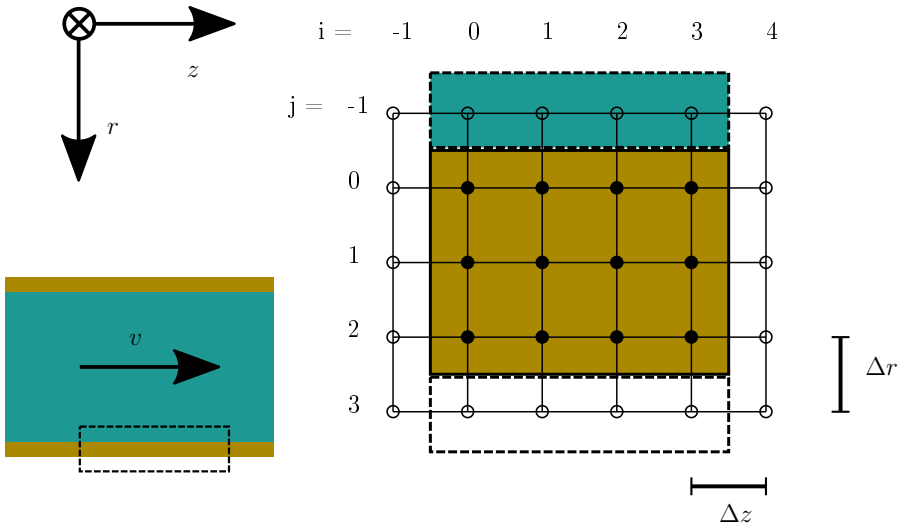

Figure 3.2: Semi-Discretised thermal pipe model diagram. The internal copper points are shown as black dots which correspond to the temperature, $T_{j,i}$ shown in the matrix below. The external, boundary condition points are shown as empty dots and correspond to the grey $T_{j,i}$ points.

In Figure 3.2 the internal copper points are clearly shown as black dots and are the only points which are simulated. The surrounding points are the external points, and the equations describing these points are used to determine the boundary condition equations for the outer internal points (to account for behaviour that occurs at the interfaces).

Using the notation of $T_{j,i}$ to represent the temperature at discrete spatial points:

$$\begin{bmatrix} T_{-1,-1} & T_{-1,0} & T_{-1,1} & T_{-1,2} & T_{-1,3} & T_{-1,4} \\ T_{0,-1} & \begin{bmatrix} T_{0,0} & T_{0,1} & T_{0,2} & T_{0,3} \\ T_{1,0} & T_{1,1} & T_{1,2} & T_{1,3} \\ T_{2,0} & T_{2,1} & T_{2,2} & T_{2,3} \end{bmatrix} & & & & T_{0,4} \\ T_{1,-1} & & & & & T_{1,4} \\ T_{2,-1} & & & & & T_{2,4} \\ T_{3,-1} & T_{3,0} & T_{3,1} & T_{3,2} & T_{3,3} & T_{3,4} \end{bmatrix} \tag{3.15}$$

The matrix representation in (3.15) shows the indexing which was used. The black inner T points form the internal copper points as in Figure 3.2 and describe the temperature of each point. The surrounding grey T points for the surrounding external points. This illustrates how the internal points for a 3×4 example interact with the external points to show general boundary conditions.

3.6.2 Copper Internal Points

The continuous form of the conduction equation that describes the internal copper wall was described in Equation (3.5). The continuous equation must be discretised to be useful in a simulation. A possible way to discretise the equation is using the second order central difference method (CDM) which has the general form shown in Equation (3.16)

$$\frac{\partial^2 f(x)}{\partial x^2} \approx= \frac{[f(x+h) - 2f(x) + f(x-h)]}{h^2} \tag{3.16}$$

The second order CDM was used to spatially discretise the continuous internal copper energy balance, Equation (3.5), to form Equation (3.17).

$$\frac{\partial T_{j,i,t}}{\partial t} \approx \alpha \frac{[T_{j,i+1,t} - 2T_{j,i,t} + T_{j,i-1,t}]}{\Delta z^2} + \alpha \frac{[T_{j+1,i,t} - 2T_{j,i,t} + T_{j-1,i,t}]}{\Delta r^2} \tag{3.17}$$

Applying the CDM to the continuous form of the internal points equation produces Equation (3.17) which is spatially discretised. For clarity the continuous time term, t, is excluded in the rest of the derivations. The system is continuous in time and spatially discretised.

$$\frac{\partial T_{j,i}}{\partial t} = \alpha \frac{[T_{j,i+1} - 2T_{j,i} + T_{j,i-1}]}{\Delta z^2} + \alpha \frac{[T_{j+1,i} - 2T_{j,i} + T_{j-1,i}]}{\Delta r^2} \tag{3.18}$$

Equation (3.18) is the semi-discretised representation of the temperature of the internal copper points which was used to simulate all the internal points of the simulated section.

3.6.3 Boundary Conditions

The boundary conditions in the semi-discrete system occur where the internal points meet the external points. Using the j,i notation the boundary conditions must be applied to the points where $i \in [0, N-1]$ and $j \in [0, M-1]$. The equation describing the temperature at these specific points must be altered from the general state (Equation (3.18)) to replace points which are not contained in the internal points.

The invalid coordinate points are replaced with values corresponding to the surrounding boundary condition. This is how the thermal boundary conditions are included in a single two-dimensional matrix which is used in the simulation.

3.6.3.1 Water Interface Boundary (j =0)

The water interfaces with the internal pipe wall, which is thus the first internal copper point in the radial direction. This means that these internal copper points at j =0 interface with the water which is modelled as external points which exist at j =-1.

The continuous water convection is described by Equation (3.10) and can be spatially discretised to form:

$$\frac{\partial T_{w(j,i)}}{\partial t} \approx -\frac{v}{\Delta z}[T_{w(j,i)} - T_{w(j,i-1)}] + \frac{1}{\rho_w c_{pw} \Delta r}\frac{2}{r}k_c[T_{w(j+1,i)} - T_{w(j,i)}] \tag{3.19}$$

where $T_{w(j,i)}$ is the water temperature. The assumption that the water has constant radial temperature enables the water to be modelled in one radial dimension and thus T_w exists only where j =-1.

At an interface the temperature and heat flux must be equal to avoid accumulation at an interface. For this reason it can be said that the internal copper points at j =0 ($T_{j=0,i}$) must be equal to the simulated water temperature ($T_{w(j=-1,i)}$) from Equation (3.19).

$$\therefore \frac{\partial T_{w(-1,i)}}{\partial t} = \frac{\partial T_{0,i}}{\partial t} = -\frac{v}{\Delta z}[T_{0,i} - T_{0,i-1}] + \frac{1}{\rho_w c_{pw} \Delta r}\frac{2}{r}k_c[T_{1,i} - T_{0,i}] \tag{3.20}$$

In Equation (3.20) the backwards difference method was used to discretise the z dependant term and the forward difference method was used to discretise the r dependant term rather than using the central difference method. The use of first order differencing in the z-axis is called "upwind differencing" and promotes stability in systems which can experience a "sharp front" [32]. This was required as the water velocity was applied as a step function. This enabled the relevant boundary conditions to be implemented thus removing outer points present in the ODEs which describe internal points without introducing unnecessary tendencies for oscillation [32].

3.6.3.2 Outer pipe boundary (j =M-1)

At the outer radial boundary the pipe can be insulated, exposed to ambient air or have an applied passive heat sink. The assumption was made that all these conditions could be roughly modelled as having a variable convective heat transfer coefficient, h, as present in the general convection equation:

$$\dot{q} = h(T - T_\infty)$$

where the flux, $\dot{q}$, is determined by the heat transfer coefficient, h, for the medium and the difference between the surface temperature and ambient temperature $T - T_\infty$. This allows for heat sinks to be simulated at certain locations only without spatial model stitching. Only the air boundary will be shown.

The final radial internal points (at j =M-1) are copper points, and the temperature and flux at this copper-air interface must be equal. Thus the conductive flux out of the copper must equal the convective flux into the air:

$$-k_c\frac{\partial T}{\partial r} = \dot{q} = h_{air}(T - T_\infty) \tag{3.21}$$

Equation (3.21) shows the continuous form of the boundary condition which is present for the discrete points at $j = M$-1. Using the forward difference method to discretise the conduction term present in Equation (3.21) (to eliminate external points later) yields:

$$\begin{aligned} -k_c\frac{\partial T_{j,i}}{\partial r} \approx -\frac{k_c}{\Delta r}[T_{j+1,i} - T_{j,i}] &= h_{air}(T_{j,i} - T_\infty) \\ \therefore \frac{[T_{j+1,i} - T_{j,i}]}{\Delta r} &= \frac{h_{air}(T_{j,i} - T_\infty)}{-k_c} \\ \therefore [T_{j+1,i} - T_{j,i}] &= \frac{h_{air}\Delta r}{-k_c}(T_{j,i} - T_\infty) \end{aligned} \tag{3.22}$$

Equation (3.22) can be used to eliminate external points on the $j = M$-1 boundary as it is the semi-discrete representation of the boundary condition at the copper-air interface.

3.6.3.3 Fixed Temperature (i =0)

When points are maintained at a fixed temperature, the discretised points are removed from the relevant equations and replaced with a constant temperature. This results in a **b** matrix being present in the final discretised representation of the system of ODEs. The boundary condition present where the pipe exits the geyser was chosen to be set to a fixed temperature. This assumes that the EWH remains at it's setpoint temperature. This means that the EWH is assumed to have a perfect control system to regulate the heating element to maintain the temperature of the water in the EWH cylinder at the set temperature.

3.6.3.4 Zero Flux (i =N-1)

When the system is simulated then it is assumed that the longitudinal length and the conductivity of copper is sufficiently high so that zero heat flux may be assumed in the longitudinal direction at the downstream end of the copper pipe. In the continuous representation this is achieved by setting the convective heat transfer coefficient, h, to zero for the general convection Equation (3.11). This means that no heat flux is assumed to occur over this interface, and that in the spatially discretised system Equation (3.23) is true

$$T_{j,N-1} = T_{j,N} \tag{3.23}$$

3.6.4 Applying Boundary Conditions

The application of the boundary conditions involves the replacement of spatially discretised terms which are not internal points with terms which describe the behaviour at each interface using only internal points. A simple M =3, N =4 example of boundary application can be found in Appendix A.

3.6.5 'l' Notation

Two-dimensional systems of ODEs such as the semi-discretised thermal pipe model are computationally expensive to solve. If the two-dimensional system is 'flattened' in the spatial directions then linear algebra can be used to compute the ODE solutions which is much more computationally efficient. To rearrange the i and j spatial representation into one representative l notation is thus required.

$$l = i + j \times N \tag{3.24}$$

Equation (3.24) shows how the two spatial dimensions (j,i) were flattened into a single spatial dimension (l). An example of this can be seen in matrices shown in (3.25). The two-dimensional (j,i) representation can be seen on the left hand side, and the l representation can be seen on the right hand side prior to being flattened into a vector.

$$\begin{bmatrix} T_{0,0} & T_{0,1} & T_{0,2} & T_{0,3} \\ T_{1,0} & T_{1,1} & T_{1,2} & T_{1,3} \\ T_{2,0} & T_{2,1} & T_{2,2} & T_{2,3} \end{bmatrix} = \begin{bmatrix} T_0 & T_1 & T_2 & T_3 \\ T_4 & T_5 & T_6 & T_7 \\ T_8 & T_9 & T_{10} & T_{11} \end{bmatrix} \tag{3.25}$$

The l notation enables characteristic matrices, **Tz** and **Tr**, to be created which represent the behaviour of the system in the z and r directions respectively. **Tz** and **Tr** are the matrices which are used generate the equations which describe each point in the two-dimensional representation. **Tz** and **Tr** can be combined using the correct Kronicker products to form the **A** matrix which can be used in the one-dimensional representation. The **A** matrix is used to describe the behaviour of the regular internal points of the system. An additional **b** column vector is present when fixed temperature boundary conditions are present to account for the irregular internal points.

3.7 Pipe Model Simulation

The spatially discretised, continuous time representation discussed in Section 3.6 can be simulated when flattened and using l notation. The semi-discrete thermal pipe model contains many simplifying assumptions. Simulation of thermal and fluid sections without the large number of simplifications usually requires a super-computer.

The thermal pipe model simulation was required to be able to operate using a laptop with 8 GB of RAM and an Intel Core i7-4720HQ CPU.

3.7.1 Python Model

The semi-discrete thermal model was implemented in the form of a simulation using Python 3.5. The model was required to allow rapid prototyping so that different conditions could be simulated in a short amount of time. This enables scenarios to be simulated before buying and installing components to a physical system for testing. Rapid prototyping was possible as the model was sufficiently flexible as boundary conditions and thermal constants could easily be altered to match existing data. This is very useful because many of the thermal constants cannot simply be obtained using first principles or lists.

The Python model was written to be object orientated. Selectable physical parameters were provided with instantiation of the object. Boundary conditions were applied using

instance methods, which alter the **Tz**, **Tr** and **b** matrices. The final **Tz** and **Tr** matrices are only used in one calculation but the stored values are manipulated many times when applying the boundary conditions; this behaviour was most efficiently handled by dense matrices. After all the boundary conditions were set then the **A** matrix was computed and converted to a sparse matrix structure. This is because the **A** matrix is present in every ODE solver iteration for each k time-step and computations are thus performed many times. The ODE solver used the flattened ('*1*' notation) dense matrix and returned a dense solution matrix containing simulated temperatures for each spatial point for each designated time step.

The solution matrices are quite memory intensive as the data contained is $M^2 \times N^2 \times k$ floating point temperature values, but due to the sparse linear operations involved in obtaining these values the computations were performed in an acceptable time span (less than a minute in most cases).

The *odeint* solver from *scipy.integrate* was used. *odeint* is a simpler interface for the *scipy.integrate.ode* class which is built on the *lsoda* package from *FORTRAN* [33]. This solver automatically switches between stiff (Backward Differentiation Formulas) and non-stiff (implicit Adams) methods depending on the system of ODEs which are to be solved [34]. The minimum time step is automatically calculated to promote stability, but only desired time instances are returned as the solution [33]. *odeint* was used to solve the initial value problem of systems of first order ODEs. This means that starting temperatures must be provided for all points prior to the start of the simulation.

For long time simulations the effect of the initial conditions becomes negligible as a steady-state solution is obtained. In cases where changing parameters occur (usually the change of fluid velocity to simulate events) then separate models were generated for the different conditions. Temporal model stitching was done to link the simulated data in time. The final conditions of the previous model object were used as the initial conditions of the current model object. A major goal of this functionality was to verify the thermal pipe model. This was attempted by matching measured temperatures for known velocity and internal temperature conditions to the output of the simulation. This theoretically allows boundary conditions to be verified as being accurate to the physical system and for physical constants (e.g. h_{air}) to be verified with measured data.

When the model is determined to be as accurate as can be expected for measured conditions, then simulations of possible scenarios can be performed. Possible applications of these are the addition of heat sinks and heat sources to the systems with the hopes of increasing the measured temperature difference to remove the effects of sensor inaccuracy as much as possible. The simulation was compared against numerical results for simple cases to verify that the implementation was correct. Parameter errors, incorrect boundary condition assumptions or inability to react due to necessary simplifications are not as simple to verify.

3.7.2 Simulation Output

The output of the simulation is the temperature profile of the pipe at different time-points. Extracts at certain time steps of a simulated water flow and cool down case are shown in Figure 3.3.

If certain coordinate points are selected then simulated time series temperatures can be generated which can be compared against measured values.

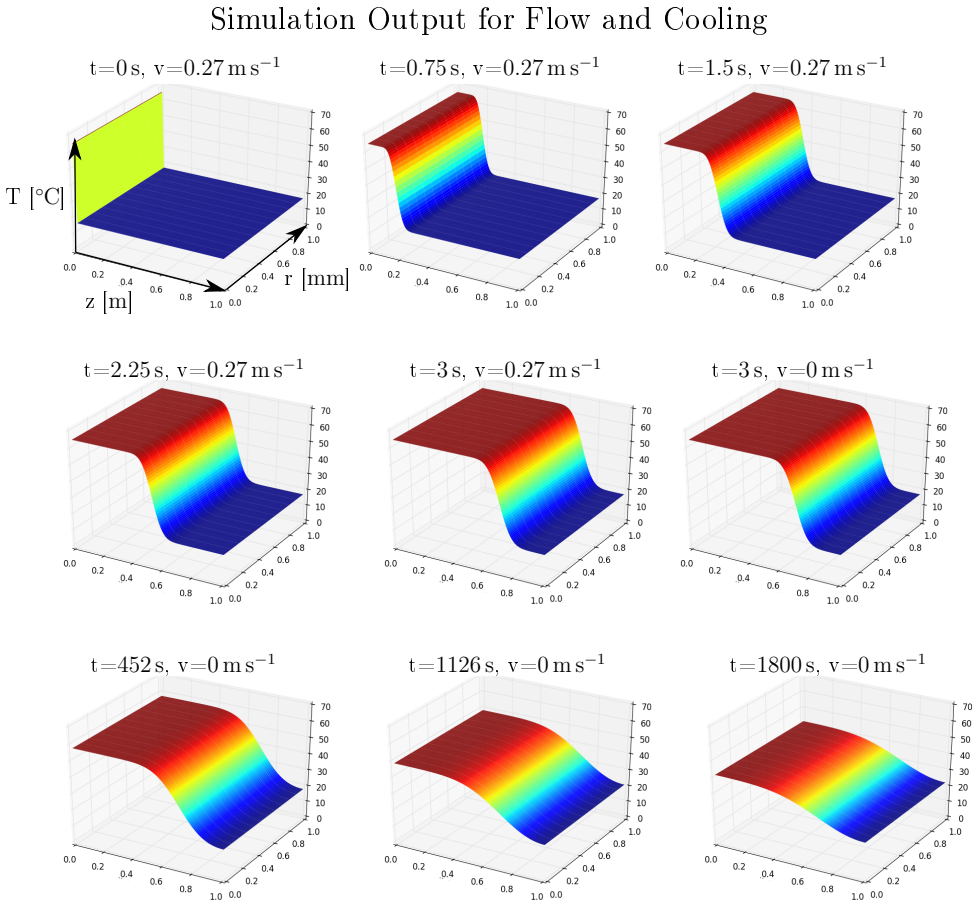

Figure 3.3: The output of the thermal simulation is shown. The top left figure shows the orientation of the z, r and T axes in addition to the starting conditions. The simulation was run with 3 s of water flow (flow velocity of 0.27 m s^{-1} or volumetric flow rate of 4.3 L min^{-1}). Model stitching was then performed to simulate 30 min of cool down time with no flow.

3.7.3 Simulation and Preliminary Thermal Test Results

The simulations performed using the Python model were used to estimate the temperature of the copper pipe. The simulated temperatures were compared to the measured temperatures for the preliminary thermal tests to discern the reason for the unexpected measured thermal behaviour. Observations were made regarding the simulated performance of transit time and steady-state temperature difference to determine fluid flow velocity. The ideal behaviour of the simulation indicated that both were possible and the measured data was analysed to determine if this was the case in practice.

The simulation also indicated that the radial heat flux in the copper pipe wall was approximately instantaneous as can be seen in Figure 3.3, where rapid radial heat transfer was simulated. This was not what the measured data indicated as will be shown.

3.7.3.1 Transit Time

When an outlet valve is opened then water from the EWH flows through the pipe. The valve cannot open instantaneously but the time between fully closed and fully open was kept below 5 s for valve toggles during the preliminary thermal tests. The fluid velocity was simulated as a step function because the rate of change of flow rate was much faster

than the rate of change of temperature. The measured flow rate, start time and stop time of events were obtained from the preliminary thermal tests. These measured flow conditions were used in the simulation.

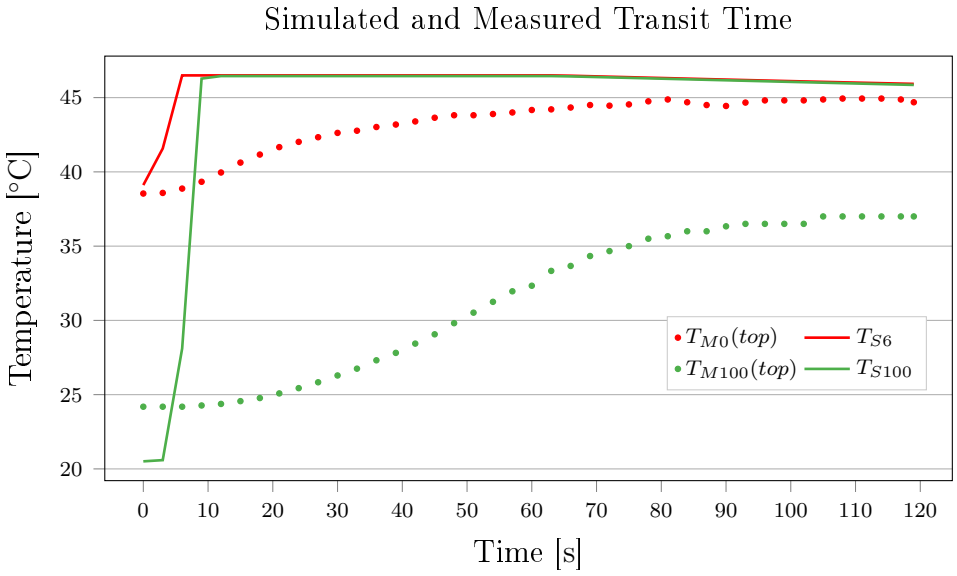

Figure 3.4: Simulated and measured transit time. Water flow occurred for the first 60 s. The subscript M denotes measured values which are shown as points. The subscript S denotes simulated values which are shown as lines. The subscripted numbers indicated the distance from the start of the pipe in cm. The sensors shown were mounted to the top of the outlet pipe. The data was down-sampled to 3 s intervals prior to display for clarity.

Figure 3.4 shows the measured and simulated temperature readings for the start of a measured flow event. The simulation reflects the ideal behaviour of the system. The simulated readings, T_{S6} and T_{S100}, react instantly to water flow and a clear delay between the near and far sensors can be seen because the water flow was modelled as a step function. The upstream temperature sensor, T_{S6}, was required to be simulated at a distance of 6 cm from the start of the pipe to match the steady-state no-flow temperature of the measured sensor, T_{M0}. The simulated radial conduction is very rapid as can be seen by the steep gradients of the simulated temperatures in Figure 3.4 and by the instant radial conduction shown in Figure 3.3. The simulated values indicate that a transit time method can be used because the time delay, distance between sensors and fluid velocity were in perfect proportion when simulated.

The measured results do not behave ideally as can be seen from Figure 3.4. $T_{M0}(top)$ and $T_{M100}(top)$ are sensors which were mounted on the top of the pipe. It can be seen that the measured reading react more slowly to temperature changes than the simulated values. This can be due to unaccounted mixing of colder water in the pipe prior to an event and warmer water from the EWH. But the fluid velocity was too high to result in a delay of more than a few seconds if water mixing was the cause. The measured results do not behave ideally. $T_{M0}(top)$ and $T_{M100}(top)$ do not reach maximum temperatures within 60 s of measured flow as shown by having a constant positive gradient for the duration of measured flow in Figure 3.4. The cause of the measured lag is more likely to do with the unaccounted thermal resistance of the sensor and unknown heat transfer capability between the pipe and sensor.

The sensor casing and electronics must first increase in temperature before the recorded results reflect this. It is not possible to determine how well heat flux can transfer between the pipe and the sensor and this thermal coupling can be another reason for the measured lag.

3.7.3.2 Steady-State Temperature Difference

The measured temperature difference between two points during an event is dependant on the distance between the temperature sensors (because of the area that the convective air losses occur over), the ambient temperature (which affects the rate of heat flux into the air) and the fluid velocity as can be seen from Equation (3.2). The convective air losses can be considered constant for time ranges in the order of several minutes as the ambient temperature can me measured and should not change rapidly.

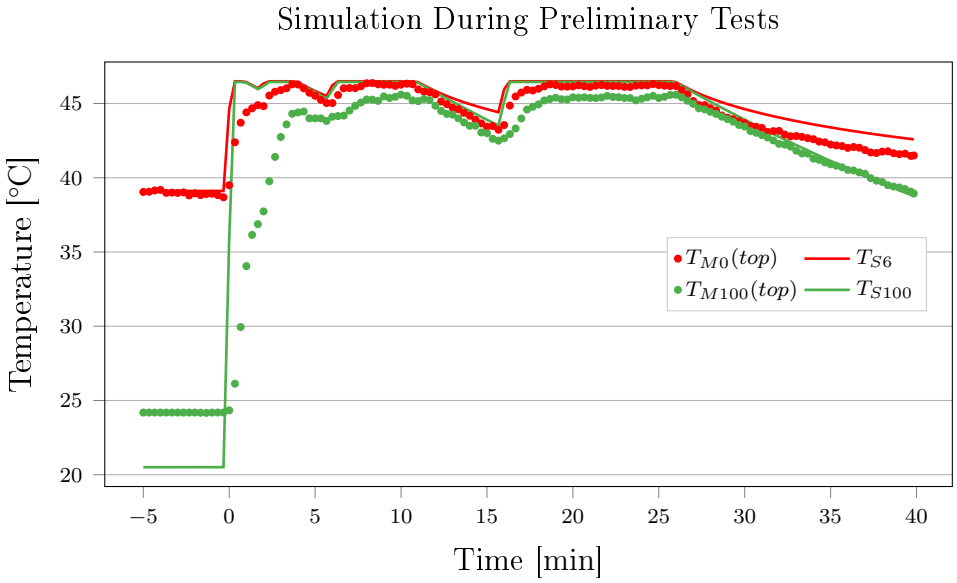

Figure 3.5: Simulated and measured steady-state differences during measured water flow. The subscripts M and S denote measured and simulated values respectively. The subscripted numbers indicated the distance from the start of the pipe in cm. The sensors shown were mounted to the top of the outlet pipe. Values were down-sampled to 20 s intervals prior to display for clarity.

As can be seen in Figure 3.5, the simulated steady-state temperature differences were small (less than 1 °C during simulated flow). Inexpensive temperature sensors cannot provide trustworthy measurements to allow for such small differences to be measured. The measured temperature differences were larger values but were not found to be consistent. The preliminary thermal tests indicated that the steady-state maximum temperature during flow was more dependant on the actual sensor being used than the location of the sensor or the fluid velocity. This can be in Figure 3.6 which shows the measured steady-state temperatures during a long flow event.

In Figure 3.6 the steady-state temperatures during a flow event must decrease as the sensor locations are further downstream as there is not energy input on the pipe. However, $T_{M33}(top)$ recorded the highest temperature even though it is 33 cm from the start of the pipe and should be at a lower temperature than $T_{M0}(top)$ as no energy input occurred. The other sensors seem to follow the correct order in Figure 3.6, but this was not always

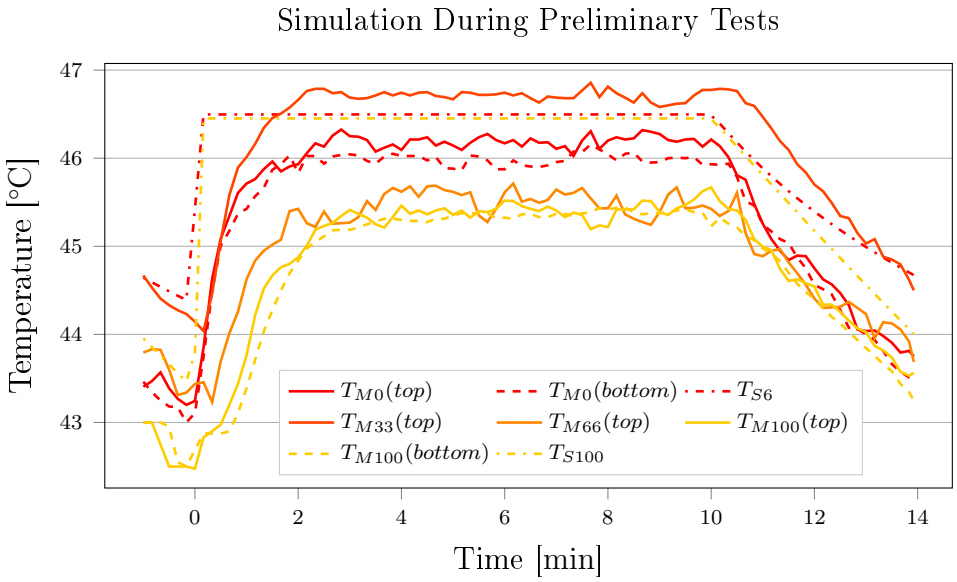

Figure 3.6: Measured and simulated steady-state temperatures for a 10 min flow event during preliminary thermal tests. For the preliminary thermal tests, 6 temperature sensors were mounted on the 1 m long outlet pipe with the distances from the outlet indicated by the subscript number. Upstream sensors are shown in red, and the colour used becomes progressively yellow as the distance from the outlet increases. Top mounted sensors, bottom mounted sensors and simulated values are shown as solid, dashed and dotted/dashed lines respectively. Values were down-sampled to 10 s intervals prior to display for clarity.

found to be the case. The maximum theoretical longitudinal temperature difference, between $T_{M0}(top)$ and $T_{M100}(top)$ can be seen to be less than 1 °C in Figure 3.6. This is a small measurable difference and the sensor variation was observed to be of similar magnitude (to the temperature drop which was intended to be measured) for conditions which should result in consistent behaviour. This is can be seen in Figure 3.7.

Figure 3.7 shows the results of two identical tests spaced 8 hours apart. Consider $T_{M100}(bottom)$ in Figures 3.7a and 3.7b. In Figure 3.7a the measured temperature at the bottom of the end of the pipe section was recorded as being similar to the temperature 33 cm upstream at $T_{M66}(top)$. But in Figure 3.7b it is the lowest temperature. All the temperature sensors can be fluctuate more between readings that the temperature difference between sensors placed at different locations. The large discrete steps seen in $T_{M100}(bottom)$ in Figure 3.7b, during the preliminary thermal tests, were later determined to be the result of electromagnetic interference affecting the temperature sensors when similar problems were experienced during the development of the experimental unit.

It can be seen that the measured longitudinal temperature difference between $T_{M0}(top)$ and $T_{M100}(top)$ in Figure 3.6 is less than 1 °C. It can be seen from Figures 3.7a and 3.7b that the variation for identical flow conditions is not significantly smaller than 1 °C. This means that sensor variation was of similar magnitude than the desired measurement, which is not good when desired for measurements.

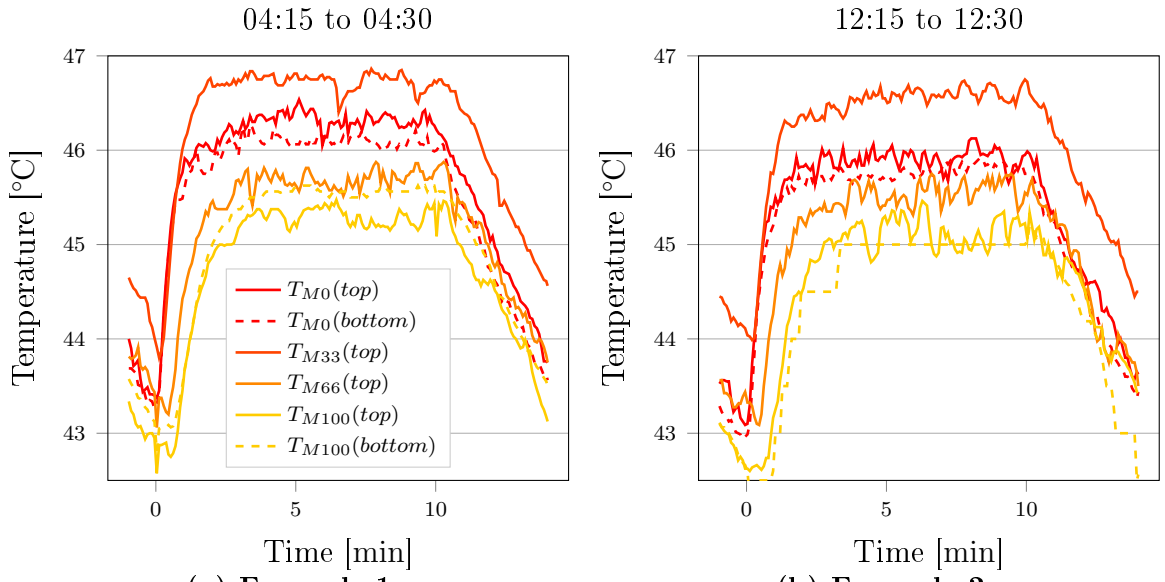

(a) Example 1 **(b) Example 2**

Figure 3.7: Examples 1 and 2 show the measured temperatures for two 10 min flow tests occurring 8 hours apart for the same flow rate. The variation in sensor temperature can be seen to be greater then the different in measured temperature at different points along the pipe.

3.7.3.3 New Usage Events

Instant temperature increases due to hot water flow were simulated but not measured as seen in Figure 3.4 (which shows the first event after several hours of no water flow). This is the case where the greatest temperature increase occurs; from resting ambient to steady-state flow temperature. Figure 3.5 shows the same event but shows the subsequent flows as well. The measured temperatures can be seen to increase when water flow occurs even if the pipe was not at ambient conditions prior to each flow event. This indicates that the start of a hot water usage event can be detected using thermal data. But the sensor lag which was observed in the preliminary tests means thermally determined flow event start times are unlikely to be accurate. If more coarse temporal resolution is acceptable (in the order of minutes) then thermal data seems likely to yield rough flow event detection capability. The slow measured cool down time also means that the end of flow events can only be determined by post-processing data and not in real time.

3.8 Thermal Difficulties

There are several difficulties present with using thermal techniques to estimate the velocity of liquid water in an enclosed pipe at domestic flow rates. Gaseous fluid velocity estimation using thermal measurements is commonly used, but the same technique is very difficult to use on liquid fluids due to the measured variations being much smaller. Domestic water velocity estimation using thermal techniques is a novel thing to do and thus several obstacles must be overcome.

Simulation Coefficient Verification was difficult as certain physical coefficient values are general approximations and have a high uncertainty. For example, the heat transfer coefficient of air, h_{air}, can vary drastically depending on temperature, humidity, external

wind and pressure. These parameters cannot be held constant or incorporated in the model for the sake of feasible complexity. Thus an estimation of the value is the only practical option.

Due to the interconnectedness of several thermal properties, each coefficient cannot be verified individually. For a thermal model, which does not contain simplifications (such as one that can only be executed using a super-computer), each individual parameter could possibly be adjusted using several test conditions to determine the most accurate set of coefficients to give consistent simulations. Even if this is possible it is unlikely to be more convenient than a the installation of an invasive flow meter.

Simulation Instability was encountered due to the dimensions of the pipe wall. The copper pipe wall is only 1 mm thick but is 1 m long. Ideally Δz and Δr should be similar to promote stability. But to achieve this N would be much larger than M but computation involving matrices with the described dimensions results in unstable ODE solutions. For this reason Δz is much larger than Δr so that N can only be hundreds of times larger than M.

Simulation of Temperature Sensor was not possible for the given application. The sensor has its own thermal behaviour. Simulating the behaviour of sensors is difficult because a sensor is supposed to provide a reference rather than an additional unknown coefficient which cannot be measured. The thermal resistance of the sensor creates additional lag as the temperature casing must change before the reported output temperature reflects the temperature. The thermal resistance of the sensors was specified but the unknown thermal coupling made this value irrelevant.

Physical Constraints Domestic EWH systems have different conditions than industrial applications. Most measurement methods are only applicable to industrial scale implementation.

Thermal Inertia present in the copper pipe and water plug after an event meant that the desired temporal resolution of flow events was not measurable using thermal methods.

The copper pipe and enclosed hot water retain heat well. This thermal inertia is thus the cause of small longitudinal temperature differences being measured in the system. The measurable temperature difference was too small to practically measure using inexpensive sensors and without a complex installation procedure.

Temperature Sensor Errors were observed to be larger than the intended measured temperature. Very precise and accurate temperature sensors are expensive. The thermal coupling between the pipe and the measurement location on the sensor was found to play a large role in the measured error.

3.9 Thermal Modelling Indications

Domestic flow rate estimation in an EWH context was not possible using thermal data in isolation for the preliminary thermal tests. The simulations and measured results showed that the longitudinal temperature difference was too small to be practically measured using relatively inexpensive sensors. The physical mounting configuration of the temperature sensors was found to have a greater effect on the measurable results than the experimental conditions did. The repeatable installation of temperature sensors to provide consistent results was found to be too difficult to be practically implementable. This

means that expensive components and intricate installation would be required to measure the expected temperature differences (which is not beneficial to potential users).

The simulated and measured results both indicated that thermal data can be used to detect the start time of a hot water flow event but the thermal inertia of the system and the observed sensor lag means that this method is likely only useful if coarse temporal flow data is acceptable.

The increased cost of suitable temperature sensors, installation complexity to ensure uniform mounting, and unlikely chance of successful flow rate estimation using thermal data alone meant that quantitative estimation of water flow rate in a domestic EWH was speculated to not be a viable alternative to the current in-line flow meters.

The necessity for a larger temperature difference and more consistent temperature sensor mounting was observed. The indications which were provided by thermal modelling and preliminary thermal results influenced the design of the experimental unit in Chapter 4.

Chapter 4

Experimental Unit Design

In this chapter the design of the experimental unit is detailed. The experimental unit was needed to gather data to design a non-invasive flow estimation algorithm using suitable non-invasive methods. Vibration and thermal methods were selected to be used in a sensor-fusion system to non-invasively detect usage events and estimate water flow rate and consumption. The methods were selected as they were determined to be the most likely to succeed and be more convenient for SGC users. Relatively inexpensive components were thus required for an implementable system as well as an easy installation process. The selection of sensors is discussed as well as the hardware design of the EWH and associated experimental components. The software design of the data acquisition system is described as well as the experiments which formed the experimental Datasets: Datasets 1, 2 and 3 which were used to design and evaluate success of the flow estimation algorithm. The performance metrics to assess the success of the flow estimation algorithm are provided.

4.1 Non-Invasive Methods Selection

Several non-invasive methods were investigated as described in Section 2.5. Thermal and vibration methods were determined to be most likely to succeed for domestic EWH applications (without using components and installations which are more impractical than the current in-line flow meter installation).

From the preliminary thermal tests performed in Chapter 3 it was indicated that thermal methods were not sufficient to estimate domestic EWH flow rates in isolation. The design of a flow estimation system which uses the combination of thermal and vibration methods was investigated. After the non-invasive methods selection was made, preliminary tests were conducted for thermal and vibration methods to assess which research objectives can be achieved using each non-invasive technology. The preliminary thermal tests were discussed in Chapter 3. The observations made during preliminary thermal and vibration tests motivated certain decisions regarding the design of the experimental unit. The experimental unit was designed to simulate domestic installation conditions and provide repeatable testing to generate enough data for controlled conditions to design the vibration and thermal based flow estimation algorithm described in Chapter 5.

4.1.1 Unsuitable Methods

Several non-invasive water flow rate measurement methods exist including ultrasonic, electromagnetic, thermal and vibration methods. For the application of a retrofit solution for domestic EWH application certain methods are not attractive alternatives. The required non-invasive water flow measurement system needs to be a more attractive option than the installation of the current in-line flow meter. This means that the cost of required components must be considered as well as the ease of installation.

4.1.1.1 Ultrasonic

For domestic EWH conditions a 22 mm nominal diameter copper pipe is expected to be used in plumbing. Ultrasonic flow rate meters can use transit time, doppler shift or cross correlation methods as discussed in Section 2.5.

Transit time USFMs require at least two ultrasonic transducers to operate. For the pipe diameter used in domestic installations this means that 2 MHz transducers are required [23]. The components costs of the transducers is greater than the current invasive in-line flow meter installation. Transit time USFM methods are thus not suited.

Doppler shift USFMs require dissolved solids or gases of at least 30 micron in size and 25 parts per million in concentration to be present in a fluid to operate [14]. South African municipal water is thus too clean if the water supply regulations in [10] regarding drinking water are adhered to. Doppler shift USFMs can be used when bubbles are present in the flow, but the requirement of vacuum breakers for EWH installations means that no bubbles are present in the pipes. Doppler shift USFM methods are thus not suited.

Cross-correlation USFMs require four transducers to operate. The components cost is at least double that of transit time USFM technology and is too expensive. Cross-correlation USFM methods are thus not suited.

4.1.1.2 Electromagnetic

Electromagnetic non-invasive flow measurement is useful for fluid with complex flow patterns and unknown velocity profiles when invasive measurement is not an alternative [29]. It is possible to measure the velocity of fluids with low electrical conductivity, such as water, using the transverse field electromagnetic method [29]. An electrically insulated pipe interior is required for electromagnetic non-invasive methods to be implementable [29, 30].

Non-invasive measurement of water velocity for retrofit domestic EWH applications is not possible. EWH units generally have copper piping which is electrically conductive. To use electromagnetic methods would thus require the replacement of a section of pipe with an electrically insulated material. The installation process thus requires the same invasive, expensive and inconvenient non-trivial plumbing which an in-line flow meter requires.

Non-invasive electromagnetic water measurement is not a practical method to use for a retrofit water flow measurement system for EWH applications.

4.1.2 Selected Methods

Thermal methods and vibration methods were selected to be used in a sensor fusion based system. The combination of thermal data and the flow rate estimation provided

using accelerometer standard deviation vibration methods (as discussed in Section 2.5.3.1) was determined to be the best system to design a flow estimation algorithm using. The component costs are low as both accelerometers and temperature sensors can be purchased in relatively low cost Microelectromechanical systems (MEMS) sensors. The performance of low cost MEMS sensors is sufficient for the purposed of the designed flow estimation algorithm. The installation process should be simple and convenient for users.

4.1.2.1 Thermal Methods

In theory, thermal methods should be able to provide quantitative flow rate estimation. In Chapter 3 it was shown that thermal methods could not be used for quantitative flow rate estimation during preliminary tests. The temperature difference was seen to be too small and consistent sensor mounting was seen to be problematic meaning that quantitative domestic flow rate estimation using thermal methods was unlikely to be a more practical alternative to an in-line flow meter.

Preliminary thermal tests were conducted as described in 3.3 and the observations indicated that quantitative flow rate estimation using thermal data alone is not possible for an EWH application. Water flowing at domestic flow rates has a temperature drop over a length of copper pipe, ΔT, which is too small to accurately measure using low cost non-invasive temperature sensors. The physical coupling of the sensors was observed to be difficult to do consistently which means that temperature data cannot be as accurate as the listed sensor accuracy. Quantitative flow rate estimation was not possible using the thermal methods investigated in the preliminary testing. It is possible to create a larger ΔT than was present in the preliminary thermal tests by installing a heat sink onto the copper pipe between the upstream and downstream temperature sensors. This increases the heat transfer coefficient from one associated with ambient air, h_{air}, to a higher $h_{heatsink}$ value. This means that greater temperature losses are experienced when water flows in the pipe. The energy losses can be considered to be negligible for users if implemented as a heat sink will only create more losses during water consumption and will not increase standing losses. For experimental purposes, the use of heat sinks results in an exaggerated thermal loss which means a larger measurable temperature difference. Four aluminium finned heat sinks were milled to have a mounting surface with a 22 mm radius to ensure maximum heat transfer from the pipe to the heat sink and the air. The heat sink essentially creates a larger surface area which convective heat transfer can take place into the air.

An EWH contains a volume of water which is maintained at a set temperature that is significantly higher than the ambient air temperature. The copper outlet pipe of an EWH transfers heat energy into the ambient air at all times and thus cools down to an steady-state no-flow temperature when no hot water flow occurs. The temperature of the outlet pipe during times of hot water flow is significantly higher than during times of no hot water flow. The thermal inertia of the water and copper pipe means that the outlet pipe stays hot after an event has stopped. This means that thermal methods are unsuited to generate temporal data relating to estimated water flows. Thermal data can be used to determine whether a hot water usage event has occurred which means that thermal data can be used for event classification. The only scenario that can lead to a rapid increase of outlet pipe temperature is when hot water from the EWH passes through the outlet pipe during a water usage event. The assumptions made are that the water in the reservoir is near the set point temperature. The duration of consecutive events must be short enough

that the flowing water is still sufficiently hot and events must have enough time between events that the outlet pipe can sufficiently cool down to enable a measurable temperature difference at the start of a new event.

4.1.2.2 Vibration Methods

Preliminary vibration tests were conducted on a 150 L EWH installed in a 4th floor test location. Vibration data was gathered using a LSM303 3-axis MEMS accelerometer mounted to the centre of the EWH outlet pipe. An Arduino was used to sample the LSM303 accelerometer during preliminary vibration tests. Only one accelerometer axis data was recorded to achieve the highest possible sample rate and provide opportunity for frequency spectrum analysis over a larger frequency range.

The preliminary vibration tests were performed with flow rates ranging between $2\,\mathrm{L\,min^{-1}}$ and $5.5\,\mathrm{L\,min^{-1}}$ due to the low pressure associated with the test location. Frequency domain analysis showed an amplitude peak present at an essentially constant frequency during flow events. The frequency shift method was too small to use to determine differences between flow rates. The standard deviation of accelerometer data, as used in [13], was also analysed. The standard deviation information showed that the presence of absence of flow could definitely be detected using vibration data captured using a mounted accelerometer. The quadratic relationship between standard deviation amplitude and fluid velocity described in [13] was not observed. Industrial fluid systems typically have larger diameter pipes and higher fluid velocities. The fluid velocity of turbulent liquids creates radial pressure fluctuations which result in proportional radial pipe acceleration which can be measured. For low flow rate domestic applications even if the fluid is sufficiently turbulent (due to smaller pipe diameters), the longitudinal water velocity is lower and the expected pipe acceleration is thus lower. Greater pressure fluctuations (associated with higher flow velocities) would move the constant mass of a section of pipe more, resulting in larger displacements and greater accelerations. After the preliminary vibration tests were performed, it was speculated that qualitative categorisation of EWH flow rates into broad categories was possible (i.e. off, low, medium, high) but that further testing was required to determine whether quantitative flow estimation was possible using vibration methods.

4.2 Experimental Unit Sensor Selection

A Raspberry Pi 3 was used to sample the relevant sensors and to control the experimental unit. The Raspberry Pi (RPi) is a powerful device to use to sample sensors and is impractical to use in real-world applications. Using a RPi and designing the software in Python provided development speed which justified the use of an RPi in the experimental unit. The RPi has Inter-Integrated Circuit (I^2C) communications and enough General Purpose Input/Ouput (GPIO) pins to communicate with all the sensors and components. The RPi is powerful enough and has sufficient memory to enable on-board data storage without negatively affecting data sampling.

TMP275 digital temperature sensors from Texas Instruments were selected. TMP275 has a guaranteed factory accuracy of 1 °C without calibration, linear operation, selectable resolution of up to 0.0625 °C, I^2C communication and a maximum sampling rate of $\approx$ 3 Hz [35]. The listed accuracy and resolution of the sensors in addition to the I^2C communication made the TMP275 an attractive option.

The same LSM303 MEMS accelerometer which was used during preliminary vibration testing was used for the experimental unit. The sensor was present on an Pololu MinIMU-9 v2 breakout board. Adafruit provides a Python module which means that the set-up of the accelerometer in software was convenient. The LSM303 accelerometer communicates using I^2C and can be set to sample up to 1.334 kHz [36].

An in-line flow rate meter was required to be installed in the test system to provide measured flow rate information. The conventional 0.5 L resolution positive displacement flow meter was installed to produce the same coarse flow resolution data as an existing SGC unit. Additionally, a fine flow meter was selected with higher flow rate resolution and thus be more useful in a system with 1 Hz sampling rate. An in-line flow meter with volumetric resolution of 380 pulses/L was acquired. Both flow meters communicate using GPIO pulses.

4.3 Hardware Design

The hardware considerations for the experimental unit were to mimic user conditions closely but additionally facilitate repeatable control tests to generate a dataset, Dataset 1, which was used to develop the flow estimation algorithm. Additional tests were performed using the experimental unit to test other factors of operation to generate Datasets 2 and 3.

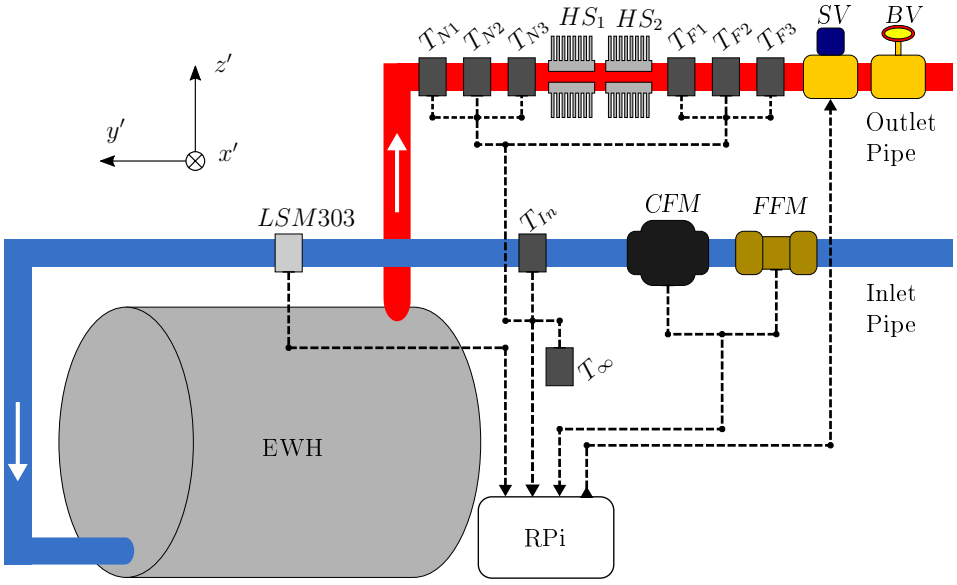

Figure 4.1: Diagram showing the experimental unit.

A diagram of the experimental unit is shown in Figure 4.1. The experimental unit was set up in a steam room on the ground floor of the Electrical and Electronic (E&E) Engineering Building at Stellenbosch University. 600 kPa Municipal water supply was available using plumbing fixtures which passed through an outside wall. The hot water outlet passed through the exterior wall before entering the drainage system. This meant that the ambient air temperature remained as close to real world conditions as possible as the hot water left the outlet pipe sufficiently far away from the EWH location.

The steam room was located next to the E&E Workshop which contains heavy machinery. Large vibrations were measured which did not correspond to water flow or experimental

unit adjustments, which indicated that the vibrations from the heavy machinery were measured by the system. A large air compressor was located very close to the EWH installation and this was suspected to be the cause of the vibration anomalies.

Photographs of the installation can be found in Section B.1.

4.3.1 Electric Water Heater

The EWH was required to be large enough to allow for extended duration usage events. A 150 L Heat Tech Geysers T150 EWH was selected. The T150 has a 3 kW heating element. The EWH setpoint temperature was set to 65 °C to maximise any thermal observations which can be made.

Municipal level water pressure, 600 kPa, was required to simulate domestic flow rates and also be able to reach greater flow rates than are typically recorded to test the system. For this reason the EWH was installed in the steam room on the ground floor to maximise the available water pressure in a safe environment. 22 mm nominal diameter copper piping was used for the cold water inlet pipe (to connect the EWH to the municipal water supply) as well as for the hot water outlet pipe. The copper pipes were arranged so that long straight sections of piping were present. This was done to ensure regions where fully developed flow could reliably be expected to facilitate vibration measurements. The outlet hot water was diverted to the existing water management system in the test location. The required vacuum breakers were installed near the EWH which was possible because the inlet and outlet pipes had to pass through a section in the wall which was higher than the EWH. The EWH was installed horizontally on a sturdy steel mounting table (to facilitate the reuse of the EWH for other experiments in the future). Figures B.1 and B.2 in Section B.1 show photographs of the EWH.

4.3.2 Flow Control

Repeat experimentation at fixed conditions is required to build a dataset which can be used to develop a flow estimation system. Thus repeatable water flow test conditions were needed. Two flow control devices were used to achieve the required flexibility at a lower experimental cost. The flow control components can be seen in Figure B.3 in Section B.1.

Ball Valve

A 22 mm manual ball valve, shown in Figure 4.1 as BV, was installed in-line on the outlet pipe. The ball valve was used to set the flow rate used in experiments. It was usually not adjusted during times of water flow except to test specific scenarios.

Solenoid Valve

A DN20 solenoid valve, shown in Figure 4.1 as SV, was installed in-line on the outlet pipe. The DN20 is operated using 12 V direct current (DC) power which was provided using an AC to DC converter (alternating current to direct current). SV was controlled using the RPi by GPIO outputs to toggle 12 V relays. The DN20 was fully opened and fully closed rather than set to open partially (which can be done to achieve various flow rates). It was found that partial valve opening resulted in a less consistent flow rates being achieved. More expensive solenoid valves may be able to provide more consistent

flow rate control but this was not found to be true for the DN20. It was found that SV required 3.5 s to open or close. Therefore only 7 s of water flow was not at maximum flow rate (while SV was opening at the start of and event and closing at the end of an event).

The combination of the manual ball valve and the electrically operated solenoid valve enabled repeat testing conditions to be achieved at discrete flow rates. When continuous flow rates were required, the solenoid valve was opened fully and the manual ball valve was used to change the flow rate during flow events.

4.3.3 Flow Measurement

The practical application for a non-invasive flow estimation system is to replace the in-line flow meter which is currently used for SGC. Accurate flow measurement to use as a reference was required to design and calibrate the flow estimation system. It was thus chosen to install two in-line flow meters to provide flow measurements using the current coarse measurement method and a more fine measurement method.

Coarse Flow Meter

The coarse flow meter, CFM, is the same 0.5 L resolution in-line flow meter which is used in the SGC. Such a flow meter was obtained and installed in-line with the intention of providing the same data format and coarse flow rate measurement as the SGC system.

The CFM used is only designed to work for flow rates greater than $2\,\mathrm{L\,min^{-1}}$. An additional fine flow rate meter was installed to measure low flow rates and verify the performance of CFM. But the coarse flow meter was damaged during installation and could not be used (illustrating an inconvenience which users may experience with in-line meters).

Fine Flow Meter

A fine in-line flow meter, FFM, was installed and provided the measured volumetric flow rate, $\dot{V}_M$, after the coarse flow meter was observed to be damaged during installation. The fine flow meter gives 380 pulses/L as opposed to the coarse flow meter 2 pulses/L. The higher flow resolution facilitated the higher sampling rate used in the experimental unit acquisition system (discussed further in Section 4.4).

The FFM was intended to use as an additional flow rate measurement device to assess the accuracy of CFM, but CFM was damaged and FFM was used as the reference flow measurement device. The measured volume which FFM reported, V_M, was verified using the volume of water that flowed into a bucket and it was found that the FFM was sufficiently accurate and more importantly the recorded values were consistent meaning that FFM was precise. The finer volumetric resolution of FFM enabled lower flow rates to be measured than the currently implemented SGC system can measure which is ideal for an experimental set up.

4.3.4 Thermal Components

The hardware design relating to the thermal aspects of the experimental unit consist of temperature sensors and heat sinks. Thermal paste with high thermal conductance and negligible electrical conductance was used between the copper pipe and all thermal com-

ponents to ensure maximum heat transfer. Figure B.4 in Section B.1 shows a photograph of the outlet pipe containing temperature sensors and the heat sink installation.

Heat Sinks

Four heat sinks were used in a configuration of two sets which were fixed to the outlet pipe. Each heat sink was milled to have a mounting surface with the same radius as the 22 mm copper pipe. This was done to maximise the contact surface area between the outlet pipe and each heat sink and thus increase the heat flux which can take place at the interface. The heat sinks were used to exaggerate the longitudinal temperature drop, ΔT, which should be measurable during times of steady state water flow. Further details regarding the heat sinks can be found in Section B.1.

Temperature Sensors

Texas Instruments TMP275 digital temperature sensors were selected for use in the experimental unit. TMP275 is listed to have guaranteed 1 °C accuracy without calibration, with typical values listed as ±0.5 °C [35]. The preliminary tests discussed in Section 3.3 showed that this was not true for the sensors mounted on the copper pipe likely due to poor thermal coupling and thermal resistance of the large break-out boards used during preliminary tests.

The sensors communicate using I^2C which is widely used by many devices meaning that I^2C development is quick and reusable. Eight TMP275 sensors can be operated using the same I^2C bus by setting the 3 −bit slave addresses on the TMP275 sensors. The sensors were set to the maximum resolution of 12 −bit which equates to 0.0625 °C [35]. Sweep I^2C sampling of all eight sensors once per second was possible at maximum resolution and power consumption was less important than high resolution data for the experimental unit.

The temperature is measured from the TMP275 ground pin so high thermal conductance was required between the mounting surface and the ground pin. The TMP275 sensors were mounted on Printed Circuit Boards (PCB) which were designed to facilitate heat transfer.

Preliminary thermal tests indicated that the thermal coupling was important for the temperature sensors and the PCBs were designed to facilitate this. The TMP275 PCBs were not manufactured according to design, so 3 mounting configurations were investigated to maximize heat transfer. Mounting configurations:

- Mounting 1: Copper wire soldered to TMP275 ground pin, passing through hole in PCB, brazed directly to copper outlet pipe (Direct connection).
- Mounting 2: Manufactured PCB with additional solder flow between ground plate and TMP275 ground pin (Standard).
- Mounting 3: Copper wire soldered to TMP275 ground pin, passing through hole in PCB, milled 22 mm mounting bracket (Maximum surface area).

Photographs of the TMP275 PCBs and mounting methods in figures B.5a and B.5b respectively, and the TMP275 mounting methods and locations can be seen in Table B.1 in Section B.1.

4.3.5 Accelerometer

The LSM303 accelerometer was used for the experimental unit. The sensor was mounted on the inlet pipe. The accelerometer does not necessarily need to be mounted to the outlet pipe. An EWH is maintained at constant pressure and has a fixed volume therefore all cold water flowing into the EWH inlet can only occur when hot water is flowing out of the EWH outlet at the same flow rate. Several components were mounted to the outlet pipe which would affect the vibration characteristics on the outlet pipe (especially the large heat sinks). The inlet pipe only had the two flow meters and one temperature sensor mounted on it meaning that the copper pipe could vibrate more freely. The LSM303 was fastened using a cable ties and insulation tape was used to prevent short circuits. The sensor was fastened 740 mm upstream from the 90° EWH inlet plumbing connection. This was done to ensure fully developed flow was present at the point of vibration measurement so significantly more than $10\,D_i$ 10 upstream and downstream of uninterrupted flow was present [8].

The LSM303 communicates using I^2C, so sweep sampling of the TMP275 sensors and the LSM303 accelerometer was convenient. The LSM303 was enabled to sample at the maximum rate of 1.344 kHz which consumes more power but ensures that the accelerometer sample rate setting was not the bottleneck for vibration sample rate. The LSM303 is a 3-axis accelerometer which measures the g-force is each axis; $g_{x\prime}$, $g_{y\prime}$ and $g_{z\prime}$. The g-force range was set to $\pm 2\,g$ which was sufficient [36].

4.3.6 Raspberry Pi

A Raspberry Pi 3 was used to sample the sensors and control the water flow experiments. The RPi has sufficient GPIO pins to receive the flow meter data (GPIO pulses sampled using GPIO interrupts) and control the solenoid valve (SV). I^2C communication is also supported to communicate with the accelerometer and temperature sensors. The RPi has 3.3 V V_{CC} lines which are sufficient for the flow meters, accelerometer and temperature sensors. The solenoid valve required 12 V to operate and this was supplied using an external power source in for form of an AC to DC converter. SV toggling was done using 12 V relays which were controlled using the RPi GPIO pins.

A breakout board PCB was designed to conveniently house all the required components and provide more I^2C connection points[1].

A photograph of the RPi and PCB with the I^2C sensor connections can be found in Figure B.6 in Section B.1. The PCB used can be found in Figure B.7.

4.4 Software Design

The software design required sampling of sensors, scheduling of function executions and flow events, and storage of the recorded data. The three aspects are interlinked and are thus difficult to explain in isolation. Experiments were designed and executed (using scheduling) to generate specific, useful data. The data generated during an experiment performed using the experimental unit created a Dataset. The generated Datasets are

[1] Thanks to Lowku Leeuwner who was provided with the design specifications and requirements and created the schematics for PCB production.

discussed further in Section 4.5. Further information relating to sampling, scheduling and storage can be found in Section B.2.

The data sampling and storage script, or "acquisition system", was executed on the RPi. The acquisition system was coded using Python 2.7 to ensure that all the required python packages were compatible. Python packages which were heavily used in the acquisition system were Pandas to store and manipulate local data, APScheduler ('Advanced Python Scheduler') to control when functions were executed, and SQLAlchemy to connect to the MySQL database to store recorded data. A library was available to setup LSM303 accelerometer which reduced the development time.

The acquisition system was used to sample all the sensors, performed the scheduled opening and closing of SV to induce flow events according to a pre-determined schedule and stored the recorded data to a local MySQL database. The data stored in the MySQL databases generated Datasets 1, 2 and 3 which were post-processed as described in Chapter 5 to create and evaluate the non-invasive flow estimation system.

4.4.1 Sampling

The sampling was executed using an APScheduler *scheduler* object which had a *job* to control the execution time of the sampling function (discussed in Section 4.4.2). The sampling can be divided into two sections for clarity: the primary sweep (time, temperatures, flow rate, state of SV) and vibration burst sampling (high frequency sampling of accelerometer data for N samples). The primary sweep was performed at 1 s intervals. Vibration burst sampling generated large amounts of data, therefore vibration priority flags were used to determine how often a burst sample was made. During low priority times, a burst sample was performed once per minute, and during high priority times a burst sample was performed once per second. Both the primary sweep and vibration burst were executed in the same function, but the execution or skipping of the vibration burst was controlled using flags.

4.4.1.1 Primary Sweep

The primary sweep was executed at a sampling frequency of 1 Hz. Once per second the following was executed:

- Store DateTime and Microsecond of current sample
- Store and clear GPIO interrupt incremented *FFM* and *CFM* pulse count values
- Store state of SV to know if water was flowing
- Perform I^2C sweep of 8 temperature sensors, store the integer representation
- If vibration sampling is required: execute vibration burst sampling
- Append the locally stored values of current sample to global 'acquisition' list

The sampled points were stored locally until the completion of the sample and then appended to the global 'acquistion' list storing the samples. GPIO interrupts on the *FFM* and *CFM* pins were enabled and the number of pulses between samples were incremented

using these GPIO interrupt handlers. The primary sweep thus recorded the samples per second value for each flow meter. The integer representation of the temperature values refers to the fact that the raw output of the TMP275 was stored directly. The output must be divided by 16 to obtain the actual temperature (to 0.0625 °C resolution). The raw values were stored as integers and not as floating point numbers to minimize storage requirements because the conversion in post processing is simple.

4.4.1.2 Vibration Burst Sampling

As stated in Section 4.4.1, burst sampling of the LSM303 accelerometer was performed in the same function as the primary sweep but during low priority times then the burst sample was not performed. Vibration sampling was performed as burst sweep of 500 samples and a sampling frequency of ≈ 1 kHz was achieved. The high frequency vibration sampling of the 3 accelerometer axes meant that a large amount of data was generated, much of which was not required for the flow estimation algorithm to function. The minimum number of samples required to produce a useful standard deviation value was unknown until after Dataset 1 was post-processed. The largest number of vibration samples which could be captured and stored each second, without affecting the primary sweep, was found to be 500. During low priority times (when no flow events were scheduled to occur) a vibration burst sample was performed once every minute. During high priority times (i.e. 5 min prior to a scheduled test start until 5 min after the completion of a scheduled test) a vibration burst sample was performed every second. Data size was thus minimized while maintaining high temporal resolution vibration data during times where water flow was known to occur for the initial data acquisition. High resolution vibration data was stored in a separate Pandas DataFrame and a separate MySQL database. The vibration data was immediately inserted into the 'vibration' MySQL database when the burst sample was completed.

The vibration priority sampling was used during the initial development of the system. When the minimum required vibration data format was established (after post-processing Dataset 1) then vibration data was gathered in real time. A high frequency sweep of 250 samples per accelerometer axis was found to be sufficient, and the standard deviation of each 250 sample burst sweep could be stored directly. This means that 1 Hz sampling is possible for the acquisition system without requiring vibration priority control, and that the generated data is not impractically large. Datasets 2 and 3 recorded the required vibration data at 1 Hz.

4.4.2 Scheduling

The scheduling was performed using the APScheduler Python module. An APScheduler *scheduler* object was created, the required *jobs* were added to the *scheduler*. A blocking *scheduler* object was used which ran in the foreground. A *job* makes a call to a function at specific times when *trigger* conditions are met.

APSchduler has 3 types of *triggers* (which are used to execute *jobs*): date, interval and cron. Date is used when the *job* must run only once at a certain time. Interval is used when the *job* must run at fixed time intervals. Cron is used when a *job* must run periodically according to date and time conditions. The following important APScheduler *jobs* were used in the acquisition system:

- Interval triggering was used to execute the primary sweep at 1 Hz for temperature, flow and *SV* state data
- Cron triggering was used to open/close *SV* to control scheduled flow events
- Cron triggering was used to toggle the vibration burst sampling intervals using an internal flag (enabling high resolution vibration sampling only for scheduled flow events)
- Cron triggering was used to write local Pandas DataFrames containing acquired data to the relevant MySQL database once hourly

It was found that certain temperature sensors occasionally reset to the default 9 −bit resolution after *SV* was toggled during scheduled water flow control. This was first observed during the preliminary thermal tests and was shown in Figure 3.7. Shielded 4-conductor wire was used for all I^2C devices in the experimental, unit but further steps were required. To ensure that maximum resolution was maintained during times of flow; the primary sweep *job* was paused after *SV* toggles were completed, the resolution of each TMP275 sensor was confirmed, and the primary sweep was resumed. This ensured that all temperature sensors were set to 12 −bit resolution during flow tests.

The automated control of the *SV* required scheduling to ensure repeatable experiments. The sampling of the data also required scheduling. The vibration priority control was performed using scheduling when relevant. The 1 Hz sample rate of the primary sweep was also controlled using scheduling and interval triggering. Data storage to the 'acquisition' MySQL database was also controlled using an APScheduler *job*.

4.4.3 Storage

A MySQL 5.5 server was hosted locally on the RPi. The Pandas Python module, which was used to store the samples prior to being inserted into the MySQL database, has many convenient features which are available when using the SQLAlchemy SQL toolkit. SQLAlchemy was thus used to connect to the MySQL server and connect the sampled data to a MySQL Database. Two separate MySQL databases were required for the first experimental unit dataset gathered (Dataset 1). The minimum vibration requirements were then determined and subsequent experiments performed vibration sampling at the same frequency as the temperature and flow rate measurements, therefore a single MySQL Database was required to store the 1 Hz data.

4.4.3.1 Acquisition Database

A Pandas DataFrame was created from acquisition samples list containing 1 Hz temperature, flow and valve state information was inserted into the 'acquisition' MySQL database at 50 min of each hour and then cleared locally. This kept the row depth of the Pandas DataFrame to under 3600 samples and MySQL insert operations on the RPi were observed to complete in an acceptable time for this interval.

The acquisition database was used to store all measured values which were sampled at a frequency of 1 Hz. The sensor values contained within each stored sample can be found in Table B.5 in Section B.2.

4.4.3.2 Vibration Database

The burst vibration sweep had a much higher sample rate than the primary sweep and thus a large amount of data was generated each second. The raw vibration data was inserted into a separate database, the 'vibration' MySQL database, after the desired number of burst sampled accelerometer readings were gathered.

The vibration MySQL database contained the accelerometer data which consisted of 500 accelerometer g-force samples per accelerometer axis for each entry (for Dataset 1). Each entry in the vibration MySQL database thus contained a DateTimeIndex value, an integer Microsecond value, and 3 integer g-force readings for x', y' and z' axes. 500 entries were stored for each burst sample. The burst sweep was performed once per second during scheduled flow events and once per minute when no flow events were scheduled to reduce the data size.

The vibration database for Dataset 1 was used to determine the minimum accelerometer samples required to calculate the standard deviation values, σ, which were used in the flow estimation algorithm discussed in Chapter 5. After the minimum vibration requirements were established then the acquisition script was altered to perform real-time vibration sampling. This improvement resulted in two benefits: vibration sampling could be performed in real time, and the amount of vibration data per second was reduced to 3 floating point values. A separate vibration database was therefore not required for any data obtained after Dataset 1 had been processed.

4.5 Dataset Generation Experiments

The experiments performed using experimental unit were done to generate Datasets 1, 2 and 3. Dataset 1 was performed to gather the maximum amount of vibration data to determine the minimum required vibration data which can be used. Dataset 1 was the largest Dataset and was used to design the non-invasive flow rate estimation system. Dataset 2 was then performed to evaluate a larger range of flow rates. Dataset 3 was performed to discover the minimum time between flow events which must occur for the flow estimation system to be successful.

An overview of the purposes of each Dataset generated using the experimental unit is provided in Table 4.1

Dataset	Purpose	Flow Control	Duration
1	Design Flow Estimation Algorithm Repeat Testing Minimum Vibration Sampling Requirements	Scheduled	5 days
2	Test Instantaneous Flow Rates Test Short Duration Events	Manual	1 hour
3	Determine Min Cool Down Time Between Events	Scheduled	1 hour

Table 4.1: Experimental Unit Dataset Summary

4.5.1 Dataset 1

Dataset 1 was generated using experiments which consisting of multiple scheduled flow events using a single flow rate for 24 h. Dataset 1 was used to design the flow estimation algorithm discussed in Chapter 5.

Dataset 1 was generated during 5 days of continuous testing. Each "Test Day" had the same automated flow event scheduling at a fixed unique flow rate (determined using BV). Each Test Day consisted of four "Test Sets" spaced 6 h apart. Each Test Set consisted of three separate flow events: a 2 min flow event starting on the hour, a 2 min flow event starting 5 min after the hour, and a 5 min flow event starting 10 min after the hour.

The repetition of Test Sets at the same flow rate provided sufficient data to design the flow estimation algorithm. The Test Sets were placed 6 h apart to ensure that the EWH system returned to steady-state no-flow thermal conditions between water flow events. This enabled the evaluation of the system to detect new usage events at various flow rates after prolonged times of no use. The short time between flow events within a Test Set was to test the ability of the system to detect consecutive usage events (as may be expected in normal use cases).

The naming convention used to identify scheduled Test Sets was such that each Test Set ID consists of: the Test Day and the Test Set number. This removed the dependence on the calendar date that a test was performed on. E.g. Test Set ID 4.2 denotes the 2^{nd} Test Set (3 scheduled flow events) which occurred on Test Day number 4 (at unique flow rate number 4).

The known times of flow events when using scheduled tests sets meant that the high frequency vibration burst sampling could be enabled 5 min prior to the start of a Test Set and disabled 5 min after the final flow event completed (to reduce the amount of unnecessary vibration data).

Figure B.8 in Section B.2 shows scheduling control used to gather Dataset 1.

4.5.2 Dataset 2

Dataset 2 was generated using half an hour of manually controlled flow events and cool down time. SV was opened at the start of testing and then BV was manually controlled to induce various flow rates and continuous flow rate variation during a flow event. The purpose of generating Dataset 2 was to provide more measured flow rates to test the accuracy of the estimation system.

Dataset 2 was generated using a vibration burst sweep of 250 samples per accelerometer axis. The standard deviation of each accelerometer axis was computed and stored with the primary sweep data as $\sigma_{x'}$, $\sigma_{y'}$ and $\sigma_{z'}$. This reduces the number of vibration data points per second from 1500 integer values to 3 floating point values which made the data acquisition much more practical.

Dataset 2 provided additional flow rates but also tested the possibility of having a half hour on-site calibration. The time between separate flow events was found to be too short, as the flow estimation system could not identify separate flow events and it was determined that additional testing was required.

4.5.3 Dataset 3

Dataset 3 was conducted to establish what the minimum time between flow events was to enable event detection. Flow events were automatically scheduled and controlled using *SV*. Each flow event was 1 min in duration. The no-flow wait-time between flow events increased from a minimum wait-time of 15 s to a maximum wait-time of 3:15 min in 15 s increments. Water was forced to flow before the experiments were performed. This was done to ensure that the outlet pipe was already warm at the start of the experiments.

The minimum wait-time was established using Dataset 3.

4.6 Performance Metrics

A summary of the performance metrics to evaluate whether the objectives stated in Chapter 1 are shown.

Objective 1: Non-invasive Usage Event Detection

The performance metrics to quantitatively evaluate the ability of the designed algorithm to identify and classify usage events using non-invasive methods is shown in Table 4.2

Obj.	Description	Metric
1a)	Vibration event temporal boundaries	Event duration and start time
1b)	Detected vibration event classification	False positives and false negatives
1c)	Low flow identification	Undetected low flow events

Table 4.2: Objective 1 Performance Metrics

Objective 1a) is to be evaluated using the difference in estimated and measured event duration and event start times. Perfect performance would be that the estimated and measured temporal boundaries of usage events are identical.

Objective 1b) is to be evaluated using the number of incorrectly classified events. Perfect performance would be that zero false positive and zero false negative event classifications are made.

Objective 1c) is to be evaluated by the number of events which were quantitatively estimated but should have been flagged as low flow rate events which can only be qualitatively identified.

Objective 2: Non-invasive Flow Estimation

The performance metrics to quantitatively evaluate the ability of the designed algorithm to estimate flow rate and volumetric eater usage using non-invasive methods is shown in Table 4.3.

Objective 2a) is to be evaluated using the percentage error between estimated and measured flow rates for instantaneous flow rates and qualitative evaluation of instantaneous flow tracking. This is to ensure that the system can estimate flow rates which fluctuate during the span of a usage event.

Obj.	Description	Metric
2a)	Instantaneous flow rate estimation accuracy	Percentage error per sample point
2b)	Mean flow rate estimation accuracy	Percentage error per detected event
2c)	Volumetric flow estimation accuracy	Volumetric error per detected event
2d)	Flow estimation restrictions	Minimum flow rate and wait-time

Table 4.3: Objective 2 Performance Metrics

Objective 2b) is to be evaluated using the percentage error between estimated and measured mean flow rates for each usage event. The required flow rate estimation accuracy is 10 % to replace the currently used in-line flow meter.

Objective 2c) is to be evaluated using the volumetric error between estimated and measured usage volumes per event. This is to ensure that large volume usage events, which most heavily contribute to the total water consumption, are accurately estimated. The required volumetric usage estimation accuracy is 10 % to replace the currently used in-line flow meter.

Objective 2d) is to be evaluated by determining the minimum flow rate for quantitative flow estimation and the minimum wait-time between usage events for usage event detection. The quantitative assessment of objective 2d) is the percentage of volumetric usage which could have been estimated using the designed system if it were installed on the 32 anonymous SGC units (Field Dataset).

Chapter 5

Flow Estimation Algorithm

The flow estimation algorithm was predominantly empirically developed due to the complex nature of vibration and thermal relationships. The flow estimation algorithm was designed using the data trends observed in Dataset 1. Research and preliminary testing led to certain vibration and thermal expectations which were first investigated and implemented when applicable.

Basic data processing was required before the raw data, which was acquired using the experimental unit, could be analysed. The flow estimation algorithm consists of non-invasive event detection using vibration and thermal data fusion to detect temporal boundaries of usage events, and non-invasive flow rate estimation using vibration data. The estimated volumetric usage, V_E in L, was estimated as an integral of the estimated volumetric flow rate, $\dot{V}_E$ in $\mathrm{L\,min^{-1}}$, over the detected temporal boundaries. The estimated volumetric usage per event is the parameter which is most important for the SGC system to be able to operate correctly.

The algorithm was found to have two factors which can limit the performance relating to flow rate and the time between events. The minimum flow rate and minimum cool down time between events were investigated.

5.1 Data Processing

The data processing and analysis was performed using a laptop with 8 GB of RAM and an Intel Core i7-4720HQ CPU. Python 3.5 was used to process the data after being read from the relevant MySQL databases into local Pandas Dataframes.

5.1.1 Measured Data Conversion

The raw data was stored in a way which minimised storage requirements by using integers where possible. Simple scaling was required to obtain the correct physical units for the measured data points.

Temperature values required simple division by 16 to return the data to the 0.0625 °C resolution which the TMP275 sensors reported.

The raw *FFM* pulses, *PulseCnt*, represent the total recorded fine flow meter pulses since the previous second. *FFM* reports 380 pulses/L of measured water flow. A volumetric

flow rate was required so scaling was performed to convert $PulseCnt$ to V_M with units of lpm.

The state of the solenoid valve, $ValveState$, indicated whether SV was open or closed. $ValveState$ was used to identify where scheduled flow events occurred and enabled convenient masking and data grouping.

5.1.2 Resampling and Interpolation

The sample timestamps were stored as two separate values; a DateTimeIndex (to s resolution) and additional value containing the µs component. The two time aspects were combined to recreate the exact sampling time. The recorded data was very clean to begin with meaning that few samples were missing. The only missing samples were during the 3.5 s which SV took to open or close and for a few additional seconds between Test Days where BV was adjusted to the next flow rate. This resulted in there being very little missing data which simplified the resampling and interpolation aspects.

Resampling is often used to convert between sampling rates [37]. For example a recorded 1 Hz signal could be downsampled resulting in a 5 Hz signal. Resampling can thus be used to reduce the number of data points prior to plotting time series data. In this case, resampling was used to ensure that the indexed Pandas DataFrame contained an index with a uniform 1 Hz sample rate to facilitate time based selection and mathematical operations to be performed. Very little missing data was present in the original data so very few additional time stamps were artificially added.

Interpolation was used to fill the artificially added time stamps with the required values. Interpolation is used in time series data to fill missing data values. The interpolation required to fill a few seconds of missing data in a full day of sampling was trivial. The temperature values (and measured vibration σ values in Datasets 2 and 3) were simply forward filled meaning that all missing data points were populated with the previous valid entry. V_M and $ValveState$ was set to zero for all missing points.

5.1.3 Filtering

The data had a uniform sample period of 1 s after resampling and was fully populated after interpolation. Constant sample rate signals are more easily filtered and for some applications it was seen that basic discrete low pass filtering was required.

The notation to indicate that filtering was performed on a signal was $f\{\}$. Certain signals were found to fluctuate more than desired between samples. Low pass filtering can be used to smooth noisy signals. Thus it was decided to use a moving average filter with a short window length. A moving average filter can be considered to be a simple low pass finite impulse response filter which uses M input points to generate one averaged output point [37].

A 10 s window was found to be sufficient to smooth noisy signals and maintain the ability to detect large magnitude changes without significant time delay. Any low-pass filtering has a phase shift which is imparted on the signal and results in a time shift in discrete signals [37]. The Pandas rolling average filter (moving average) method, *Rolling*, was used to filter the required noisy signals [38]. *Rolling* has an argument to control where the filtered data point is inserted relative to the window and centre-shifting was selected.

This was done to maintain the time relation of the filtered and original signals as much as possible.

5.1.4 Vibration Standard Deviation Calculation

High frequency vibration data from Dataset 1 was used to calculate the standard deviation values. The minimum burst sample length for acceptable performance were determined by post-processing the high frequency vibration data in Dataset 1. The minimum requirements were then reflected in the acquisition system before subsequent experiments were performed. This enabled the real time σ recording used for Datasets 2 and 3 (as described in Section 4.4).

The standard deviation was calculated for each second of burst sampled vibration data, using the full 500 samples and progressively shorter windows. It was observed that using 250 samples occurring at the end of each second produced similar and adequate standard deviation values to using the full 500 samples.

$$s = \sqrt{\frac{\sum(X - \bar{X})^2}{n-1}} \approx \sigma = \sqrt{\frac{\sum(X - \mu)^2}{n}} \tag{5.1}$$

Equation (5.1) shows the close connection between general equations for sample and population standard deviation, s and σ respectively. $\bar{X}$ is the sample mean, μ is the population mean, and n is the sample length.

The sample standard deviation and population standard deviation formulae for a sample size of 250 can be considered to be approximately equal as demonstrated in equation (5.1). The standard deviation of the accelerometer axes data will be denoted using the population standard deviation, $\sigma_{x'}$, $\sigma_{y'}$ and $\sigma_{z'}$, for clarity.

The required sample length of 250 was determined for suitable σ to be calculated using the high frequency vibration data in Dataset 1. Datasets 2 and 3 were recorded with the σ values calculated and stored once per second which simplified the acquisition process and reduced the complexity of data processing.

Datasets 2 and 3 maintained 1 Hz sampling frequency for the duration of the conducted experiments and the σ values calculated before storage so no post-processing of raw vibration data was required in these cases.

5.1.5 Measured Data Manipulation

The measured data represents the parameters which can be directly measured using the sensors. These include the absolute temperatures, measured flow rate, state of SV and vibration standard deviation. Other useful information can be obtained by further manipulating the available data.

Additional information which can be derived using the temperature readings are the temperature drop over the heat sink and first time derivative of temperature. The recorded data from 3 temperature sensor mounting methods, as mentioned in Section 4.3.4, were analysed and mounting method 2 was found to produce the most useful data (the temperature sensors which used the original PCB with additional solder added). T_{N2} and T_{F2}

were thus used for the near and far temperatures in the rest of the report, T_N and T_F respectively.

The temperature drop over the heat sink, $\Delta T = T_N - T_F$, is the parameter which would be used to estimate the flow velocity if the temperature could be more precisely measured as Chapter 3 required.

The time differential of the temperature signals were investigated and it was found that $\dot{T}_N$ produced the most consistent behaviour during measured flow events.

$$\dot{T}_N[n] = \frac{f\{T_N\}[n] - f\{T_N\}[n-h]}{h} \tag{5.2}$$

Equation (5.2) shows the backward difference method used to calculate the discrete derivative was performed on filtered near temperature to calculate $\dot{T}_N$. Filtering the raw T_N signal prior to taking the derivative resulted in more clearly observable trends. $\dot{T}_N$ was observed to reach a peak at the start of water flow. This trend is expected as the thermal inertia of the copper pipe wall is low compared to the hot water contained within the pipe during water flow. The copper pipe thus quickly increases in temperature until the copper temperature is approximately equal to the water temperature. $\dot{T}_N$ thus provides a means to determine whether new flow events occur.

The vibration standard deviation values, σ, were filtered prior to use in vibration event detection. The smoothed $f\{\sigma\}$ signals were much more useful to determine when water flow occurred.

5.2 Event Detection

Event detection encompasses vibration event detection, thermal event classification and usage event detection. Vibration event detection non-invasively identifies sample points where flow is likely to have occurred, and groups the consecutive samples into separate vibration events which required grouped analysis. Vibration event detection provides the temporal boundaries of possible water usage events. Thermal event classification consists of the development of thermal criteria which were observed to only occur during scheduled flow events. Thermal event classification was used to classify the cause of detected vibration events. Usage event detection consists of the fusion of vibration event detection and thermal event classification to determine when hot water was used using only non-invasive methods. Usage event detection uses the temporal boundaries which vibration event detection provides and the hot water flow detection which thermal event classification provides. Vibration analysis at the usage event detection stage enabled reliable events to be identified (meaning that quantitative estimation could be reliably used). The classifications and flags determined were transferred to the time series data when usage event detection was completed.

Figure 5.1 shows the sequence and flow of the tests performed to execute vibration event detection, thermal event classification and usage event detection. Each component of event detection is then discussed in more detail.

5.2.1 Vibration Event Detection

Vibrations which can be measured using an externally mounted accelerometer are generated when water flows within a closed pipe. Preliminary vibration testing indicated that the presence or absence of water flow could be determined using accelerometer data in isolation, even at low flow rates. This prompted the development of a method to identify times when water flow occurred using σ values.

Time series σ values were analysed during scheduled flow events. The σ magnitude increased when flow was measured as was expected. The longitudinal velocity of turbulent water flow within a pipe is comprised of an average and fluctuating component as described in [13]. The fluctuating water velocity component is proportional to transverse pressure fluctuations. The pressure fluctuations cause the measurable vibrations, and the standard deviation of the measured vibrations are proportional to the average longitudinal flow rate [13]. Higher water flows cause larger vibrations and result in σ values with greater magnitudes. The vibration event detection was calibrated using the lowest flow rates in Dataset 1 which occurred on Test Day 1. This was done so that all scheduled flow induced vibration events (usage events) could be detected for higher flow rate events.

5.2.1.1 Vibration Thresholds

Minimum vibration threshold levels were empirically determined for each accelerometer axis using the smoothed $f\{\sigma\}$ values present during the lowest measured flow rates. The filtered signals were used for this application to ensure single events were not identified as several short events when a fluctuating raw σ value briefly dropped below the corresponding threshold level.

$\sigma_{x'min}$, $\sigma_{y'min}$ and $\sigma_{z'min}$ are the minimum threshold levels for each axis, with the general vibration threshold being denoted as σ_{min}. Each sample which had all 3 measured σ values greater than the corresponding threshold levels was marked with a flag, σ_{flag}, which can be considered to be a non-invasive equivalent of $ValveState$.

Axis	Measured		Threshold
	mean(σ_{closed})	min(σ_{open})	σ_{min}
$f\{\sigma_{x'}\}$	3.64	3.82	3.75
$f\{\sigma_{y'}\}$	3.49	4.94	5.00
$f\{\sigma_{z'}\}$	4.60	7.18	6.00

Table 5.1: Vibration event σ threshold motivation. The mean measured standard deviation when *SV* was closed, mean(σ_{closed}), gives an indication of the average standard deviation values for no flow conditions. The minimum measured standard deviation when *SV* was open, min(σ_{open}), shows the minimum measured σ values during flow tests for each accelerometer axis for Dataset 1. σ_{min} shows threshold levels which were selected for each axis.

Table 5.1 shows the measured σ values which motivated the selection of σ thresholds, σ_{min}, for each accelerometer axis. The threshold levels for each accelerometer axis were adjusted so that low flow rates could be identified as single vibration events but that unnecessary vibration events were minimized.

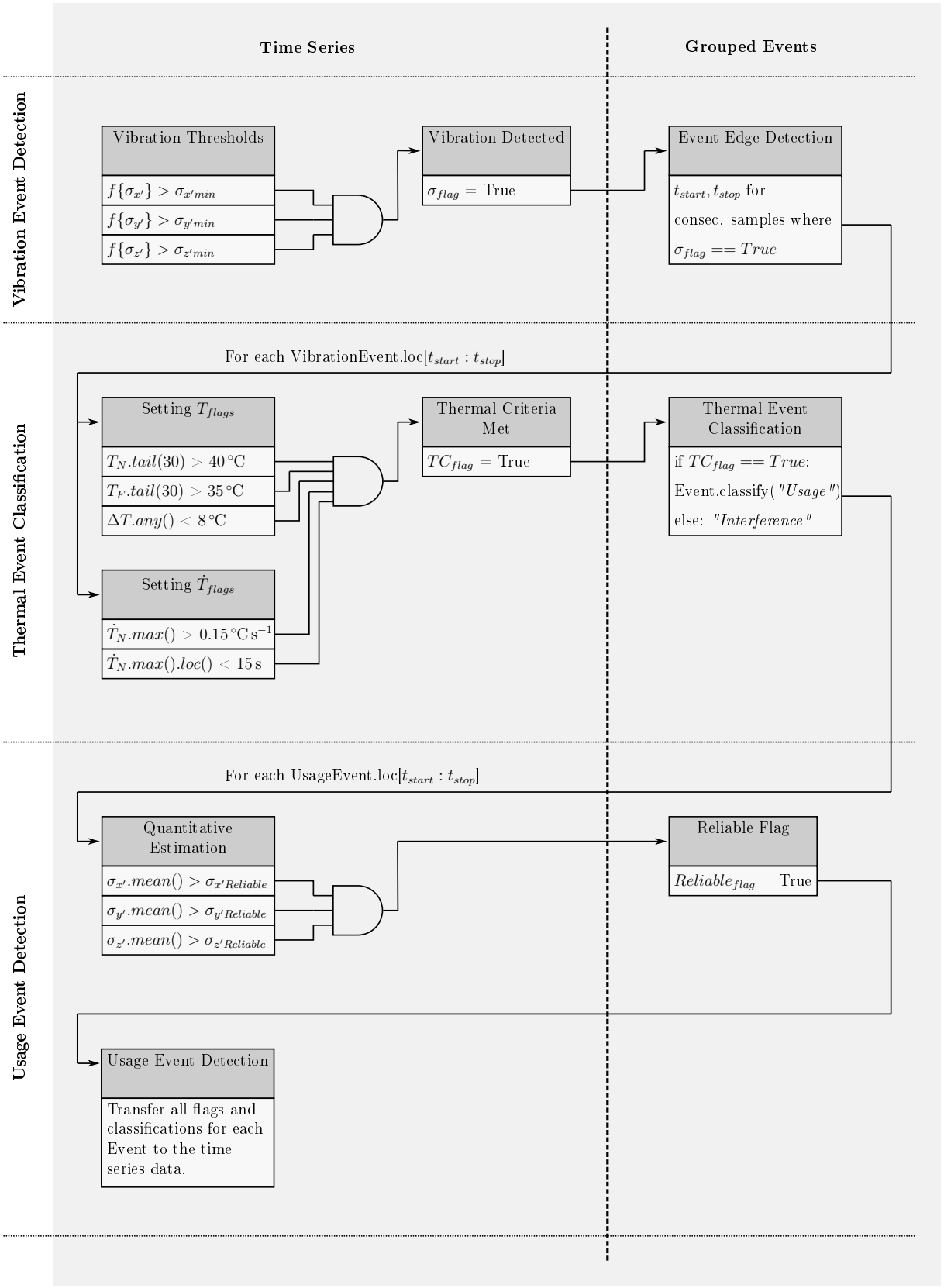

Figure 5.1: Event Detection Flow Diagram. Time series analysis was performed on the full dataset containing 1 Hz sample points. Analysis was also required for the grouped events (consecutive samples were grouped to form discrete events which contain the start and stop times of the detected event, and summed measurements for events)

Water usage events with low flow rates have the smallest σ values and are thus the most difficult to detect using a minimum threshold level. Test Set 2 from Test Day 1 (Test Set ID 1.2) is shown in Figure 5.2 to illustrate how σ_{min} was implemented to identify the temporal boundaries of a scheduled flow event.

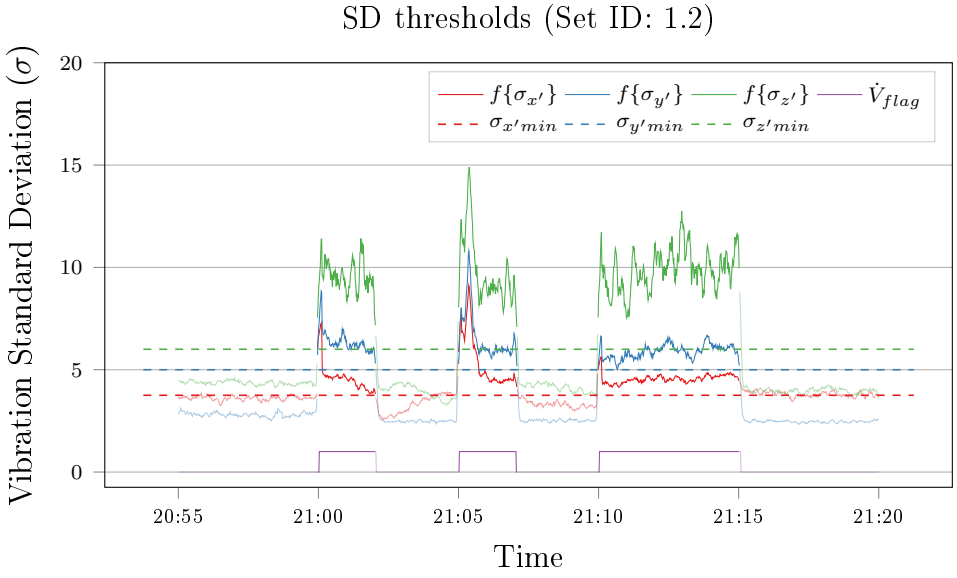

Figure 5.2: Vibration event detection using σ_{min}. Detected vibration events are indicated on the figure as dark lines. The semi transparent sections are where at least one $f\{\sigma\}$ value was below its respective threshold and thus no vibration event was detected for those sample points. $\dot{V}_{flag}$ is a flag which shows where water flow was measured.

Figure 5.2 shows $f\{\sigma\}$ for each axis and the associated σ_{min} values used for vibration event detection during Test Set 1.2. It can be seen that $f\{\sigma_{x'}\}$ and $f\{\sigma_{y'}\}$ are sometimes close to the minimum threshold levels during Test Set 1.2 which justifies the threshold levels to avoid detecting single vibration events as several separate events in close succession. It also demonstrated the requirement to filter the σ values prior to performing vibration event detection.

5.2.1.2 Vibration Event Grouping

Consecutive samples containing σ_{flag} were grouped together to form vibration events. Grouping consecutive samples into separate vibration events was required to analyse each scheduled flow events separately. This grouping was possible using $ValveState$ but this data would not be available in an implemented non-invasive system. The vibration event grouping was thus performed using the non-invasive methods to provide the same data which would be available in a retrofit non-invasive implementation.

Edge detection was performed on the σ_{flag} flag and the start and stop times were stored. A separate Pandas DataFrame was created to store each vibration event as a new entry. Each detected vibration event was chronologically numbered. The full DataFrame was given the same vibration event numbering system, so that time series data corresponding to vibration events was available. This enabled access to the time series data within the non-invasively determined temporal boundaries of each vibration event.

5.2.1.3 Interference

The measured flow rate, $\dot{V}_M$ in $\mathrm{L\,min^{-1}}$, within each vibration event's temporal boundaries was used to check whether water flow had occurred. A boolean equivalent, $\dot{V}_{flag}$ was used to indicate the presence or absence of measured water flow. It was found that certain vibration events did not contain any measured water flow. These vibration events were caused by external interference (e.g. the vibrations caused by a compressor pump which was located outside the experimental location). The magnitude of the interference vibrations were thus greater than the magnitude of the measured σ values during the lowest flow rates.

In the Dataset 1 there were 2 separate extended duration vibration events were caused by external interference which occurred during scheduled flow tests. Figure 5.3 shows an example of external vibration interference which can be seen to not be related to flowing water in the pipe during Test Set 1.4.

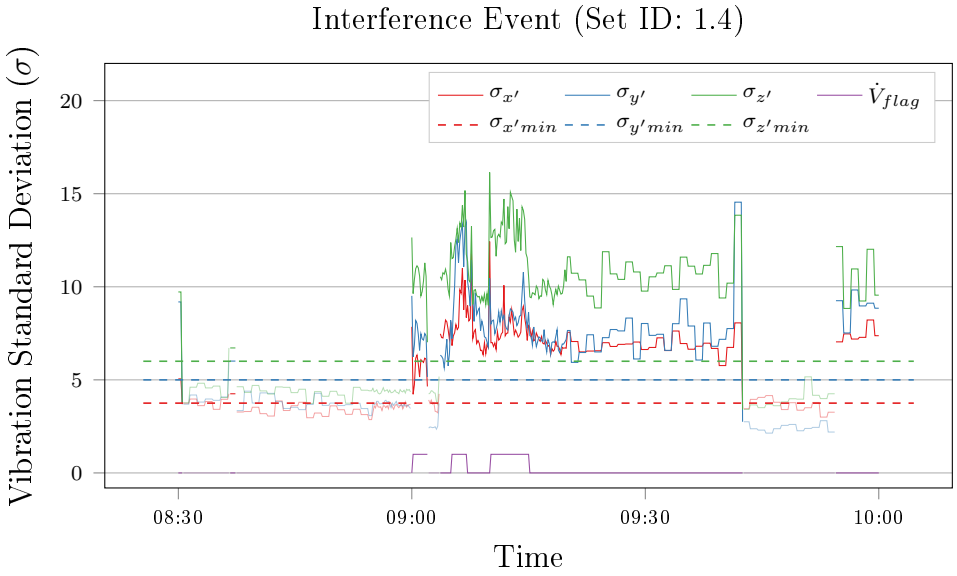

Figure 5.3: External vibration interference occurring during low flow rate tests. The σ values for the x', y' and z' accelerometer axes are shown as solid lines and the associated σ_{min} values are shown as dashed lines. The regions where flow pulses were measured are indicated by $\dot{V}_{flag}$ and the regions where vibration event detection occurred are indicated by darker lines. The external interference occurred between 09:03:40 and 09:42:32 during the second and third scheduled flow events of Test Set 1.4. The signals were resampled to 10 s for clarity prior to display.

Figure 5.3 shows where an external interference resulted in vibration event detection which occurred over 2 flow events during Test Set 1.4 (09:05 to 09:07, and 09:10 to 09:15 scheduled events). The magnitude of the σ values caused by the external interference was seen to be larger than the magnitude of σ values caused by water flow (09:00 to 09:02). The magnitude of vibration interference combined with the low threshold levels required to detect low flow rate water flows meant that usage event detection would not be possible using accelerometer data in isolation.

Figure C.1 in Section C.1 shows the extended duration interference event which occurred during Test Set 5.4.

5.2.2 Thermal Event Classification

After vibration events were detected further analysis of each grouped event was required to perform thermal event classification. Thermal data within the temporal boundaries of detected vibration events was analysed and trends were discovered. Thermal criteria were developed which were only observed when hot water flow was measured in Dataset 1. If the thermal criteria were met for a specific vibration event then it was classified as a usage event as it was caused by hot water flow. Vibration events which did not meet the thermal criteria were classified as interference events.

Thermal event classification involved the generation of thermal criteria using the measured data. The temperature thresholds for a specific EWH are likely to require specific analysis to calibrate the thermal criteria for a EWH unit. This is anticipated due to the observed impact of temperature sensor mountings on the reported data. The thermal criteria are required to perform usage event detection on new data in an implemented system during normal operation (without measured data used in calibration).

5.2.2.1 Energy Transfer

The energy transfer which occurs within the outlet pipe is comprised of longitudinal conductive heat transfer within the copper pipe and radial energy transfer from the water within the pipe, through the copper pipe via radial conduction and terminating with convective transfer into the ambient air. Energy transfer and thus measurable temperature changes have two separate modes of operation: resting and flow conditions.

The temperature profile of the resting system is most strongly determined by the radial conduction along the pipe. The water and copper pipe reach the ambient temperature of the surrounding air as time passes if no heat energy is input into the system. The experimental EWH maintains set point temperature of the contained water, so the EWH is at a higher temperature than ambient.

When water flow occurs then hot water from the EWH fills the outlet pipe and a temperature increase can be measured.The thermal behaviour of the system was thus measurably different during times of water flow than during extended times of no water flow. Vibration event detection provided temporal boundaries where water flow was likely to have occurred. The measurable thermal behaviour was analysed within each vibration event to determine if the conditions were met which correspond to observed flow state thermal behaviour.

The measurable observations were made using T_N and T_F. T_N and T_F reach their respective resting temperatures when no flow has occurred for a sufficiently long period of time. These resting temperatures are higher than ambient air temperature due to heat conduction occurring in the longitudinal direction of the copper pipe. The longitudinal conduction increases the temperature of the copper pipe and the convective radial heat loss into the air means that T_N has a higher resting temperature than T_F. During a flow event hot water travels in the longitudinal direction of the pipe and radially transfers energy into the pipe which raises the temperature of the pipe at all longitudinal points. This means that T_N and T_F rapidly increase in temperature at the start of a hot water flow event.

5.2.2.2 Thermal Criteria

Empirically determined thermal criteria were set up to determine whether the conditions for flow state were met for each vibration event. The measured near and far temperatures, T_N and T_F, were used to establish minimum threshold values. The temperature drop between T_N and T_F over the heat sink, ΔT, was used to establish a maximum threshold value. The first time differential of T_N ($\dot{T}_N$) was also investigated. If all thermal criteria shown in Table 5.2 were met for a specific vibration event then the vibration event was classified as a usage event.

Name	Criteria	Time During Event
TC_1	$T_N > 40\,°C$	Event end
TC_2	$T_F > 35\,°C$	Event end
TC_3	$\Delta T < 8\,°C$	Any time
TC_4	$\dot{T}_N > 0.15\,°C\,s^{-1}$	$< 15\,s$ of events start

Table 5.2: Thermal Criteria for Thermal Event Classification

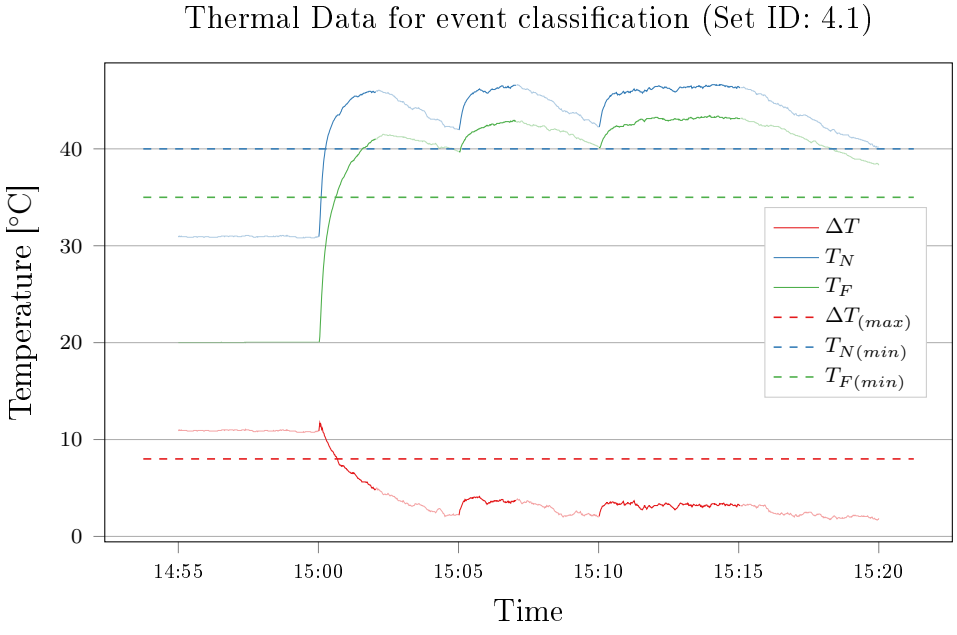

Figure 5.4: Temperature measurements during hot water flow for Test Set 4.1. The opaque line sections indicate where hot water flow was measured and the semi transparent line sections indicate where no water flow was measured. The dashed lines show the selected temperature thresholds which form TC_1, TC_2 and TC_3.

Figure 5.4 shows the measured raw temperature data gathered during times of hot water flow during Test Set 4.1. T_N and T_F can be seen to rise above their threshold values by the end of the measured flow event. ΔT can be seen to be below the required value at the end of each vibration event.

The measured temperature checks were performed at the end of each vibration event to ensure that for short water flow durations the heat transfer could have occurred as much as possible and thus the measured temperature could be high enough for valid events.

TC_4 considers the rate of temperature increase, $\dot{T}_N$. It was observed that a maximum rate of temperature increase was present near the start of hot water flow. The magnitude of this peak was found to be related to the temperature increase of the sensor during a flow event. $\dot{T}_N$ peaks were seen to have a larger magnitude when the pipe was at resting steady state temperatures prior to the event. Convective heat transfer from the pipe into the air always occurs, so the magnitude of the peak is determined by the amount of time which the pipe was able to cool down (time between flow events). For this reason there is a minimum time which must elapse between hot water usage events so that the pipe can cool enough for a sufficient peak to be present.

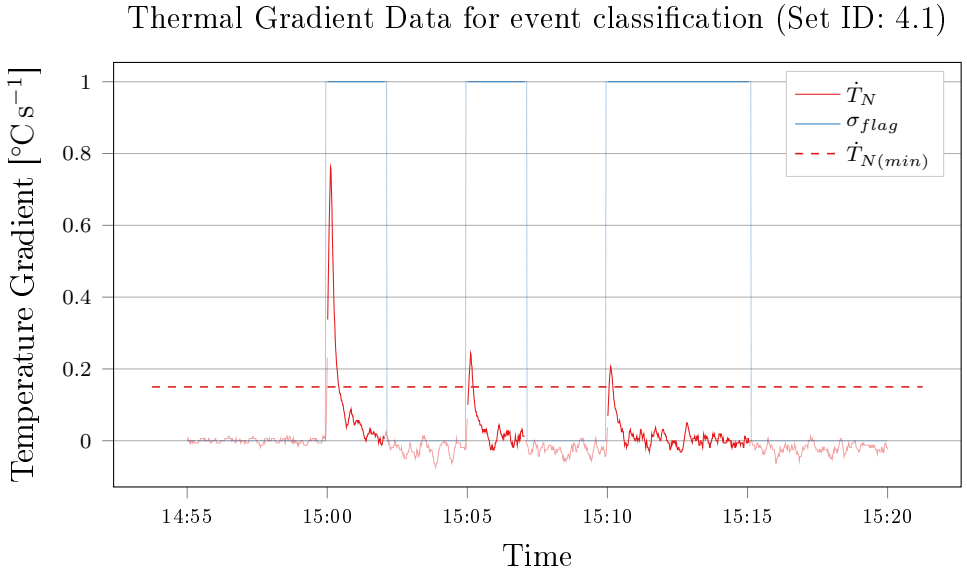

Figure 5.5: Temperature gradient during hot water flow. The opaque line sections indicate where hot water flow was measured and the semi transparent line sections indicate where no water flow was measured. The dashed line shows the value which $\dot{T}_N$ must exceed within 15 s of the start of a vibration event. The flag used to indicate vibration events is shown as σ_{flag}. The figure shows how TC_4 was determined.

Figure 5.5 shows the temperature gradient which is measured during times of hot water flow for the nearest temperature sensor. It can be seen that the rate of change of measured temperature reaches a pronounced peak. It was observed that this peak was above $0.15\,°C\,s^{-1}$ for all hot water flow events in Dataset 1. The peak had to occur within 15 s of the start of the vibration event to meet the criteria. A peak threshold and time-of-peak were required rather than just the time-of-peak. This was to ensure that coincidental gradient peak locations in interference events did not result in erroneous usage event classification.

5.2.2.3 Minimum Temperature Sensors Required

It was found that only T_N was required to classify vibration events in Dataset 1 using thermal event classification. T_N or $\dot{T}_N$ were always the criteria which resulted in events being correctly classified as interference events. T_F and ΔT comparison values could be set to always be 'True' and the thermal event classification results for Dataset 1 were identical.

The redundant thermal criteria were still used in the system design and testing. Additional testing could confirm that the performance is possible using only one externally mounted vibration sensor and temperature sensor but one Dataset is not sufficient to confirm this as it may only be possible for the conditions considered in the experimental unit.

5.2.3 Usage Event Detection

Usage event detection is simply the fusion of vibration event detection and thermal event classification. The temporal boundaries of vibration events were provided using vibration event detection indicating where vibration data indicated that flow was expected. The time-series thermal data within the detected time boundaries was analysed using thermal event classification resulting in the entire vibration event was classified as a usage event or an interference event.

During the iterative algorithm design process it was observed that low flow rate usage events had unacceptably large estimated flow rate errors as is discussed in Section 5.3. Vibration analysis of detected usage events was performed during the grouped data analysis stage, and events could be identified which were likely to have accurate flow rate estimation values. Usage events with average σ values which were larger than the $\sigma_{Reliable}$ values were flagged as being reliable, meaning that reliable results could be provided using quantitative flow estimation. Qualitative flow estimation was required for unreliable usage events, where a constant low flow rate approximation was required as quantitative estimations were likely to be unreliable.

The classifications and flags generated for the grouped events were then transferred to the time series data. This enabled the selection of all the time-series data of usage events which were non-invasively detected. The detected usage events and classifications were then available when analysing individual data points.

5.3 Flow Rate Estimation

After usage event detection was determined to be successful then the flow rate estimation system was designed. The flow rate estimation was performed using the measured vibration data. The filtered vibration standard deviation values, $f\{\sigma\}$, were used in vibration event detection to detect event flow start and stop times. The raw standard deviation values, σ, were used for quantitative flow rate estimation.

The purpose of the flow estimation algorithm described in this section is to provide the same level of accuracy for the total volumetric water consumption as the current in-line flow meter used in SGC systems. The design of the flow rate estimation system was based on the fluid velocity estimation used in [13]. Due to the incompressibility and constant density of water for domestic scenarios the fluid velocity, u, and volumetric flow rate, $\dot{V}$, are directly proportional based internal area of the pipe opening. Thus $\dot{V}$ could be estimated directly as it is a scaled equivalent to u.

5.3.1 Calibration

Calibration was required to design the system due to the complexity of vibration propagation in real world systems. The experiments used to generate Dataset 1 were designed to enable system calibration by providing multiple automated flow events at the same

flow rate. A large amount of data was available for 5 discrete flow rates which enabled average values to be used. The relationship between measured flow rate, $\dot{V}_M$, and vibration accelerometer standard deviation, σ, were investigated.

The relationship between measured flow rate and measured σ was found to be different based on the location of the sensor mounting [17]. It was found to be quadratic for accelerometers mounted to the centre of pipe sections and linear for accelerometers mounted on 90° bends [17]. The LSM303 accelerometer was mounted to a long section of straight inlet pipe more than 10 pipe diameter distances from any up- or downstream disturbances to facilitate fully developed flow [8]. Domestic flow rates and pipe diameters result in lower fluid velocities and thus lower pipe accelerations. Linear and quadratic relationships were investigated due to the lack of data at domestic flow rates.

Each usage event was separately analysed. This means that in Dataset 1 there were eight 2 min duration flow events, and four 5 min duration flow events recorded per day at a fixed flow rate. The average measured flow rate, $\bar{\dot{V}}_M$, was compared to each σ value. It was found that a basic linear relationship provided more uniform constant values for events with the same measured flow rate.

The calibration consisted of isolating each usage event and determining a scaling constant for each accelerometer axis for each second within the usage event: $c_{x'}$, $c_{y'}$ and $c_{z'}$. Mean scaling constants for each axis were then determined per usage event.

Where i is the usage event number and n_i is the duration of the usage event in seconds:

$$\bar{c}_{x'i} = \frac{\sum c_{x'i}}{n_i}, \qquad \bar{c}_{y'i} = \frac{\sum c_{y'i}}{n_i}, \qquad \bar{c}_{z'i} = \frac{\sum c_{z'i}}{n_i} \tag{5.3}$$

The mean scaling constants shown equation (5.3) were multiplied by the associated time-series σ values. It was seen that $\dot{V}_M$ for each event could be quite accurately approximated using the mean scaling constants for that event. This indicates that the relationship between $\dot{V}_M$ and σ values were consistent throughout the duration of a usage event. This led to the mean of the scaling constants for each event to be investigated. The intention was to generate a single scaling constant for each accelerometer axis.

Where i is the usage event number and N is the number of usage events within Dataset 1:

$$C_{x'} = \frac{\sum_{i=0}^{N} \bar{c}_{x'i}}{N}, \qquad C_{y'} = \frac{\sum_{i=0}^{N} \bar{c}_{y'i}}{N}, \qquad C_{z'} = \frac{\sum_{i=0}^{N} \bar{c}_{z'i}}{N}, \tag{5.4}$$

Equation (5.4) shows the final scaling constants relating to each accelerometer axis which was used to estimate the flow rate. Initially the full set of usage events within Dataset 1 was used to calculate the final scaling constants. It was observed low flow rate experiments were not accurately estimated using this method. The final scaling constants were recalculated using only the usage events which occurred from Test Day 2 to Test Day 5 in Dataset 1 (which had larger flow rates). This was found to yield better results for the remaining usage events. It was also apparent that the calibration and thus quantitative flow rate estimation was not possible for low flow rates. This is not surprising as low flow rates are likely to have a transitional flow regime (rather than turbulent). Difficulty measuring transitional flow was experienced in [20] as well.

5.3.2 Reliable Flag for Quantitative Estimation

It was not possible to use low flow rate events in the calibration and thus estimation sections of the algorithm design. It was however possible to determine that low flow rate flows occurred using only vibration data. This was implemented during the usage event detection stage as discussed in Section 5.2.3 where a 'reliable' flag could be determined to indicate whether flow rates could be quantitatively estimated for each event. The necessity for the identification of low flow events and acceptable reliable events was discovered during the design of the flow estimation section of the algorithm but was best implemented in the usage event detection stage.

Low flow rate events could be detected by the system but the linear proportionality which was present for other flow ranges did not yield accurate results. A constant low flow rate approximation value was speculated to be useful for unreliable usage events.

5.3.3 Instantaneous Flow Rate Estimation

Instantaneous flow rate estimation was the first step to developing the quantitative flow estimation system. The time-series estimated flow rates were analysed for separate usage events.

The estimated flow rate, $\dot{V}_E$, was the product of respective scaling constants and σ time-series values.

$$\dot{V}_{E[n]} = \frac{1}{3}\left(C_{x'}\sigma_{x'[n]} + C_{y'}\sigma_{y'[n]} + C_{z'}\sigma_{z'[n]}\right) \tag{5.5}$$

Equation (5.5) shows the formula used to calculate the estimated flow rate. The average of the estimated flow rates using each vibration axis on the time series σ values was used. $\dot{V}_E$ is obviously time-series data and was thus compared to the measured flow rate. It was found that $\dot{V}_E$ was able to track instantaneous flow rate changes and estimate a fluctuating $\dot{V}_M$ accurately. This further suggested that the linear approximation was valid for the experimental unit.

5.3.4 Mean Flow Rate Estimation

The mean estimated flow rate, $\bar{\dot{V}}_E$, was compared to the mean measured flow rate, $\bar{\dot{V}}_M$, for each usage event. This was found to be accurate and means that the 1 Hz sampled data could be reduced to a lower sample rate if a system required it in the future as long as local sampling was performed at 1 Hz.

The mean flow rate was found to be useful for usage events with fluctuating flow rates as were present in Dataset 2. This means that usage events data can be further summarised to give users feedback on a particular usage event which may be beneficial in the future (e.g. to provide brief summary of the day's water usage per event for a mobile application for users, or full resolution data for system analysis for installers).

5.4 Volumetric Consumption Estimation

If the temporal boundaries of valid usage events and the qualitative flow rate estimation accuracy can be verified then the estimated volumetric consumption, V_E, per event or per day can be used as a reliable parameter. The integration of high frequency data can provide volumetric usage estimation values which can be compared to measured volumes to determine the effectiveness of the flow estimation system.

The current in-line flow meter provides volumetric usage information in a SGC unit. The non-invasive flow meter is intended to replace the in-line flow meter so V_E must be confirmed to match V_M closely for the system to be implementable as a retrofit solution.

5.5 Usage Limitations

Two usage limitations were discovered during the development of the system. The first was that a minimum flow rate was required for quantitative flow rate estimation to be possible. The second was that a minimum time of no flow between usage events (or 'cool down time') was required.

The parameters for each limitation were established using Datasets 2 and 3. The expected performance of the system (operating within these restrictions) was then investigated on the Field Dataset to give an indication of the expected performance if applied to domestic SGC units.

5.5.1 Flow Rate Limitation

Dataset 2 was generated with the intention of testing more flow rates to assess estimation accuracy at various flow rates as described in Section 4.5. Some manually controlled flow events occurred at low flow rates which provided more data to discern what the minimum flow rate, $\bar{\dot{V}}_{(min)}$, was for the experimental unit.

The maximum flow rate which was attainable in the preliminary vibration tests was $5.5\,\mathrm{L\,min^{-1}}$ as mentioned in Section 4.1.2.2. The same diameter copper pipe was used so the flow regime of the contained water can be expected to be similar at similar flow rates. Quantitative flow rate estimation was not possible for the flow rates measured in the preliminary vibration tests. This gave an indication of the minimum flow rate. The flow rate limitation is likely the result of low flow rates having a transitional flow regime for the given pipe diameter.

Low flow rate usage events can be identified and an analysis was performed on the effect which using a fixed low flow rate approximation had on the volumetric estimation. Low flow rate events contribute less to total volumetric consumption in the same time frame. The flow rate estimation capability is negatively affected by the flow rate limitation. The total volumetric consumption estimation could be less affected by the limitation depending on the individual usage patterns.

5.5.2 Cool Down Time Limitation

Dataset 3 was generated to test specifically for the minimum wait-time or cool down time, t_{cd}, between usage events as discussed in Section 4.5. The Field Test Dataset was used

to evaluate what percentage of anonymous users' consumption patterns would result in usage events not being detected due to being too closely spaced.

The cool down time limitation exists because the outlet pipe needs to cool down between usage events. A temperature increase is required on T_N to perform thermal event classification. When usage events are spaced too closely together then subsequent usage events are classified as interference events because the thermal criteria (specifically TC_4 in Table 5.2) were not met even though the vibration events in question would be caused by water flow.

Chapter 6

Results

The results obtained using the experimental unit are discussed in this chapter.

Section 6.1 is concerned with Hypothesis 1. Temperature results are provided using the experimental unit relating to the temperature difference method (Chapter 3).

Sections 6.2 to 6.6 are concerned with Hypothesis 2. The performance of the flow estimation algorithm (Chapter 5) is evaluated.

Section 6.2 examines the performance of the system to detect and classify usage events in Dataset 1 to fulfil research objective 1 which is the non-invasive detection of valid usage events including temporal boundaries. The ability to identify which usage events contain flow rates which can be quantitatively estimated is assessed. The limitations of the flow estimation algorithm regarding minimum flow rate and minimum cool down time between events is shown in Section 6.3. The performance of flow rate estimation during detected usage events is shown in Section 6.4. The performance of the designed system to estimate the volume of hot water used per event and per day for the experimental unit Datasets (1, 2 and 3) is shown in Section 6.5. The expected performance of the flow estimation algorithm on a Field Dataset is shown in Section 6.6. The Field Dataset contains the anonymous water consumption of 32 SGC clients gathered over four weeks. The anonymous consumption patterns were analyses as a grouped set and individually to determine the grouped and individual consumption patterns, respectively. The flow estimation algorithm limitations were applied to the Field Dataset to simulate the expected performance if the designed non-invasive flow estimation system were applied to each field test SGC unit. The performance benefits of using a constant low flow rate approximation value for detected low flow rate events is shown to represent the relevance of the designed system in real world applications.

6.1 Temperature Difference

The theoretical explanation of how longitudinal temperature difference during steady-state flow relates to fluid velocity was discussed in Chapter 3. Preliminary tests indicated that in practice, thermal methods alone could not be used to predict flow rates for domestic EWH conditions as observed temperature losses were too small to practically measure. The experimental unit (Chapter 4) was designed to maximise temperature differences with the addition of heat sinks. Temperature sensors were mounted in such a way to maximise thermal coupling and promote heat transfer.

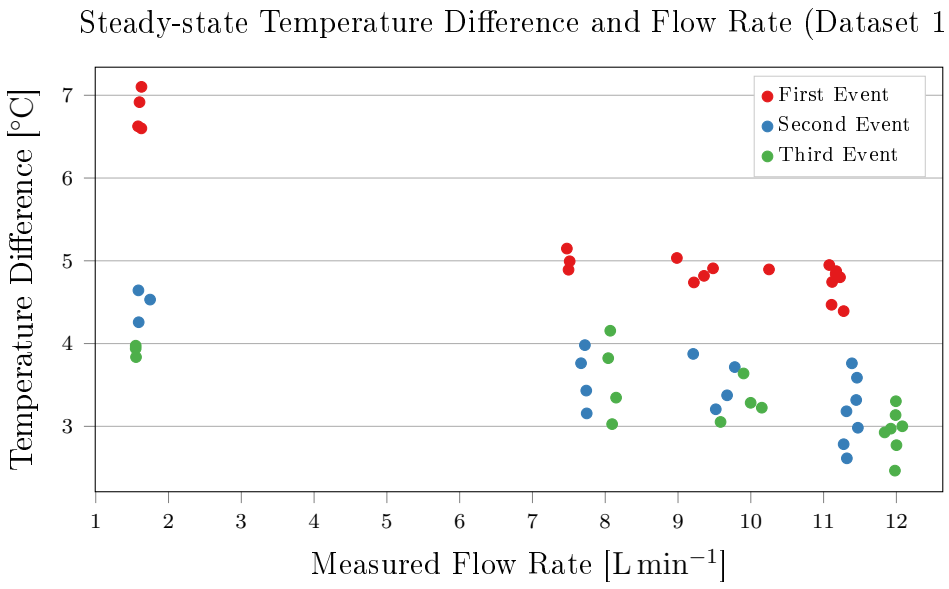

Figure 6.1: Temperature difference during steady-state flow and measured flow rate scatter plot for detected usage events in Dataset 1. The average steady-state temperature difference over the heat sinks, $\bar{\Delta T}$, is shown for the first, second and third flow events in each Test Set in Dataset 1.

Figure 6.1 shows the link between steady-state temperature drop over the heat sinks, $\bar{\Delta T}$, and measured flow rate for each detected usage event in Dataset 1, $\bar{\dot{V}}_M$. The first 60 s of temperature data per event was omitted when calculating $\bar{\Delta T}$ to facilitate steady state conditions as best possible. It can be seen that there are usually two clusters which correspond at each flow rate used: the upper clusters are attributed to the first flow event during each Test Set (red) and the lower cluster corresponds to subsequent flow events (blue and green).

For the first event T_N increases more than T_F within the two minutes of measured flow, because $\bar{\Delta T}$ is consistently larger than the subsequent events (the points in red are always the largest). This means that the system takes long to reach steady-state temperature during flow events. Only long duration flow events would thus be able to be estimated using measured temperature differences. This slow response when using inexpensive sensors which require simple installation was first observed in the preliminary thermal tests in Section 3.7.3 (Figure 3.5 illustrates this well). The large variation between the first events and subsequent events (at each discrete flow rate) means that despite the additional thermal coupling used in the experimental unit, the thermal data gathered was not useful.

If the points occurring during each Test Day at each discrete flow rate (approximately 2, 8, 10, 11 and 12 L min^{-1}) are considered, then a large temperature variation can be seen for controlled experimental conditions which should yield consistent temperature differences. The same flow durations, flow rates and time between flow rates was used for each Test Day so the measured steady state temperatures should be consistent. This was not observed (as shown by the vertical temperature difference range which occurs at the listed flow rates in Figure 6.1) which indicates that the inexpensive sensors used and the installation procedure did not yield repeatable results.

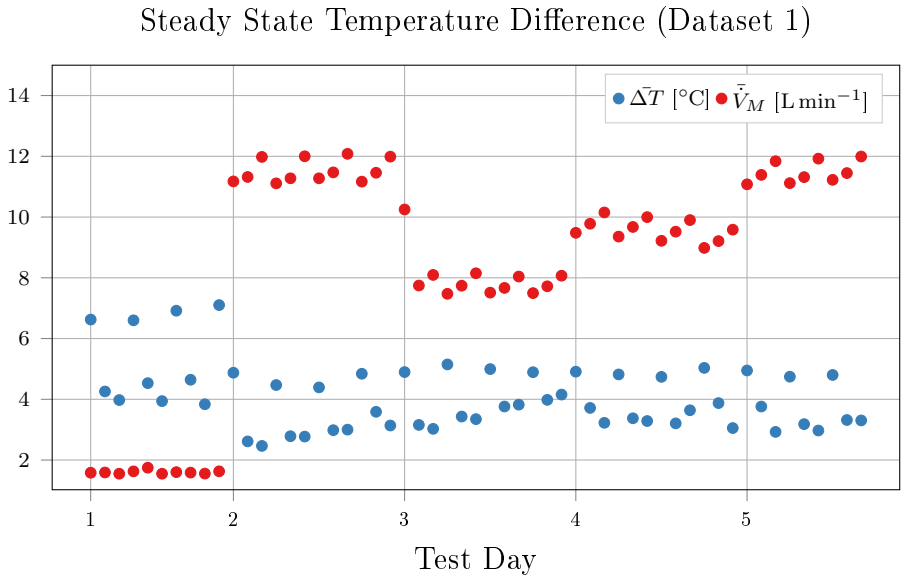

Figure 6.2: Longitudinal temperature difference measured during steady-state water flow is shown as observed during Dataset 1. The average temperature drop over the heat sinks used in the experimental unit is shown in blue as $\bar{\Delta T}$. The average measured flow rate during events is shown as $\bar{\dot{V}}_M$ in red.

Figure 6.2 shows the steady-state thermal difference and measured flow rate during usage events in Dataset 1. The heat sinks provided larger temperature differences in the longitudinal direction during water flow as was desired. This can be seen as the temperature differences shown in Figure 6.2 range between 2 °C and 8 °C, whereas in the preliminary tests the measured differences were less than 1 °C (Figure 3.6). But the magnitude of $\bar{\Delta T}$ at different flow rates was still consistent when variation was expected. This can be seen for Test Days 2 and 5 where $\bar{\Delta T}$ spans very similar temperature ranges event though different flow rates were used.

It can be seen from Figures 6.1 and 6.2 that measured temperature differences are not strongly related to hot water flow rate even when heat sinks were used to exaggerate the temperature drop and special care was taken to facilitate good heat transfer.

6.2 Event Detection

The flow estimation algorithm discussed in Chapter 5 used the combination of vibration data and temperature data to detect hot water flow.

Event detection consists of vibration event detection, thermal event classification and usage event detection as detailed in Section 5.2. Vibration event detection was used to non-invasively determine the temporal boundaries of possible usage events. The accuracy of the event durations was thus assessed as a measure of success. Thermal event classification was used to create the thermal criteria, using data provided from the in-line flow meter, to non-invasively classify events as usage events or thermal events as described in Section 5.2.2. Usage event detection is the combination of the non-invasively determined temporal boundaries and empirical thermal criteria to non-invasively detect usage events. The success of usage event detection was determined by ability to non-invasively determine when water flow occurred.

6.2.1 Vibration Event Detection

The temporal boundaries of usage events were non-invasively obtained using vibration event detection. The duration of each usage event was required to be accurate to ensure that volumetric flow estimation could be performed later. The start time of a usage event was required to be accurate so that thermal event classification could be performed.

Dataset 1 was comprised of scheduled flow events and repeat experimentation. The evaluation of the temporal boundary detection was performed for the scheduled flow events within Dataset 1. There were 60 scheduled flow events in the 5 days of experimentation and the durations of the 60 corresponding detected vibration events were assessed.

The duration of detected usage events (using vibration data) was observed to be longer than the measured duration of flow events (using in-line flow meter data). This can be explained by the smoothing filtering used to design the vibration event detection to ensure that the vibration threshold technique used was reliable. The difference between the estimated and measured usage event duration was performed to assess the capability of using vibration event detection to determine the duration of known flow events.

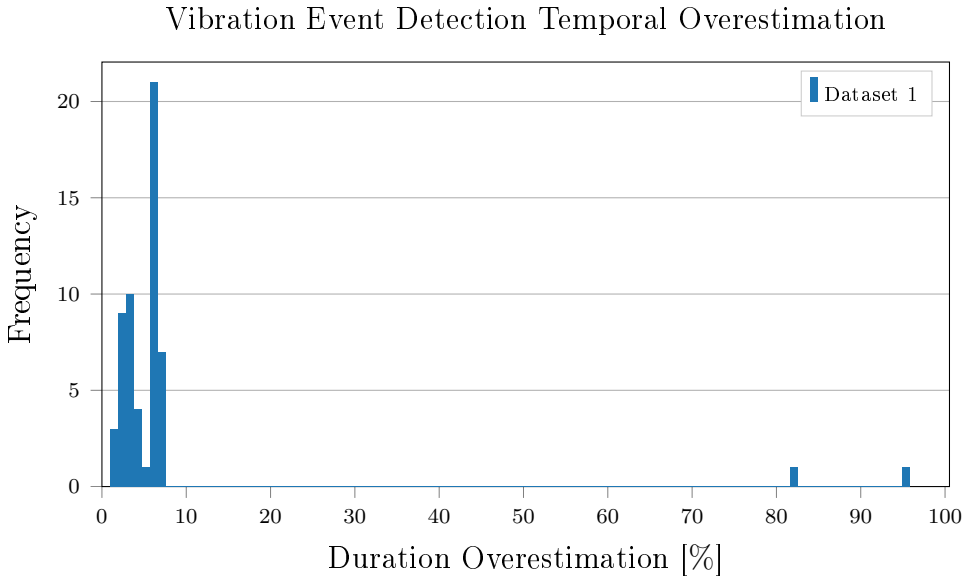

Figure 6.3: Percentage duration overestimation of vibration events containing measured flow in Dataset 1. The histogram shows the percentage difference between the duration of detected vibration events and the measured duration of flow. The outliers were due to external vibration interference spanning over scheduled flow events.

It can be seen from Figure 6.3 that the temporal boundaries obtained using vibration event detection are typically accurate. The durations of scheduled flow events were within 10 % for normal cases (where vibration interference did not occur during a scheduled flow event). The primary temporal boundary detection analysis was performed on Dataset 1 as it contained the greatest number of automated flow events.

Scheduled flow events were 2 min or 5 min in duration in Dataset 1. The maximum overestimation was 9 s for normal cases which is acceptable. The two outliers depicted in Figure 6.3 are due to scheduled water flows occurring during periods of externally caused vibration interference. These occurred in Test Sets 1.4 and 5.4 spanning over 2 and 3 flow

events respectively. When the interference events in Dataset 1 are excluded then a more accurate representation of the temporal boundary estimation is given. *SV* has a toggle time of 3.5 s, so usage events may have contained larger vibrations than were related to the flow rate (during toggles). This may explain the consistent temporal overestimation values observed in Dataset 1.

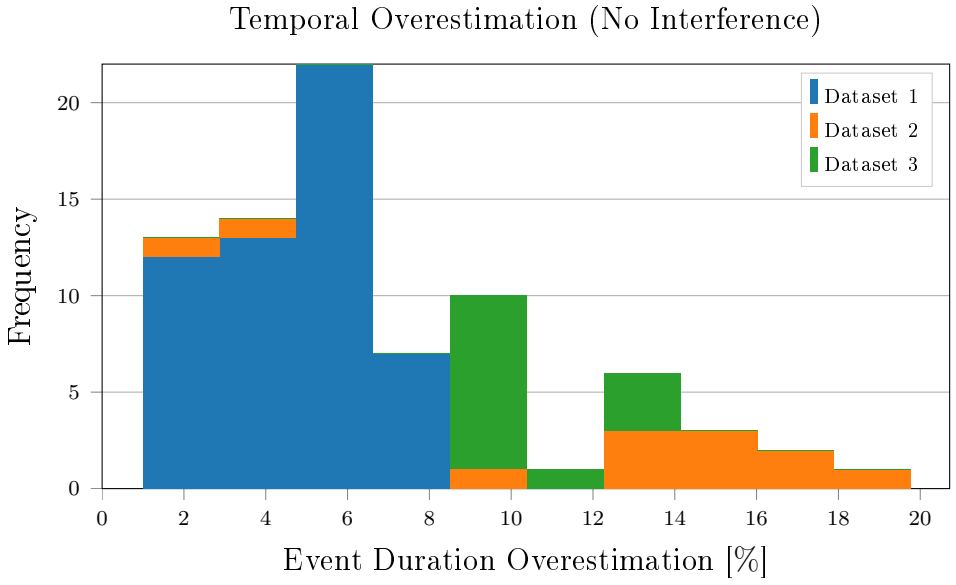

Figure 6.4: Percentage duration overestimation of flow induced vibration events. The histogram shows the spread of the accuracy of the temporal boundaries of the events contained in each Dataset. The histogram is cumulative.

It can be seen from Figure 6.4 that event detection in Dataset 1 performed well and the duration overestimates were low when interference events were excluded. Dataset 2 contained short duration, manually controlled flow events. This resulted in longer overestimations occurring for shorter events and thus greater percentage error. Dataset 3 consisted of 1 min long scheduled flow events. It can be seen that Datasets 1 and 3 are quite consistent unlike Dataset 2. This indicates that the scheduled *SV* operation produced less extra vibrations than the manually operated *BV*.

The overestimations are likely caused by the valves which are mounted on the outlet pipe. In a real world setting the valve to control flow operation is further downstream than for the experimental unit. This should improve the temporal boundary detection ability of the algorithm using vibration event detection.

It can be seen that the temporal boundaries obtained using vibration event detection were sufficient. The duration of known flow events were successfully determined using vibration data from a non-invasively mounted accelerometer meaning that vibration event detection was successful.

6.2.2 Thermal Event Classification

Thermal event classification consists of using the thermal criteria, established using Dataset 1, to determine the cause of vibration events and was thus designed to perform successfully for the dataset.

Thermal event classification was successful for all scheduled flow events within Dataset 1 where external vibration did not occur. All other flow events within Dataset 1 were correctly identified using the thermal criteria and comparing to periods of measured flow. Thermal event classification was not successful for any manually controlled flow events in Dataset 2 (due to insufficient wait-time between flow events). Dataset 3 consisted of tests to establish the minimum time required between successive flow events so that thermal event classification was successful and is discussed in Section 6.3.

In Datasets 1, 2 and 3 there were interference events which met the thermal criteria. Thus the thermal criteria used to perform thermal event detection did not give any false positives when classifying possible usage events.

False negatives (vibration events which were classified as interference events instead of usage events) did occur. Each false negative occurred during external vibration interference (as in Dataset 1) or due to insufficient wait-time between flow events (as in Dataset 2). The extended duration vibration interferences which caused missed usage events in Test Sets 1.4 and 5.4 in Dataset 1 were due to the close proximity of heavy machinery to the EWH installation. Vibration interference of this magnitude should not be expected in domestic installations but no data is available to verify this.

Due to the fact that no false positives were observed when using the thermal criteria to classify measured events; the thermal criteria used can be confirmed to be correct and resulted in correct classification of events. However due to the the presence of false negative classifications, thermal event classification can be considered to be successful when operating within the algorithm limitation of 2 min cool down time between events.

6.2.3 Usage Event Detection

The temporal boundaries of usage events were shown to be accurately determined using non-invasive means in Section 6.2.1. Thermal event classification was observed to be successful for all flow events which met the limitations of the system (discussed in more detail in Section 6.3.) Usage event detection combines the 2 aspects to use only non-invasive methods to detect usage events.

Sensor fusion is the combination of more than one sensor data type to obtain more insight than either sensor data type can provide in isolation. Usage event detection is thus the sensor fusion of the temporal data obtained using vibration event detection and the non-invasive detection of hot water flow using thermal event classification. Usage event detection consists of classifying vibration events as 'interference events' (caused by external vibration interference) or as 'usage events' (caused by hot water events) using non-invasive data only.

Dataset	Usage Events		Reliable Events	
	Expected	Detected	Expected	Detected
1	60	55	45	45
2	12	0	8	8
3	13	6	13	13

Table 6.1: Experimental unit event detection summary. The number of expected and detected usage events are analysed as well as the effectiveness of the reliability flag.

Table 6.1 shows that usage event detection was generally successful for Dataset 1 as can be seen from the 'Usage Events' column. 55 usage events were detected of the 60 expected scheduled flow events. The 5 incorrectly classified interference events were due to external vibrations in Test Sets 1.4 and 5.4 as discussed in Section 6.2.2. A detailed analysis of the usage event detection in Dataset 1 is presented in C.2. The severity of the vibration interference which occurred during Test Set 5.4 is shown in Section C.1.

The success of usage event detection was determined using Dataset 1. Datasets 2 and 3 were designed to test other factors and the experiments did not allow the necessary time between flow events for usage event detection to be effective. The duration composition of detected usage events within Dataset 1 was 96.04 % correct which reiterates that the temporal boundaries are accurate.

Event Classification	Valid [%]	Invalid [%]
Usage	86.7	3.6
Interference	8.7	1.0
Total	95.4	4.6

Table 6.2: Dataset 1 Usage Event Detection Summary. Valid percentages denote the duration of correctly classified events of duration of the considered subset. The considered subset is all vibration events which took place near scheduled flow events. Vibration interference events are included in this set.

Including the interference events in Dataset 1, the overall usage event detection was 86.7 % by duration as can be seen in Table 6.2. The overall event classification of vibration events which occurred within the subset (of vibration events occurring within scheduled Test Set times, as depicted in Table 6.2 was 95.4 % correct by duration.

For all vibration events in Dataset 1 the total correct event classification (as usage or interference events) was 97.7 % correct. The total valid duration of detected usage events within Dataset 1 comprised 96.04 % correct (obtained using Table C.1.)

Usage event detection was successful for Dataset 1 with 96.04 % overall correct classification by duration, indicating that only 4 % usage event duration overestimation occurred.

6.2.4 Estimated Flow Rate Reliability

During flow rate estimation analysis within Dataset 1 an order of magnitude difference for flow rate estimation error was observed for usage events occurring below and above a minimum flow rate threshold, $\bar{\dot{V}}_{(min)}$, of $5\,\mathrm{L\,min^{-1}}$. The iterative design process then gained an additional event detection step which was best executed during usage event detection: reliability detection. For usage events which were correctly detected, an additional flag was created using vibration data to determine whether quantitative flow rate estimation can be considered to be reliable for each usage event. The 'reliability' flag is thus a secondary vibration threshold to non-invasively determine when quantitative flow rate estimation for an event can be considered to be reliable.

The vibration and thermal data for Dataset 1 was analysed and empirical trends were found. Usage events with estimation errors an order of magnitude larger than others all occurred on Test Day 1. This was the lowest flow rate which contained σ values large enough to register as a vibration event, but smaller than the smallest σ for accurately estimated flow rates. Thus vibration analysis was employed to automatically flag usage events as 'reliable' in Dataset 1. The same threshold levels were then used on Datasets 2 and 3 to determine the validity of the reliability threshold levels for more usage events.

Table 6.1 shows the total number of expected and detected usage events for the experimental unit. 55 of the 60 scheduled flow events within Dataset 1 were correctly detected and classified as usage events. Test Set 1.4 and 5.4 contained interference events which account for the missed events. Out of the 55 detected usage events, 45 were expected and detected to be correctly classified as reliable. This means that 100 % of usage events which should have received quantitative flow rate estimation did so.

For Dataset 2 none of the flow events were detected as usage events. The manually controlled flow events did not have the minimum wait-time between flow events and the events were classified as interference events due to the thermal criteria not being met. Usage events were thus manually classified (i.e. simulated correct usage event detection) and reliability detection was once more universally successful.

Dataset 3 was gathered specifically to determine the minimum wait-time for events to meet the thermal criteria for usage event detection to be successful. All of the 13 scheduled flow events were above the minimum flow rate threshold and reliability detection was also correctly performed for Dataset 3.

It can be seen that detected usage events which can be quantitatively estimated can confidently be identified using non-invasive means only. A constant, approximate low flow rate was investigated for low flow rate events. The success of this flow rate approximation method was tested on the Field Dataset as it contained multiple users' normal usage patterns for a month. The effectiveness of the low flow approximation on the Field Dataset is discussed in Section 6.6.

6.3 Algorithm Limitations

The flow estimation algorithm was observed to have 2 limitations which inhibited universal operating conditions. The first limitation was that a minimum cool down time,$xtcd$, between usage events must be present. This is so that the pipe and water can sufficiently cool down so that usage event detection can be successfully performed using the thermal

criteria. The second limitation was that quantitative flow rate estimation was not possible for flow rates below $\bar{\dot{V}}_{(min)}$ 5 L min^{-1}. Events which cannot be quantitatively estimated were correctly identified in 100 % of cases observed in Datasets 1, 2 and 3 as demonstrated in Section 6.2.4.

- t_{cd} : 2 min Cool down time between flow events for thermal event classification to be possible
- $\bar{\dot{V}}_{(min)}$: 5 L min^{-1} Minimum flow rate for reliable quantitative flow rate estimation

6.3.1 Cool Down Time Limitation

The thermal criteria explained, in Section 5.2.2, were used to classify vibration events as usage events or interference events using thermal data. The thermal inertia of the copper pipe and enclosed water meant that the pipe cooled down at a certain rate. Temperature gradients had to be used as one of the thermal criteria to eliminate interference events which could occur shortly after the end of a valid usage event. If sufficient time was not given between usage events for the system to cool down then the thermal criteria were not met and flow events were classified as interference events.

Insufficient cool down time, t_{cd}, between events caused all flow events in Dataset 2 to be incorrectly classified as interference events as shown in Table 6.1.

Further experiments were conducted to establish t_{cd} as discussed in Section 4.5.3 to generate Dataset 3. Dataset 3 showed that a minimum cool down time, t_{cd}, of 2 min was required for usage event detection to perform as expected (meaning that the thermal criteria were met).

In Section 6.6 the cool down time limitation is applied to the Field Dataset to establish what number of measured usage events would not have been detected because of this limitation.

6.3.2 Flow Rate Limitation

Quantitative flow rate estimation was observed to be relatively consistent for certain flow events. Low flow rates were observed to have an order of magnitude larger error than the rest of the usage events. It was possible to identify usage events which contained low flow rate measurements using vibration analysis as shown in Section 6.2.4. Qualitative estimation was thus possible for low flow rates, and quantitative estimation was possible for flow rates greater than a minimum threshold.

The minimum flow rate threshold, $\bar{\dot{V}}_{(min)}$, was observed to be 5 L min^{-1}. This value was determined by isolating flow events which had the largest estimation error and investigating trends. Measured flow rates which fell below the minimum threshold had inaccurate estimations, and the corresponding σ values all fell below certain vibration thresholds which were consistently identified as shown in Table 6.1.

Only reliable flow rates were quantitatively estimated for the experimental unit; low flow regions were marked as unreliable meaning that qualitative estimation would not yield accurate results. The application of a fixed approximated value was investigated to give at least some indication of the contribution of low flow rates to total volumetric consumption.

In Section 6.6 the $\bar{\dot{V}}_{(min)}$ limitation for quantitative flow rate estimation was applied to the Field Dataset. This showed the contribution that low flow rates (which can receive qualitative estimation only) had to the total monthly water consumption in real world applications.

6.4 Flow Rate Estimation

Flow rate estimation was performed for detected usage events. Quantitative flow rate estimation was found to be possible above $\bar{\dot{V}}_{(min)}$ of $5\,\mathrm{L\,min^{-1}}$. Instantaneous flow rate estimation, $\dot{V}_E$, was first performed and confirmed to be accurate which to show that the linear proportionality between fluid velocity and accelerometer standard deviation, σ, was correct. Mean flow rate estimation, $\bar{\dot{V}}_E$, was then performed and confirmed to be accurate which indicates that the temporal boundaries and instantaneous flow rate estimation were accurate.

6.4.1 Instantaneous Flow Rate Estimation

The first stage of flow rate estimation is calculating an instantaneous flow rate estimate using the σ values for each sample in conjunction with their respective calculated constants as explained in Section 5.3. The instantaneous estimated flow rate, $\dot{V}_E$, accurately tracks the measured flow rate, $\dot{V}_M$, when the flow rate is adjusted during an event. There was only one example of such a scenario in the Dataset 1 during Test Set 3.1.

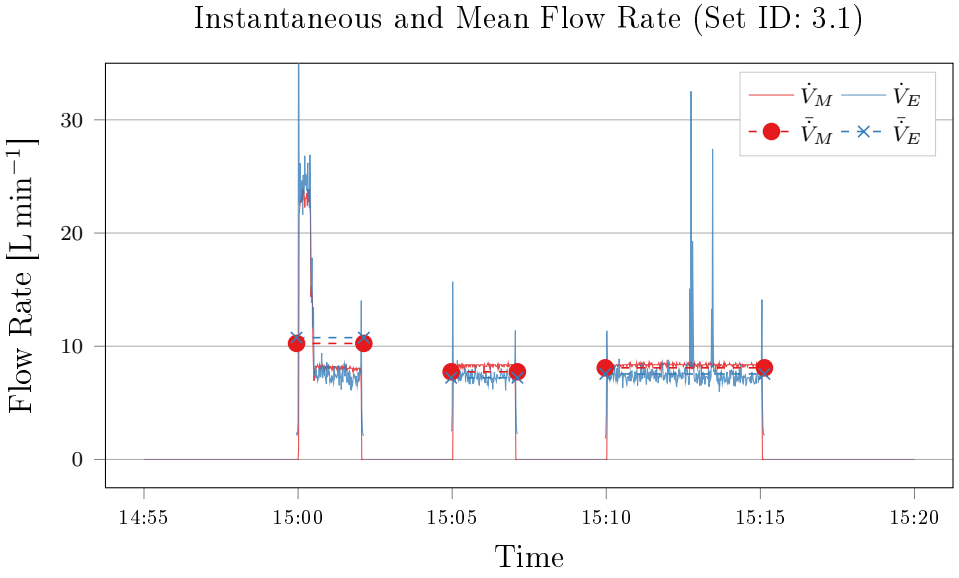

Figure 6.5: Instantaneous and mean flow rate estimation. The instantaneous measured and estimated flow rates, $\dot{V}_M$ and $\dot{V}_E$, are shown as solid lines and can be seen to fluctuate. The mean measured and estimated flow rates, $\bar{\dot{V}}_M$ and $\bar{\dot{V}}_E$, for each usage event are shown using dashed lines and end markers. The opaque line sections indicate regions where usage events were detected and the semi-transparent sections were not detected as events.

Figure 6.5 shows the measured and estimated instantaneous flow rates gathered during Test Set 3.1 in Dataset 1. The flow rate was adjusted while the automated solenoid valve

was open during the shown experiment. The flow rate was decreased during a scheduled flow event because the flow rate was observed to be too high. The 15:00:00 to 15:02:00 scheduled event is the only event in Dataset 1 where the flow rate was adjusted while water was flowing. It can be seen from Figure 6.5 that the estimated flow rate corresponds well with the measured flow rate for a changing instantaneous flow rate.

Additional experiments were performed to generate Dataset 2 where varying flow rates were intentionally executed. The manually controlled flow events in Dataset 2 occurred with insufficient cool down time between events, so thermal event classification was not possible for flow events in Dataset 2. Detected vibration events were manually confirmed to be usage events using the flow meter data (which would not be available for a non-invasive system)

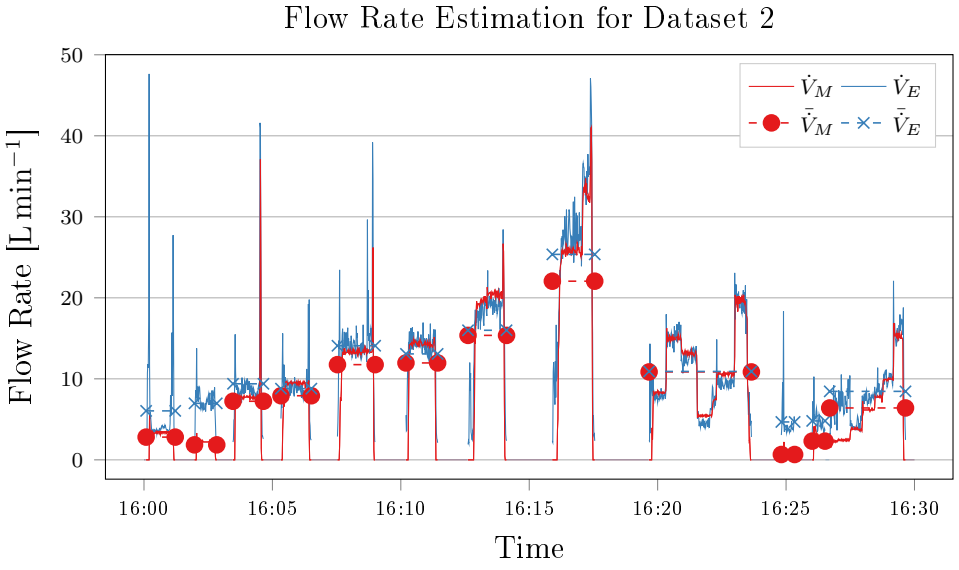

Figure 6.6: Dataset 2 flow rate estimation. The instantaneous measured and estimated flow rates are shown as solid lines, $\dot{V}_M$ (blue) and $\dot{V}_E$ (red) respectively. The mean measured and estimated flow rates for each usage event are shown as dashed lines with end markers, $\bar{\dot{V}}_M$ and $\bar{\dot{V}}_E$ respectively. The regions where vibration events were detected are shown as opaque lines and regions where not vibration events were detected are shown as semi transparent lines.

Figure 6.6 shows the instantaneous and mean flow rates for Dataset 2. The data in Dataset 2 did not contribute to the calculation of the flow rate estimation constants used in the system. The information from Dataset 2 can thus be viewed as the first new flow information after calibration was completed (or after the algorithm was designed using Dataset 1).

It is apparent from Figure 6.6 that measured flow rates less than $5\,\mathrm{L\,min^{-1}}$ cannot be accurately estimated. It can also be seen from the flow occurring between 16:20 and 16:23 that instantaneous flow rate estimation is possible for an extended duration event.

It can be seen from figures 6.5 and 6.6 that $\dot{V}_M$ and $\dot{V}_E$ correspond closely for flow rates greater than $5\,\mathrm{L\,min^{-1}}$ even for fluctuating usage during single events. Fluctuating behaviour can be expected in real world use patterns (e.g. adjusting the hot water during a shower). The ability to track instantaneous flow rates was thus important and determined to be possible. The accuracy of $\dot{V}_E$ was not quantitatively assessed due to the large number

of samples which would be required to be analysed as well as the fluctuating nature of the estimated flow rate. The quantitative assessment of estimated flow rate accuracy was performed on the mean estimated flow rate, $\bar{\dot{V}}_E$.

6.4.2 Mean Flow Rate Estimation

It was shown in Section 6.2.1 that the estimated duration of flow events using vibration event detection is reliable. It was shown in Section 6.4.1 that the estimated instantaneous flow rate, $\dot{V}_E$, is reliable above $5\,\mathrm{L\,min^{-1}}$. $\bar{\dot{V}}_E$ is the normalised integral of $\dot{V}_E$ over the temporal boundaries of the event. If the temporal boundaries as well as $\dot{V}_E$ are accurate then $\bar{\dot{V}}_E$ accuracy can be assessed.

It can be seen from figures 6.5 and 6.6 that although $\dot{V}_E$ closely follows $\dot{V}_M$, the estimated flow rate fluctuates. The mean flow rate per event, $\bar{\dot{V}}$, is a consistent value to use as the fluctuations are disregarded. Analysis of the measured and estimated mean flow rates per event, $\bar{\dot{V}}_M$ and $\bar{\dot{V}}_E$ respectively, was performed for Datasets 1, 2 and 3.

Figure 6.5 shows that the mean flow rates, $\bar{\dot{V}}_M$ and $\bar{\dot{V}}_E$, are accurate for fluctuating flow rates (15:00 to 15:02 scheduled event) and constant flow rates (15:05 to 15:07 and 15:10 to 15:15 scheduled events). Figure 6.6 contains a usage event between 16:20 and 16:23 which shows the same trends of accurate instantaneous and mean flow rate estimation.

The flow event occurring between 16:20 and 16:23 in Figure 6.6 is the longest duration flow event which only contains flow rates greater than $5\,\mathrm{L\,min^{-1}}$. Flow events with shorter durations were observed to overestimate the mean flow rate. Many short duration flow events have prominent $\dot{V}_E$ spikes at the start and end of each event. Larger σ values were thus present at event edges, which means that vibrations from the manually controlled BV may have caused these spikes and contributed to $\dot{V}_E$ overestimation in Dataset 2. The peaks at event edges contribute less to longer duration events which corresponds to the observation that the longest duration flow event in Dataset 2 has the lowest estimation error for mean flow rate as can be seen in Table C.2.

Constant hot water flow rates are not expected in real world applications for the entire duration of a usage event. The presented data shows that the instantaneous flow rate can be used to calculate a mean value which appears to be accurate. Varying flow rates per usage event should be the most prone to average errors if the linear approximation is invalid but this is not the case - calculated mean flow rates for varying flow rates during events seems to be possible. This provides justification to focus on the measured and estimated mean flow rates per usage event and analyse the accuracy of the estimated mean flow rates.

Figure 6.7 shows the percentage $\bar{\dot{V}}_E$ error of the system for mean flow rates per identified reliable usage event in the experimental unit. The histogram shows that the majority of usage events have a low estimation error. Dataset 2 consisted of short duration, manually controlled flow events, therefore the overestimation due to start and stop vibration peaks contributed to larger estimation errors. Datasets 1 and 2 contained automated flow event control only and do not contain outliers like Dataset 2. This indicates that the manually controlled BV caused larger vibrations which resulted in higher estimated flow rates when BV was adjusted, and thus larger $\bar{\dot{V}}_E$ values.

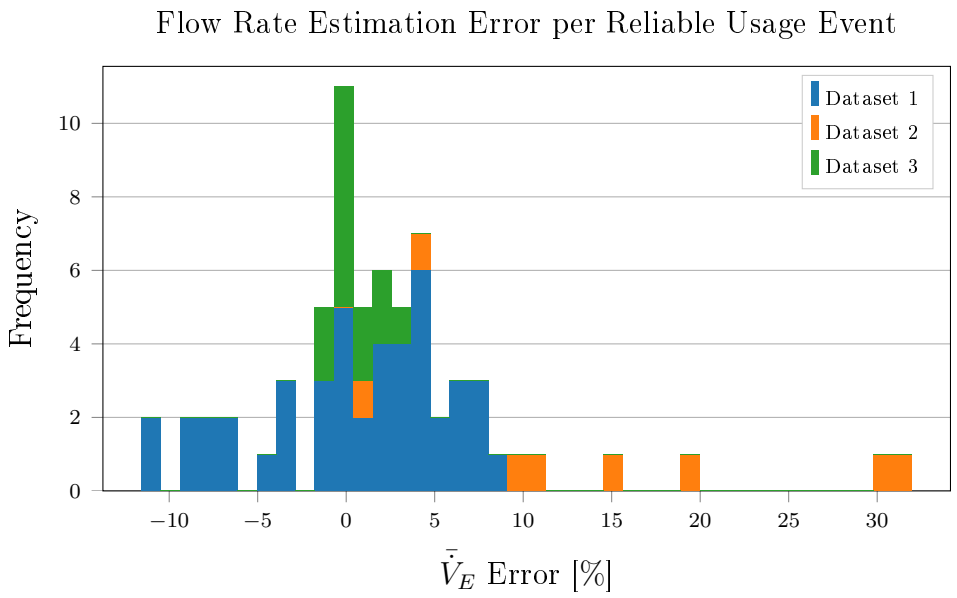

Figure 6.7: Flow rate estimation error per reliable usage event in Datasets 1, 2 and 3. The histogram shows the frequency and flow rate estimation error, $\dot{\bar{V}}_E$ Error, as a percentage of $\dot{\bar{V}}_M$. Only flow events which were marked as reliable by the algorithm are shown. The histogram is cumulative.

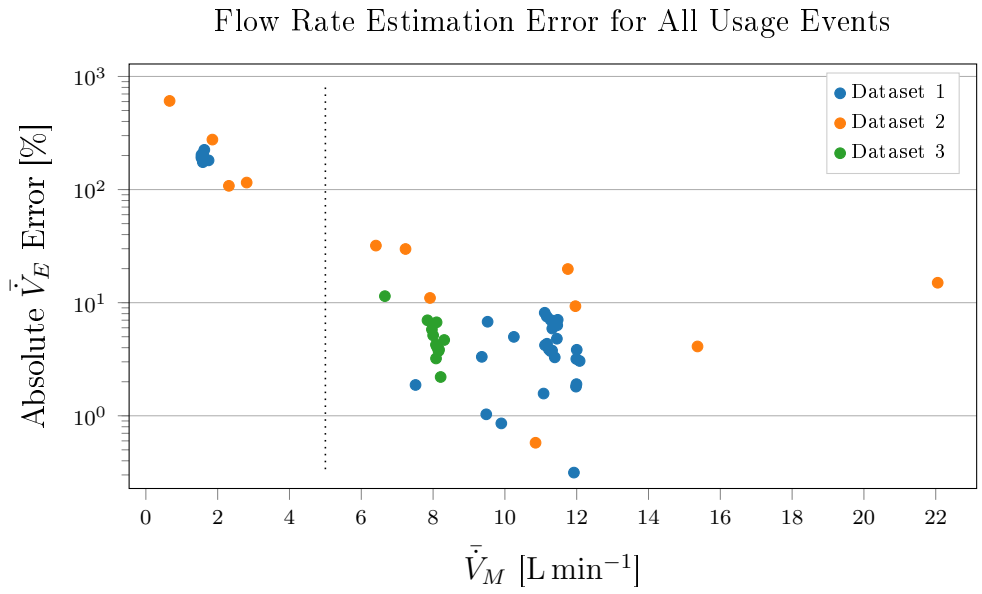

Figure 6.8: Absolute usage event flow rate estimation error relating to measured flow rate. The minimum flow rate threshold for quantitative estimation, $\dot{\bar{V}}_{(min)}$ of $5\,\mathrm{L\,min^{-1}}$, is indicated by a black dotted line.

Figure 6.8 shows the absolute error of $\bar{\dot{V}}_E$ as a percentage as a function of the measured flow rate. It can be seen that the system performs significantly better when used to estimate flow rates which are greater than $5\,\mathrm{L\,min^{-1}}$. Figure 6.8 represents the absolute estimation error for all experimental unit flow events. For usage events with measured flow rates greater than $5\,\mathrm{L\,min^{-1}}$ in Dataset 1 the estimation error was below 11 %.

The relationship between estimation error and $\bar{\dot{V}}_M$ does not appear to be inversely proportional. Low flow rate estimations are not reliable and the highest flow rates are not the significantly more accurately estimated than medium flow rates. The linear estimation method is successful and the estimation error decreases by an order of magnitude for measured flow rates above $\bar{\dot{V}}_{(min)}$.

6.5 Volumetric Estimation

Section 6.2 showed that the duration of usage events can be accurately estimated using vibration event detection and that usage events are accurately identified for normal conditions using thermal event classification. Section 6.4.2 showed that $\bar{\dot{V}}_E$ is within the specified accuracy for flow rates greater than $\bar{\dot{V}}_{(min)}$ $5\,\mathrm{L\,min^{-1}}$. Because the flow rate and duration of estimated events is reliable, the time integral of $\bar{\dot{V}}_E$ gives the estimated volumetric consumption V_E. Greater flow rates result in larger water volumes in the same time frame, therefore $\bar{\dot{V}}_E$ accuracy at greater flow rates is important and low flow rate estimation error may be less significant when the total volumetric consumption is considered.

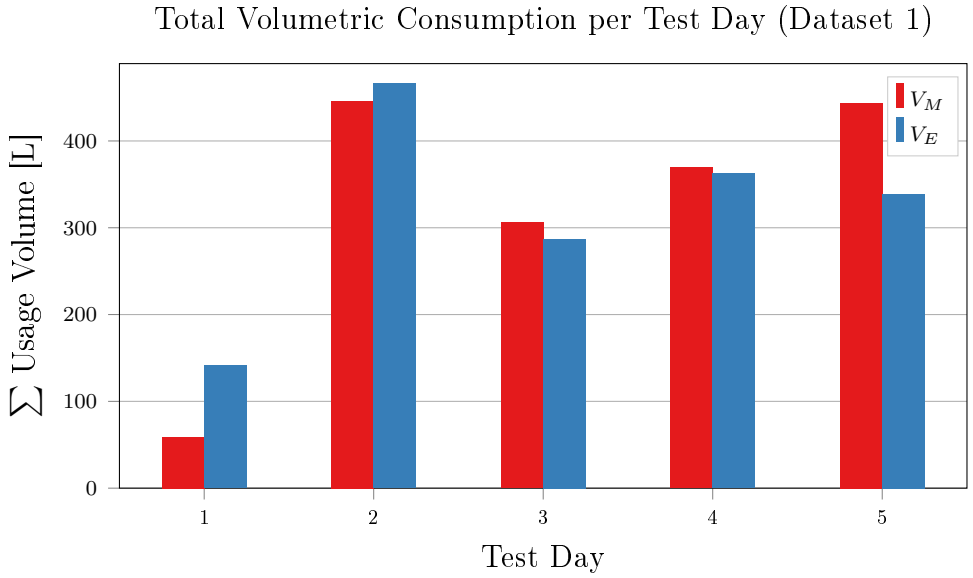

Figure 6.9: Total volumetric consumption per Test Day for Dataset 1. The total measured consumption, V_M, is shown and the total estimated consumption, V_E includes the effect of external vibration interference which prevented correct usage event detection on Test Days 1 and 5

Figure 6.9 shows the total measured and estimated volume usage during each Test Set in Database 1. All flow events within Dataset 1 were either 2 min or 5 min in duration. The volumetric estimation is more accurate for events which contained greater flow rates.

The difference between measured and estimated volumetric consumption for Test Days 2, 3 and 4 can be seen to small in comparison to the volumes being considered. Table 6.3 shows a breakdown of events volume usage details as a sum per Test Day.

Test Day	$\bar{\dot{V}}_M$ [L min^{-1}]	$\sum V_M$ [L]	$\sum V_E$ [L]	ΔV [L]	Error [%]
1	1.62	58.99	141.02	82.04	139.08
2	12.23	446.09	465.82	19.73	4.42
3	8.40	306.22	287.03	-19.18	-6.26
4	10.08	369.19	362.62	-6.57	-1.78
5	12.13	443.91	338.97	-104.94	-23.64

Table 6.3: Total volumetric estimation for Dataset 1. The total measured and estimated volumetric consumption is shown. This shows the results of the system in a simulated real world application

Table 6.3 shows the information displayed in Figure 6.9. It can be seen that the total volumetric error for Test Days 2, 3 and 4 are 4.42 %, −6.26 % and −1.78 % respectively. These results are well below the design goal of 10 % accuracy. Test Days 1 and 5 contained external vibration interference meaning that certain scheduled flow events were not detected.

Test Day	$\bar{\dot{V}}_M$ [L min^{-1}]	$\sum V_M$ [L]	$\sum V_E$ [L]	ΔV [L]	Error [%]
1	1.63	47.69	141.02	93.34	195.72
2	12.23	446.09	465.82	19.73	4.42
3	8.40	306.22	287.03	-19.18	-6.26
4	10.08	369.19	362.62	-6.57	-1.78
5	12.13	332.86	338.97	6.10	1.83

Table 6.4: Controlled volumetric estimation for Dataset 1. The temporal boundaries of non-invasively detected events were used (rather than the total measured consumption) to exclude the effect of interference events. The measured volume for each day is thus the sum of the flow meter pulses which occurred during detected usage events.

Table 6.4 shows the volumetric consumption capability of the designed algorithm after removing the effect of interference events. The non-invasively determined temporal boundaries were used to compare the measured volume during detected usage events with the estimated volume. It can be seen that the volumetric error for Test Day 5 in Table 6.4 is 1.83 % which is much lower than the −23.64 % error shown in Table 6.3. Thus it can be seen that the estimated volumetric consumption is accurate for detected events which are marked as reliable under normal circumstances.

Figure 6.10 shows the volumetric estimation error for all reliable usage event in Datasets 1, 2 and 3. V_E Error for the interference events during Test Sets 1.4 and 5.4 in Dataset 1 are not shown (as they were classified as interference events) but were −11.22 L and −111.04 L respectively because the flow events were not detected and estimation was thus

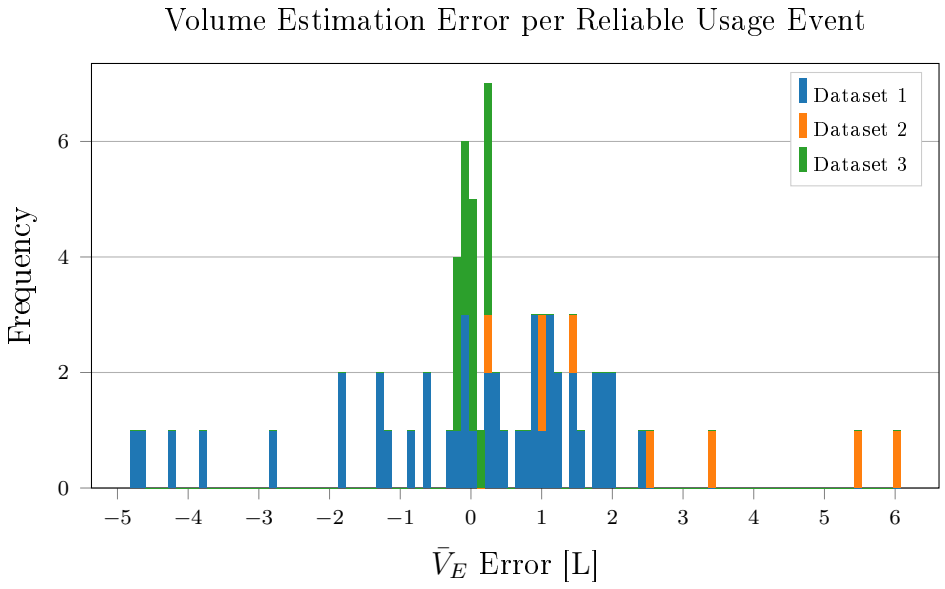

Figure 6.10: Usage Volume estimation error per usage event. The histogram shows the frequency and volumetric difference between $\bar{V}_M$ and $\bar{V}_E$. The frequency of the volumetric error bars are stacked.

not performed. It can be seen from Figure 6.10 that the volumetric discrepancy for each event is small when flow conditions are within the limitations of the algorithm.

The volumetric estimation capability can thus be considered to be accurate and sufficient for the application of providing the same accuracy and higher flow rate resolution than the current in-line flow meter. The algorithm provides sufficient results when operating within the limitations described in Section 5.5 and shown in Section 6.3.

6.6 Expected Performance in Field Units

The algorithm was shown to operate within the desired volumetric estimation accuracy boundaries for events which were classified as being reliable. The algorithm limitations mean that the flow estimation system can only perform accurately under certain conditions. The prevalence of these conditions in real world anonymous data and the expected performance of the system in real world scenarios was investigated. This was done by analysing 34 anonymous SGC user's water consumption data gathered over a period of 28 days. The data was contained in the Field Dataset which was acquired using the existing SGC system.

The Field Dataset was gathered using SGC and reflects real world usage events for 34 anonymous users in September 2016. The current SGC gathers data with 1 min temporal resolution with 0.5 L volumetric flow usage resolution. The Field Dataset thus has low sample rate and low flow resolution data structure as the existing SGC unit provided the data (Datasets 1, 2 and 3 consisted of 60 times greater temporal resolution and 170 times greater volumetric resolution).

The Field Dataset was acquired after the data was cleaned[1]. The data is anonymous so no information about the installation can be obtained (e.g. bachelor flat, house, kitchen,

[1]Thanks to Marcel Roux (marcel.roux@gmail.com) who supplied the cleaned Field Dataset.

etc). The Field data has a 1 min sampling rate and the in-line flow meters used measure water volume. The volumetric measurement for each Field Dataset sample can thus be considered to be equivalent to the mean flow rate used in Datasets 1, 2 and 3 ($\bar{\dot{V}}_M$).

Grouped usage behaviour from all 34 units was first analysed. The dispersion of flow rates which can be expected in real world use was established to determine which percentage of real world flow durations could be quantitatively estimated using the algorithm. The contribution of different flow rates to the total grouped volumetric consumption was shown to determine which percentage of the total volumetric consumption could be quantitatively estimated. Considering the usage information as a grouped set removes the information about usage event durations and the unique consumption behaviour of each unit. This grouped behavioural analysis is shown in Section 6.6.1.

Analysis of each unit individually was required in order to assess which portion of usage events could be estimated using the algorithm for each individual unit. This was necessary because the installation details of the units were not known which means that heavy users within the sample group can skew the trends which would be present in the total grouped set. The expected performance of the flow estimation algorithm can be assessed for individual users with specific consumption patterns. Individual analysis is shown in Section 6.6.2.

6.6.1 Grouped Behaviour

The grouped Field Data provided a breakdown of the duration and volumetric contribution of flow rates which can be quantitatively estimated using the algorithm. Temporal information is lost when grouping data in this way so the context of usage events is lost but a less complex breakdown of the large dataset is possible. The minimum flow rate algorithm limitation, $\bar{\dot{V}}_{(min)}$, was applied to the grouped data to determine the prevalence of flow rates which can be quantitatively estimated.

6.6.1.1 Grouped Summary

$\dot{V}_M$	$\dot{V}_E$ Type	Volumetric Composition [kL]	[%]	Temporal Composition [hour]	[%]
$< \bar{\dot{V}}_{(min)}$	Qualitative	46.3	**32.7**	367	**66.0**
$\geq \bar{\dot{V}}_{(min)}$	Quantitative	95.3	**67.3**	189	**34.0**

Table 6.5: Grouped Field data flow rate summary. The grouped analysis of the Field Data showed that only 34 % of the time which flow was measured in was above $\bar{\dot{V}}_{(min)}$. But the total volumetric contribution of these higher flow rates was 67.3 % of the total consumption for all units. The majority of the volumetric consumption could be quantitatively estimated.

Table 6.5 shows the total volumetric and temporal proportion of usage events which can be quantitatively estimated as the measured flow rate was greater than $\bar{\dot{V}}_{(min)}$. Both the measured units and percentage are shown. It can be seen that 67 % of the total volumetric consumption is composed of high enough flow rates that quantitative estimation is possible using the algorithm. Considering the total data alone is unwise and individual analysis of

each field test unit must be performed to see which users could benefit from non-invasive flow rate measurement.

6.6.1.2 Grouped Flow Rates

The flow rate composition of the Field Dataset was established. This relates to the portion of the duration of all measured flow rates which were observed to be above or below $5\,\mathrm{L\,min^{-1}}$.

The 1 min reporting time of the SGC means that the shortest possible recorded duration of a measured event was 60 s. Each sample can thus be considered to be $\bar{V}_M$. A sum of the number of unique flow rates was performed for the total dataset.

Figure 6.11 shows that $1\,\mathrm{L\,min^{-1}}$ flow events compose over 25 % of the total duration of usage events for the Field data. It can be seen that high flow rate samples comprise a much smaller percentage of the total event time that low flow rates. It is incorrect to assume that the non-invasive flow rate estimation system will not be useful in real world applications because higher flow rates contribute much more heavily to the volumetric water consumption than low flow rates.

Low flow rate events comprise 66 % of the total samples where flow occurs meaning that the majority of the duration of flow events are low flow rates. So the majority of flow events in the Field data can only be qualitatively estimated using the algorithm. Low flow events do not contribute as heavily to the total volumetric consumption as high flow rate events for the same duration.

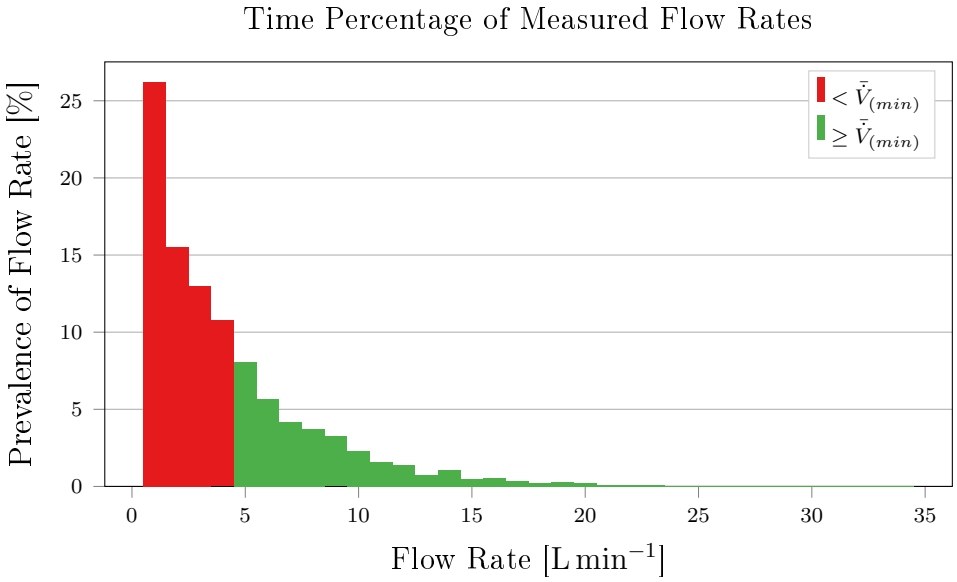

Figure 6.11: Histogram showing event duration composition at various flow rates. The amount of time which each flow rate was measured in the Field Data is shown. Red bars indicate samples where the flow rate is too low to be quantitatively estimated using the proposed system. Green bars indicate samples which can be estimated.

6.6.1.3 Grouped Volumetric Consumption

The grouped volumetric consumption was analysed to determine what portion of the total volumetric consumption of the Field data could be quantitatively estimated.

Although high flow rate events only form 34 % of the total time which flow was measured, high flow rate events contribute much more heavily to volumetric consumption than low flow rates for a fixed duration. The grouped volumetric consumption discards information about event duration and unit contributions and only investigates the total volume of water used at different flow rates.

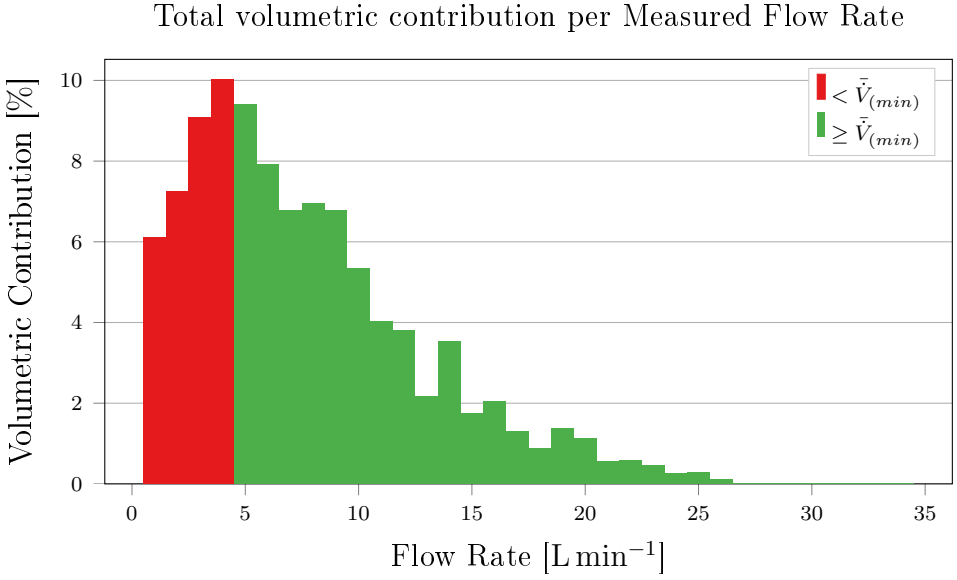

Figure 6.12: Volumetric Contribution By Flow Rate for Field Data. The Histogram shows the percentage volumetric usage contribution related to flow rate.

It can be seen in Figure 6.12 that higher flow rates are more prominent in the composition of the total grouped volumetric consumption measured in the Field data. 67.3 % of the total volumetric consumption occurred from flow rates which can be quantitatively estimated using the algorithm. This means that the non-invasive system, which is effective at medium and high flow rates, can estimate the usage events which most heavily contribute to grouped water usage each month.

6.6.2 Individual Analysis

Analysing the water consumption of each field test unit enables the usefulness of a non-invasive flow rate estimation system to be simulated for each field test unit.

Individual analysis of each unit enables access to temporal data. The algorithm limitations of 2 min cool down time between events and flow rates greater than 5 L min^{-1} can be investigated for each user.

6.6.2.1 Individual Consumption Composition

It was found that low flow rates more heavily contributed to conditions unsuited to quantitative estimation than insufficient cool down time between events for the grouped Field data.

The individual analysis of the Field units in terms of flow rate composition is given in Table C.3 and Figure C.3 for more details. Observations regarding individual flow rate and volumetric consumption were made. The volumetric contribution of sufficiently high flow rates to each unit's total consumption was determined.

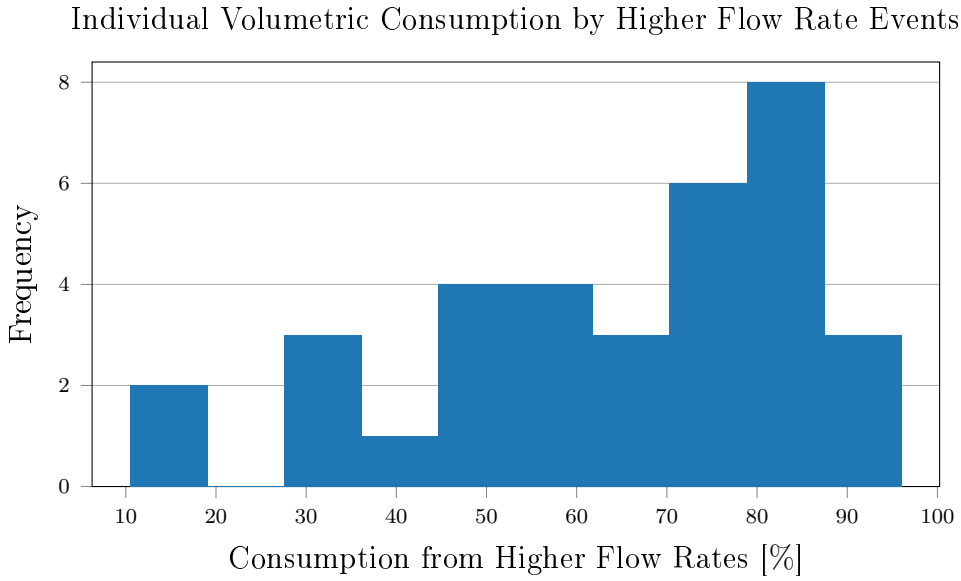

Figure 6.13: Individual volumetric consumption by higher flow rate events. The histogram shows the number of Field units (out of 34) and the fraction of each total consumption volume which was contributed by flow rates which can be quantitatively estimated using the algorithm. It can be seen that the majority of users' total consumption consists of flow rates which are greater than $\bar{\dot{V}}_{(min)}$.

It can be seen from Figure 6.13 that individual units typically contain mostly higher flow rate events. The flow estimation algorithm was determined to be accurate for the flow rate ranges which the histogram in Figure 6.13 depicts. This means that the majority users have monthly volumetric consumption values which are contributed to by flow rates which the algorithm has been shown to produce accurate flow estimations.

6.6.2.2 Simulated Event Detection

The only reason for an expected event detection failure is insufficient cool down time. The time between measured flow events was analysed for the 34 units to determine how often less than 2 min occurred between events in the Field data. Both algorithm limitations, t_{cd} and $\bar{\dot{V}}_{(min)}$, could be applied to individual anonymous users to simulate the performance of the designed system if applied to each user. Including the cool down limitation relating to event detection allowed for simulated usage event detection. Further analysis of the measured flow rates during detectable events enabled reliability classification to be simulated for the Field data.

Simulated event detection was performed and measured events which had more than 2 min of no-flow before the start of flow were marked as detected events. The volumetric consumption which was measured during detected events was identified. This value, $V_{M(Ideal)}$, can be thought of as the volume of water which would be estimated if estimation was 100 % accurate at all flow rates (i.e. only applying t_{cd} limitation) and thus excludes all water consumption which would not have met the thermal criteria.

Simulated reliable estimate values, $V_{E(Reliable)}$, were created to simulate the performance of the algorithm to estimate volumetric consumption with both $\bar{\dot{V}}_{(min)}$ and t_{cd} limitations applied. Reliable estimates consisted of detectable events (more than 2 min of no flow prior to event) which contained measured flow rate values greater than $5\,\mathrm{L\,min^{-1}}$. The reliable estimation is the simulated performance of the system without low flow rate approximation.

The percent of the total monthly consumption which would have been quantitatively estimated, $V_{E(Reliable)}$, was found to vary between 8.5 % and 93.7 % for different users. This is a large range of the total consumption measured for different users which can be quantitatively estimated, meaning that the algorithm cannot be deemed to be effective for all users. It was established in Section 6.2.4 that the algorithm can consistently classify low flow rate events (unreliable events). Low flow rate approximation was investigated to improve the estimation ability for users who have larger numbers of flow rate events.

6.6.2.3 Low Flow Rate Approximation

The mean measured flow rate for all measured flow rates below $\bar{\dot{V}}_{(min)}$ was $\approxeq 2\,\mathrm{L\,min^{-1}}$. This value was selected to be the constant approximation value to substitute for qualitative low flow rate estimation. The constant flow rate was applied to each sample where flow rates below $\bar{\dot{V}}_{(min)}$ were detected to form the estimation with approximation value, $V_{E(Approx)}$.

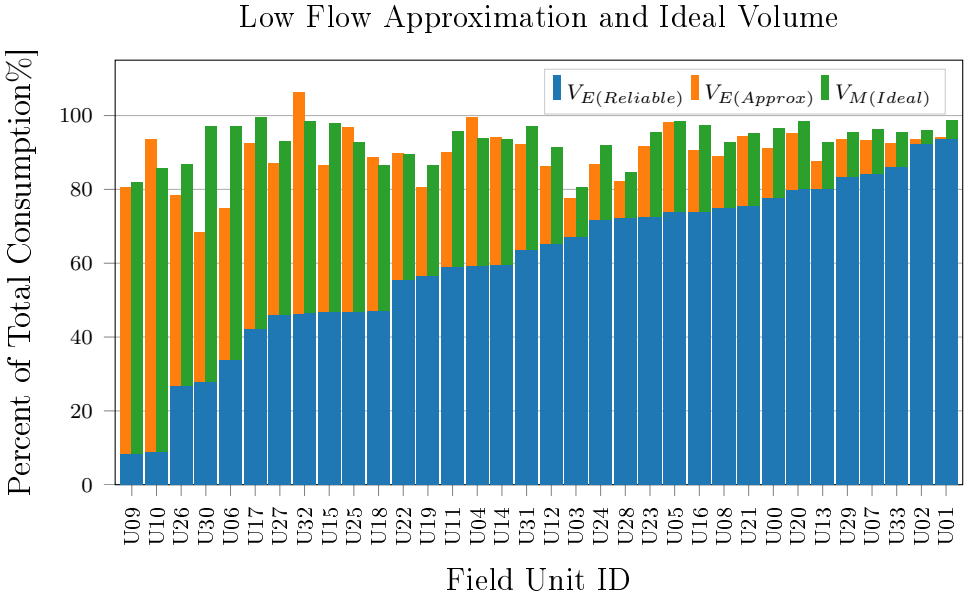

Figure 6.14: The effect of low flow approximation is shown. The values are shown as a percentage of the total measured volumetric consumption for each unit. The reliable estimation, $V_{E(Reliable)}$ (blue) forms the baseline to show the quantitative estimation which was simulated for each unit. The additional approximation of low flow rates during flagged events, $V_{E(Approx)}$ (orange). The ideal measurement of low flow rate events, $V_{M(Ideal)}$ (green) are shown. The Field units are arranged in ascending order of $V_{E(Reliable)}$.

The positive effect of low flow rate approximation can be seen in Figure 6.14. The Field units on the left hand side of Figure 6.14 (which had the worst consumption estimation

performance) were substantially improved. After approximation was performed the lowest consumption estimation was 68.4 % and the most accurate estimation was 99.4 %. The approximation had a drastic improvement on previously badly performing users and little detriment to previously better performing users. It can be seen from Figure 6.14 that the estimated volume when using an approximated constant low flow rate, $V_{E(Approx)}$, results of consumption volumes which are generally close to the ideal volume $V_{M(Ideal)}$ (the measured volume when only t_{cd} is applied).

Field unit U32 was the only unit to have an overestimated consumption value. A more detailed discussion relating to the simulated performance of the system and user consumption patterns can be found in Section C.4.2. Field unit U32 is discussed in particular. The total volumetric Field data can be found in Figure C.4.

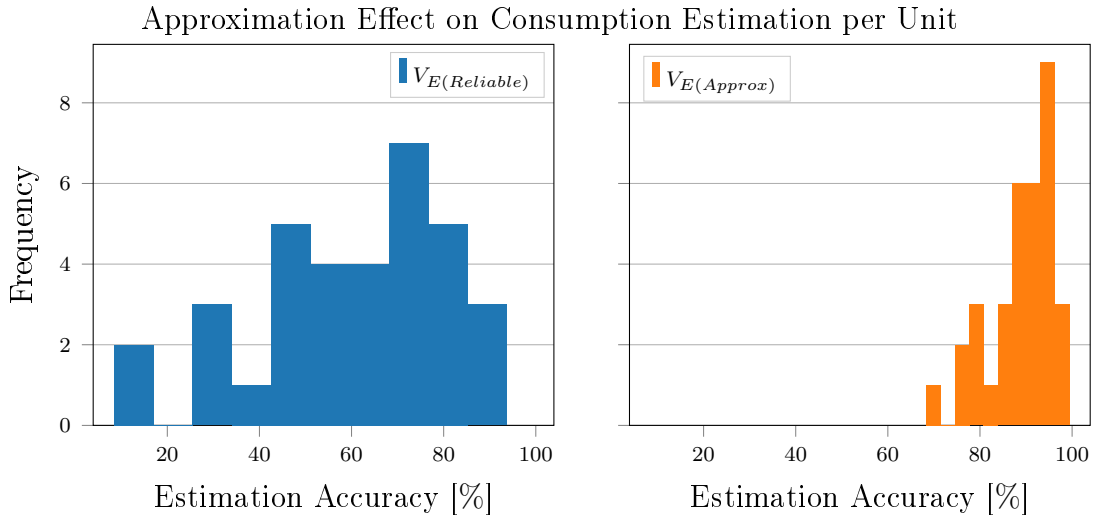

Figure 6.15: Histograms showing the accuracy of the estimated consumption for the 34 Field units as a percentage of the total measured consumption. The distribution using no low flow approximation, $V_{E(Reliable)}$, is shown in blue. The distribution using low flow approximation, $V_{E(Approx)}$, is shown in orange.

The simulated performance of the algorithm with and without low flow approximation is shown in Figure 6.15. The histograms show the prevalence of the consumption estimation performance for each Field unit. It can be seen that the field units performed better when approximation was applied, $V_{E(Approx)}$ (orange). This shows that low flow rate approximation means that a larger proportion of users can benefit from the non-invasive flow estimation algorithm. Certain user consumption patterns do not fall within the algorithm limitations, but low flow approximation removes the severity of this effect for users with consumption patterns which do not agree with the algorithm limitations as can be seen in Figure 6.15 where the majority of users have higher estimation accuracy after low flow approximation is performed.

Table 6.6 shows that low flow approximation increased the simulated volumetric estimation when using the algorithm (as a percent of total measured volumetric consumption for each unit) from 61 % to 89 %. This means that the volume estimation using the algorithm for the population was improved with low flow approximation.

Method	Percentage of Total Measured consumption [%]						
	Mean	Std	Min	Q1	Q2	Q3	Max
$V_{E(Reliable)}$	60.61	21.92	8.46	46.89	64.44	75.41	93.73
$V_{E(Approx)}$	89.01	6.96	68.45	86.74	90.88	93.64	99.38

Table 6.6: Effect which low flow rate approximation has on the simulated performance of the algorithm on Field units. The algorithm limitations mean that many flow events cannot be detected or quantitatively estimated based on user behaviour. Low flow approximation gives more consistent and better performance for simulated real world applications. The mean, standard deviation, minimum, first quartile, median, third quartile and maximum volumetric estimation values are given as a percentage of total measured consumption for the 34 individual Field units.

It can be seen from Figure 6.15 that the simulated estimation accuracy improved with the use of approximation because the grouping of the histogram shifts to higher percentage values. It can also be seen that the simulated performance seems to be more consistent throughout the 34 users as indicated by the tighter grouping of the $V_{E(Approx)}$ histogram. This is quantitatively confirmed by the reduction of the standard deviation, 'Std' in Table 6.6 from 22 % to 7 %. This indicates more consistent performance of the algorithm for most users, at a higher percent of their monthly consumption value.

Constant low flow rate approximation can thus be seen to improve the performance of all users but most improve users who often use low flow rates (which is indicated by a small $V_{E(Reliable)}$ value in Figure 6.14). These users would definitely not be suitable for non-invasive flow estimation without using low flow rate approximation. But these poor performing users had the greatest benefit when using low flow approximation. The lowest percentage of monthly consumption which could be estimated increased from 8.46 % to 68.45 % ('Min' in Table 6.6). The first quartile, 'Q1', also increased from 46.89 % to 86.74 %, which is a large 40 % improvement.

Better performing users (more to the right hand side of Figure 6.14) also received improvement although not as dramatically as the poorly performing users. This can be seen as the third quartile, 'Q3', can be seen to have improved by approximately 20 % in Table 6.6.

Low flow rate approximation was seen to be very effective when applied to the Field Dataset. It was observed to be effective for all users.

Chapter 7

Conclusion and Recommendations

7.1 Conclusion

The purpose of the research was to design a non-invasive water flow meter with the intention of applications in smart geyser system. The research question for the project was:

Can non-invasive flow measurement reduce installation costs and user inconvenience, while providing the required flow estimation accuracy for domestic EWH applications?

7.1.1 Hypothesis Testing

Two hypotheses were presented regarding the possibility of the design of a non-invasive flow rate meter for EWH applications.

Hypothesis 1 *It is not possible to design a non-invasive flow estimation algorithm using only thermal methods for a domestic EWH application.*

A simplified steady-state thermal difference model was shown to be insufficient for quantitative flow rate estimation using only non-invasive thermal data in Section 3.2. Preliminary thermal experiments did not correlate with the expected behaviour given by steady-state model.

A more complex thermal pipe model was developed. The thermal pipe model was simulated in software to determine whether a more complex thermal model is sufficient or whether physical constraints of the system mean that thermal methods cannot be used in isolation. It was determined that the measurable longitudinal temperature decrease over lengths of pipe which can be expected in domestic installations is too small to measure with practical temperature sensors. The measured thermal data did not correlate with the simulated thermal behaviour and it was concluded that the accuracy of temperature measurement is heavily dependant on the mounting configuration.

Heat sinks were installed on the experimental unit outlet pipe and care was taken to ensure that the thermal coupling was conducive to heat transfer between the temperature sensors and outlet pipe. The results obtained using the experimental unit reflected the results obtained from preliminary thermal testing. A greater temperature difference was measured when a heat sink was used, but the temperature readings at each flow rate

were inconsistent when constant readings were expected. This suggests that the measured temperature difference and measured flow rate were not closely correlated for the experimental conditions.

The impractically small temperature difference and intricate installation of temperature sensors meant that Hypothesis 1 was confirmed. The use of thermal data for quantitative domestic EWH flow rate estimation is not possible in a more convenient manner than the invasive installation of an in-line flow meter.

Hypothesis 2 *It is possible to design a non-invasive flow estimation algorithm using the combination of vibration and thermal methods to provide suitable flow esimation accuracy for domestic EWH application.*

A non-invasive flow estimation algorithm was designed using the fusion of thermal and vibration methods as shown in Section 5. The designed flow estimation algorithm was able to sufficiently fulfil the research objectives and was thus confirmed.

7.1.2 Objectives Fulfilment

The flow estimation algorithm was required to be able to reliably detect water consumption events and to provide sufficiently accurate volumetric flow estimation. The objectives were set up in order to test the methods use to achieve the desired performance.

Objective 1: Non-invasive Usage Event Detection

Develop a non-invasive system which can detect the temporal boundaries of water usage events, determine which events are caused by hot water flow and which events can receive reliable quantitative flow rate estimation.

Objective 1 was divided into three sub-objectives relating to usage event detection:

1(a): Temporal boundary detection of possible usage events.

1(b): Classification of the cause of possible usage events.

1(c): Low flow rate usage event identification.

Objective **1(a)** was accomplished using vibration event detection. The temporal boundaries of all vibration events which contained flow were identified in the experimental unit (excluding external vibration interference in Dataset 1). The duration of usage events had an estimation error of less than 10 % for normal conditions. In Dataset 1 the longest duration over estimation which was measured was 9 s for no vibration interference. Objective **1(a)** was successfully achieved.

Objective **1(b)** was accomplished by usage event detection. Temporal boundaries of events were obtained using vibration data and thermal event classification was performed based on whether thermal criteria were met. Usage event detection was successful when no vibration interference was present and when usage events had sufficient cool down time between events. The minimum cool down time, t_{cd}, was determined to be 2 min. In Dataset 1 there were 60 scheduled flow events of which 55 were correctly detected and classified with usage event detection. The 5 usage events which were incorrectly

classified as interference events occurred during times of measured external vibration interference. 95.4 % of the total duration of events in Dataset 1 were correctly identified and classified. There were no detected usage events which did not correspond to measured flow in Datasets 1;2;3 meaning that no false positives were present. Objective **1(b)** was successfully achieved.

Objective **1(c)** was successfully achieved using 'reliability' detection using vibration standard deviation thresholds. Vibrations thresholds were established to non-invasively determine when the flow rate was greater than $\dot{\bar{V}}_{(min)}$ for a detected usage event meaning that quantitative flow rate estimation was possible. The detection of reliable usage events was 100 % successful in Datasets 1, 2 and 3. Objective **1(c)** was successfully achieved.

Objective 2: Non-invasive Flow Estimation

Develop a non-invasive flow estimation algorithm using sensors which can be installed on an EWH without skilled labour as a retrofit solution, and is able to provide similar flow usage data as the invasive flow meter which is currently used..

2(a): Instantaneous flow rate estimation.

2(b): Mean flow rate estimation accuracy.

2(c): Volumetric consumption estimation accuracy.

2(d): Determine the algorithm limitations and practicality of the estimation algorithm limitations for real world implementation.

Objective **2(a)** was verified using Dataset 2. The quantitative flow estimation using vibration standard deviation was determined to be successful as demonstrated by the ability of the algorithm to track the instantaneous flow rate changes deliberately performed in Dataset 2. Instantaneous flow rate estimation was not successful for measured flow rates less that $\dot{\bar{V}}_{(min)}$ of $5\,\mathrm{L\,min^{-1}}$. Due to the fluctuating nature of flow-induced vibrations the instantaneous flow rate estimation was determined to be successful by examining instantaneous flow data in a qualitative way. Objective **2(a)** was determined to be successful within identified flow rate limitations.

Objective **2(b)** was deemed to be successful by comparing the estimated and measured mean flow rate for detected reliable usage events. For flow rates greater than $5\,\mathrm{L\,min^{-1}}$ the estimation error was below 11 % for Datasets 1 and 3. Estimation error in Dataset 2 was up to 30 % for the certain usage events. It is suspected that the manually controlled flow adjustment using the ball valve, which was only used in Dataset 2, created larger vibrations during shorter duration flow events contributed to the greater mean flow rate estimation errors. Objective **2(b)** was successfully achieved for expected use conditions and with identified flow rate limitations.

Objective **2(c)** was successfully achieved as demonstrated by the analysis of experimental unit Datasets. For reliable detected usage events in Dataset 1 the maximum volumetric error for repeat testing was 6.26 %. For the reliable usage events in Datasets 1, 2 and 3 the estimated consumptions per event ranged between 5 L below to 6 L above the measured consumption. Objective **2(c)** was successfully achieved.

Objective **2(d)** was to determine the expected performance of the flow estimation algorithm for real world conditions. The Field Dataset was analysed and the algorithm limitations of at least 2 min between usage events and a minimum flow rate of 5 L min^{-1} for quantitative estimation to be possible. It was seen that only 34 % of the total measured duration of flow was within these limitations. But it was found that 67.3 % of the volumetric consumption was within these limitations. Individual users were assessed and the poorest and best performing users had 8.5 % and 93.7 % of the total measured consumption which was estimable using the algorithm with limitations. The mean percentage of total consumption which fell within the limitations was 60.6 %. A fixed low flow rate approximation of 2 L min^{-1} was made for unreliable detected events which improved the simulated performance of the estimation algorithm considerably. For individual users the range became between 68.5 % and 99.4 % with a mean value of 89.1 % of the measured monthly consumption being correct. With the additional low flow rate approximation Objective **2(d)** can be considered to be successful. The individual user behaviour was seen to affect the number of events which can be detected and estimated. Users who frequently use low flow rate events for short durations are unlikely to be able to have non-invasive flow estimation using the algorithm. Users who usually have more than 2 min between usage events and consume higher flow rates are likely to benefit from the designed non-invasive flow estimation algorithm.

7.1.3 Overall Evaluation

The designed non-invasive flow estimation algorithm was determined to perform sufficiently on the experimental EWH unit used. The minimum required sensors for algorithm to be successful using the experimental unit were an inlet pipe accelerometer and an outlet pipe temperature sensor. Volumetric consumption estimation for expected use conditions was found to be below the required 10 % error margin to consider the project to be successful. The objectives were achieved for all measured cases or achieved for cases which fall within identified algorithm limitations. The identified algorithm limitations were applied to measured water consumption data from 32 anonymous SGC users and it was determined that certain users had consumption patterns which would facilitate the implementation of the estimation algorithm with a high success rate. Approximate values for low flow rate events were inserted and this improved the performance of the algorithm especially for previously poorer performing users.

The non-invasive flow estimation algorithm can be seen as a successful proof of concept which performs well for the specific EWH used in the experiments. The minimum temporal and flow rate limits for the specific EWH indicate that sufficient performance may be expected when applied to measured consumption patterns of existing SGC users. Non-invasive flow estimation was performed using a system which did not require expensive components or a complex installation procedure.

For this reason the research question can be positively answered: Non-invasive flow measurement can reduce installation costs and user inconvenience, while providing the required flow estimation accuracy for domestic EWH applications.

7.2 Recommendations

More field data is required to verify the success and implementability of the designed algorithm. It is advised that a sample of SGC users receive an additional system to measure the required accelerometer and temperature data during real-world usage conditions. Several factors can then be analysed:

- Universal validity of vibration thresholds used in vibration event detection.
- Universal minimum flow rate required for sufficiently accurate quantitative flow rate estimation using vibration data.
- Universal validity of vibration thresholds used to identify reliable events.
- Whether consistent vibration and flow rate proportionality are present.
- Develop a more detailed understanding of how user consumption patterns affect the performance of the non-invasive flow estimation algorithm.
- Determine the minimum sensor requirements for thermal event classification.

If sufficiently large quantities of useful data can be gathered it is advised to use machine learning to attempt to design an on-site calibration system to determine the thermal and vibration threshold values for event detection and the parameters for flow estimation to be accurate. It may be possible that tests like the ones performed in Datasets 2 and 3 may be sufficient to gather enough data at various flow rates and with spacing between flow events for individual calibration for a specific installation. If an installation technician can take an in-line flow meter with for the installation and make sure that no unaccounted hot water is consumed during the installation process then this may be possible. The in-line flow meter can be temporarily attached to e.g. the hot water outlet of a bath and flow can be induced according to a determined 'installation plan' to measure flow rates for the duration of the calibration process. The high resolution data can then be processed and the required calibration parameters applied to the system. It was indicated that a single temperature sensor and accelerometer could be used for thermal event classification for the experimental EWH and provide sufficient results. But the experimental unit was kept in controlled conditions. Additional real world consumption data is required before the minimum requirements can be determined.

More real world usage data is required before progress and refinements are possible.

Appendices

Appendix A

Thermal Modelling Appendix

A.1 Semi-Discrete Boundary Conditions Application

To illustrate the process of applying boundary conditions a simple M =3, N =4 example can be considered. Explicitly writing the ODEs for the simple system for certain boundary conditions shows why certain discretisation decisions were made. Only the internal points can be described by the model, thus the external points must be eliminated using boundary conditions. The boundary conditions implemented in the model are:

- j =0: • Water interface
- j =M-1: • Air interface
- i =0: • Fixed temperature
- i =N-1: • Zero flux

A visual depiction of the relevant $M \times N$ section is displayed for clarity:

$$\begin{bmatrix} T_{-1,-1} & T_{-1,0} & T_{-1,1} & T_{-1,2} & T_{-1,3} & T_{-1,4} \\ T_{0,-1} & \begin{bmatrix} T_{0,0} & T_{0,1} & T_{0,2} & T_{0,3} \end{bmatrix} & & & & T_{0,4} \\ T_{1,-1} & \begin{bmatrix} T_{1,0} & T_{1,1} & T_{1,2} & T_{1,3} \end{bmatrix} & & & & T_{1,4} \\ T_{2,-1} & \begin{bmatrix} T_{2,0} & T_{2,1} & T_{2,2} & T_{2,3} \end{bmatrix} & & & & T_{2,4} \\ T_{3,-1} & T_{3,0} & T_{3,1} & T_{3,2} & T_{3,3} & T_{3,4} \end{bmatrix}$$

Thus each time an external point appears in an equation describing an internal point it must be eliminated using the relevant boundary condition. A list of the $M \times N$ ODE's is listed showing which boundary condition was used to eliminate external points.

$$
\begin{aligned}
\frac{\partial T_{0,0}}{\partial t} &= -\frac{v}{\Delta z}[T_{0,0} - \cancel{T_{0,-1}}] + \frac{1}{\rho_w c_{pw} \Delta r}\frac{2}{r}k_c[T_{1,0} - T_{0,0}] + \frac{v}{\Delta z}T_{fixed} \\
\frac{\partial T_{0,1}}{\partial t} &= -\frac{v}{\Delta z}[T_{0,1} - T_{0,0}] + \frac{1}{\rho_w c_{pw} \Delta r}\frac{2}{r}k_c[T_{1,1} - T_{0,1}] \\
\frac{\partial T_{0,2}}{\partial t} &= -\frac{v}{\Delta z}[T_{0,2} - T_{0,1}] + \frac{1}{\rho_w c_{pw} \Delta r}\frac{2}{r}k_c[T_{1,2} - T_{0,2}] \\
\frac{\partial T_{0,3}}{\partial t} &= -\frac{v}{\Delta z}[T_{0,3} - T_{0,2}] + \frac{1}{\rho_w c_{pw} \Delta r}\frac{2}{r}k_c[T_{1,3} - T_{0,3}]
\end{aligned}
$$

$$
\begin{aligned}
\frac{\partial T_{1,0}}{\partial t} &= \frac{\alpha}{\Delta z^2}[T_{1,1} - 2T_{1,0} + \cancel{T_{1,-1}}] + \frac{\alpha}{\Delta r^2}[T_{2,0} - 2T_{1,0} + T_{0,0}] + \frac{\alpha}{\Delta z^2}T_{fixed} \\
\frac{\partial T_{1,1}}{\partial t} &= \frac{\alpha}{\Delta z^2}[T_{1,2} - 2T_{1,1} + T_{1,0}] + \frac{\alpha}{\Delta r^2}[T_{2,1} - 2T_{1,1} + T_{0,1}] \\
\frac{\partial T_{1,2}}{\partial t} &= \frac{\alpha}{\Delta z^2}[T_{1,3} - 2T_{1,2} + T_{1,1}] + \frac{\alpha}{\Delta r^2}[T_{2,2} - 2T_{1,2} + T_{0,2}] \\
\frac{\partial T_{1,3}}{\partial t} &= \frac{\alpha}{\Delta z^2}[\cancel{T_{1,4}} - 1T_{1,3} + T_{1,2}] + \frac{\alpha}{\Delta r^2}[T_{2,3} - 2T_{1,3} + T_{0,3}]
\end{aligned}
$$

$$
\begin{aligned}
\frac{\partial T_{2,0}}{\partial t} &= \frac{\alpha}{\Delta z^2}[T_{2,1} - 2T_{2,0} + \cancel{T_{2,-1}}] + \frac{\alpha}{\Delta r^2}[(-1 - \frac{h_{air}\Delta r}{k_c})T_{2,0} + T_{1,0}] + \\
&\quad \frac{\alpha h_{air}}{k_c \Delta r}T_\infty + \frac{\alpha}{\Delta z^2}T_{fixed} \\
\frac{\partial T_{2,1}}{\partial t} &= \frac{\alpha}{\Delta z^2}[T_{2,2} - 2T_{2,1} + T_{2,0}] + \frac{\alpha}{\Delta r^2}[(-1 - \frac{h_{air}\Delta r}{k_c})T_{2,1} + T_{1,1}] + \frac{\alpha h_{air}}{k_c \Delta r}T_\infty \\
\frac{\partial T_{2,2}}{\partial t} &= \frac{\alpha}{\Delta z^2}[T_{2,3} - 2T_{2,2} + T_{2,1}] + \frac{\alpha}{\Delta r^2}[(-1 - \frac{h_{air}\Delta r}{k_c})T_{2,2} + T_{1,2}] + \frac{\alpha h_{air}}{k_c \Delta r}T_\infty \\
\frac{\partial T_{2,3}}{\partial t} &= \frac{\alpha}{\Delta z^2}[\cancel{T_{2,4}} - 1T_{2,3} + T_{2,2}] + \frac{\alpha}{\Delta r^2}[(-1 - \frac{h_{air}\Delta r}{k_c})T_{2,3} + T_{1,3}] + \frac{\alpha h_{air}}{k_c \Delta r}T_\infty
\end{aligned} \tag{A.1}
$$

The MxN example boundary condition elimination shown in equation array (A.1) should illustrate why certain discretisation decisions were made. All the points present in the ODE describing an internal point need to be accounted for. External points are present in equations describing boundary points, and thus the external points must be eliminated using the relevant boundary conditions. In certain scenarios then only forward differencing or backward differencing enabled external points to be eliminated.

Appendix B

Experimental Unit Appendix

B.1 Hardware Design

Installation Photographs

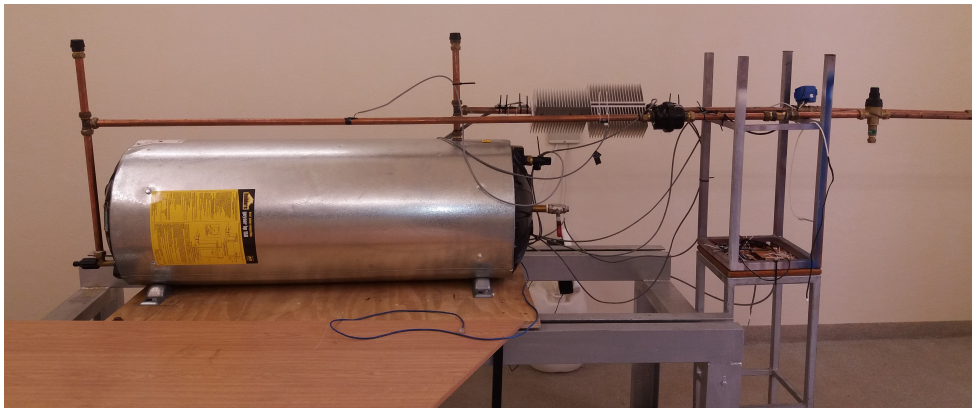

Figure B.1: Experimental Unit Photograph.

Figure B.2: A side view of the experimental unit showing the plumbing configuration of the inlet and outlet pipes.

Figures B.1 and B.2 show photographs of the experimental unit. The EWH can be seen to be mounted horizontally to to a sturdy table with a metal frame. The inlet an outlet pipes can be seen on the right of the picture, where they rise above the level of the vacuum breakers and pass through a wall to the exterior to fulfil the installation regulations for EWH units. The support system holds the inlet and outlet pipes up, simulating how the water pipes are fastened to (typically) wooden supports.

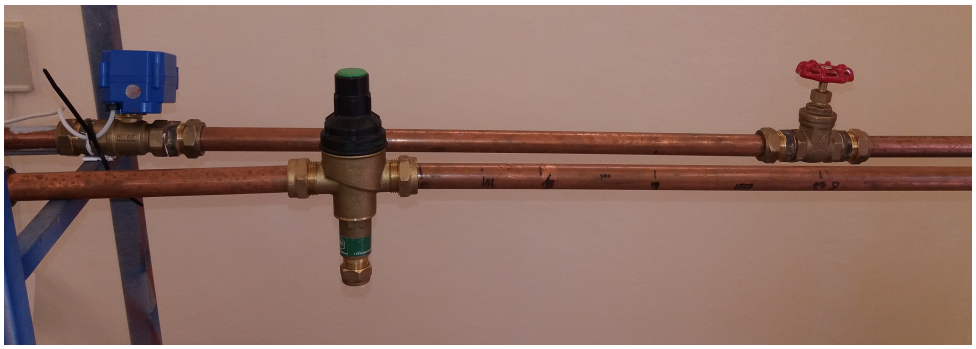

Figure B.3: Photograph showing the flow control components. The blue DN20 automatically controlled solenoid valve, *SV*, is shown on the left. The red manually controlled ball valve, *BV* is shown on the right of the photograph. The pressure control valve is the valve with green which is required to be installed in the cold inlet pipe.

Figure B.3 shows the flow control components. SV controls the flow by opening and closing fully when scheduled using the Raspberry Pi and acquisition system. The flow rate during experiments was manually controlled using BV.

Figure B.4: EWH Outlet Pipe. The 'near' temperature sensors can be seen mounted on the left side of the image on the outlet pipe, the two pairs of heat sinks can be seen mounted downstream, and further downstream the 'far' temperature sensors. *CFM* can be seen on the inlet pipe in the right of the photograph.

Heat Sink Analysis

The two pairs of heat sinks, shown in Figure B.4, were installed on the experimental unit outlet pipe to maximise the longitudinal temperature losses during water flow in order to test Hypothesis 1 for a 'best-case' scenario. The heat sinks were installed to investigate whether thermal data could be used for quantitative flow rate estimations when ideal conditions were present.

The heat sinks used were 510-3U produced by Wakefield-Vette. Four heat sinks 187 mm in length and were milled to have a 22 mm radius to enable mounting to the pipe. The heat sinks were modified to be mounted in opposing pairs to cover the external pipe surface area. The combined cost of the four heat sink was similar to the EWH unit, thus the expensive heat sinks were only intended to be used on the experimental unit. The addition of the heat sinks provided an ideal scenario to investigate using thermal data in isolation to measure domestic hot water flow (using inexpensive sensors which required a simple installation). If the addition of the heat sinks resulted in a system which could use thermal data in isolation then further investigation would be required into the minimum heat sinks needed for successful operation. If the ideal scenario provided the same limitations as experienced in the preliminary thermal tests, discussed in Section 3.7, it could be determined that the use of thermal data in isolation is not a practical solution for domestic hot water flow.

Non-insulated copper pipe has thermal losses of approximately $60\,\mathrm{W\,m^{-1}}$ for domestic EWH conditions [39]. The additional heat loss provided by the four heat sinks was 41 W. The installed heat sinks approximately the same effect as having an additional length of 0.66 m of non-insulated copper pipe near the EWH outlet. Measured temperatures associated with the lowest water flow rate were used, where the maximum heat loss associated with heat sinks was experienced.

The heat loss calculation pertaining to the heat sinks are shown in Equation (B.1):

$$Q = \frac{T_{pipe} - T_{\infty}}{R_{HS}} = \frac{43.0 - 19.9}{0.56} \tag{B.1}$$

where Q is the heat loss associated with the heat sinks (in W), T_{pipe} in the average of the upstream and downstream temperature measurements (in °C), T_{∞} is the measured ambient temperature (in °C), and R_{HS} is the rated thermal resistance of the heat sinks of $0.56\,^{\circ}\mathrm{C\,W^{-1}}$ [40].

Temperature Sensors

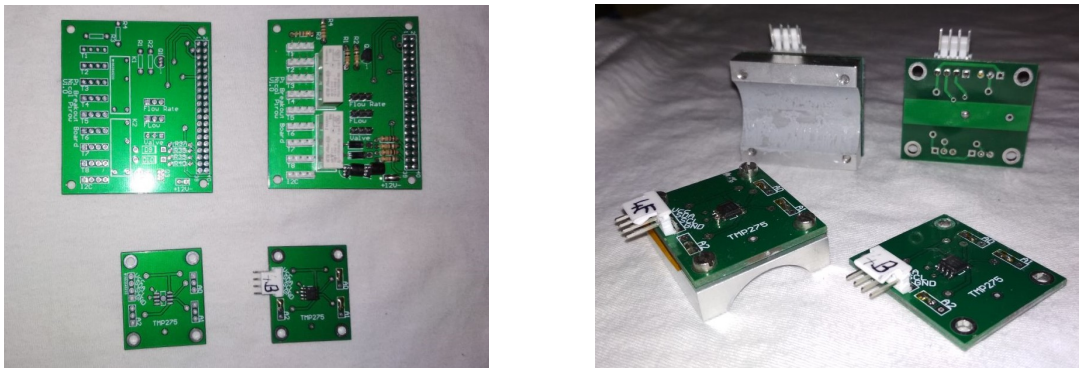

(a) Unpopulated and Populated PCBs (b) TMP275 mounting methods 2 and 3

Figure B.5: PCB Photographs.

ID	Address	Location	Distance [mm]	Mounting
T_{N1}	0x49	Outlet	105	1
T_{N2}	0x4B	Outlet	145	2
T_{N3}	0x4D	Outlet	185	3
T_{F1}	0x4A	Outlet	595	1
T_{F2}	0x4E	Outlet	645	2
T_{F3}	0x4F	Outlet	685	3
T_{In}	0x4C	Inlet	1550	2
T_{∞}	0x48	Suspended	X	2

Table B.1: TMP275 mounting details.

Table B.1 shows the addresses, locations and mounting configurations used for each sensor. The distance shown is in relation to the nearest right angle plumbing connection found on the EWH side of the each respective pipe section. T_{∞} was suspended as far from the EWH and from any metal surfaces as possible. The 'near' sensors, denoted by the subscript N, are upstream and the 'far' sensors (subscript F) are downstream in relation to the heat sinks on the outlet pipe.

Raspberry Pi

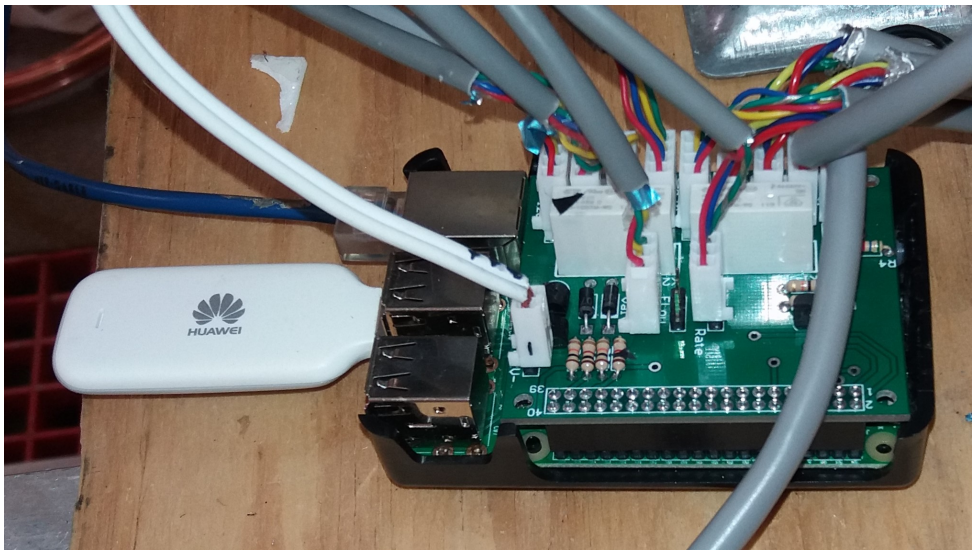

Figure B.6: The Raspberry Pi 3 used to sample sensors for the experimental unit.

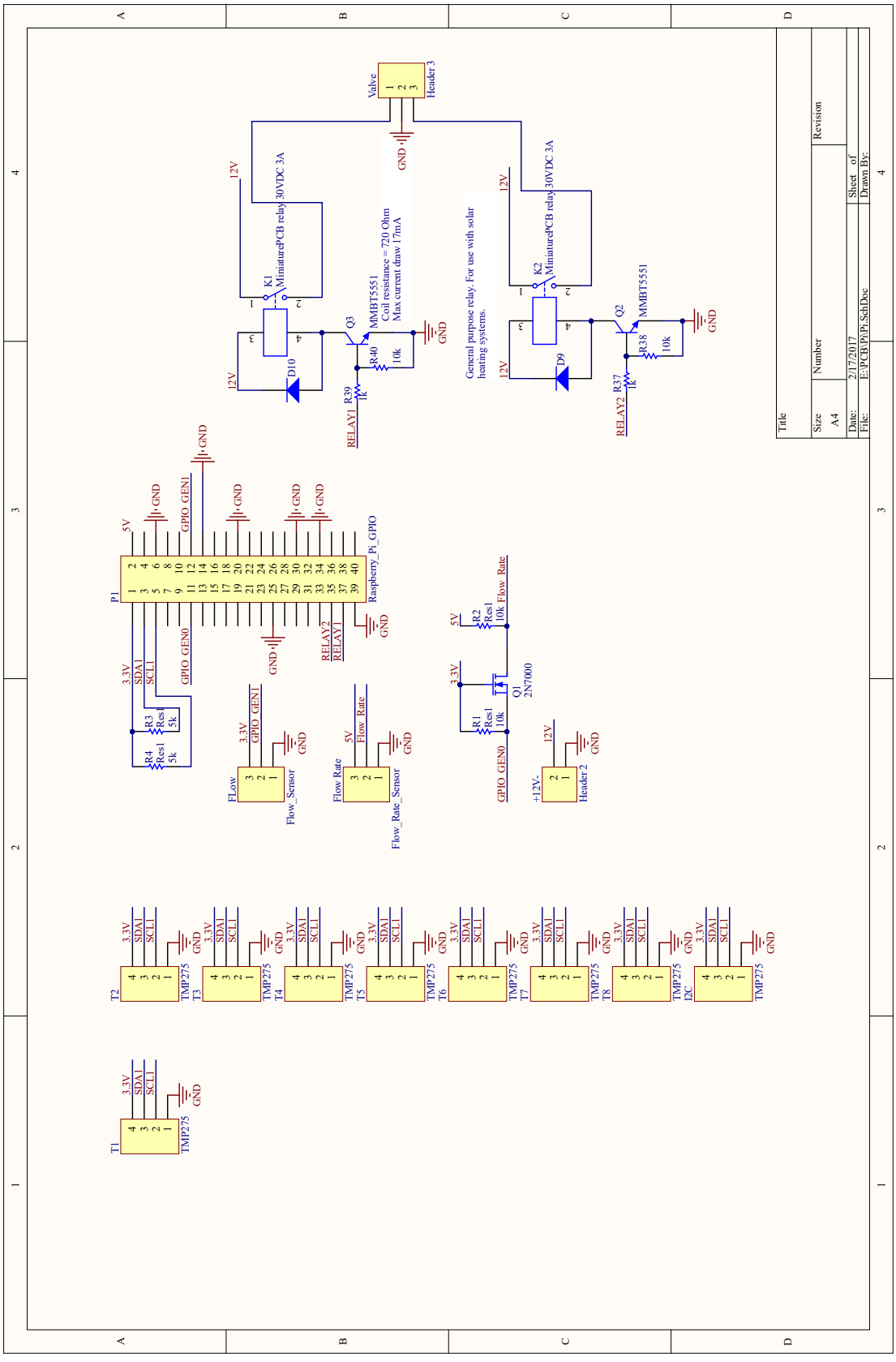

Figure B.7: Raspberry Pi PCB schematic.

B.2 Software Design

B.2.1 Sampling

The primary sweep is the main aspect related so the sampling used in the experimental unit and a representative version of the relevant aspects are provided. The primary sweep was performed using a function, **PrimarySweep()**. **PrimarySweep()** was executed by an APScheduler job which ensured 1 Hz sampling rate. Vibration burst sampling was performed in the same function call when required.

B.2.1.1 Variable and Object Names

Tables B.2 and B.3 show the variables and objects required to explain how the data sampling was performed.

Name	Description
Ven	Global flag to enable vibration burst sampling
VN	Number of burst samples
PulseCnt	Global counter, incremented when *FFM* GPIO interrupts occur
VolCnt	Global counter, incremented when *FFM* GPIO interrupts occur
SampleList	Global list which stores the samples from PrimarySweep() calls
TMP275List	List containing the eight TMP275 objects
currAcqTable	Name of current 'acquisition' table in MySQL database
currVibTable	Name of current 'vibration' table in MySQL database

Table B.2: Relevant variable names and descriptions

Name	Description
bus	SMBus object for I^2C communications
engine	SQLAlchemy engine object, connect to MySQL database
sched	APScheduler BlockingScheduler object, controls jobs
TMP275	TMP275 object, methods: get_resolution(), set_resolution_12(), read_16()
LSM303	Modified Adafruit_LSM303 object, methods: read_acc()
VH	ValveHandler object, methods: Open_Valve(), Close_Valve()

Table B.3: Relevant object names and descriptions

B.2.1.2 Functions Pseudocode

BurstSampleLSM(LSM303, VN, engine, currVibTable):

```
burstSampleList=[ ] #list to store VN vibration burst samples
for i in [0:VN]: #required number of samples in burst
    get dt,ms #DateTimeIndex and microsecond of current sample
    currSample = [dt,ms]
    currSample.append(LSM303.read_acc())#3 g-force readings:x,y,z
```

burstSampleDF = pandas.DataFrame(burstSampleList) *#Pandas DF for burst sample*
burstSampleDF.to_sql(currVibTable, engine) *#insert VN samples into vibration table in MySQL database*

stdDevVals = burstSampleDF.standardDeviation() *#vibration standard deviation:* $\sigma_{x',y',z'}$

return stdDevVals *#return vibration standard deviation*

PrimarySweep(TMP75List, bus, LSM303, engine, VH, currVibTable, VN):

global PulseCnt,VolCnt *#GPIO interrupt incremented FFM and CFM pulses*
global Ven *#enable vibration burst sampling for the current sample?*
global SampleList *#list storing previous samples*

get dt,ms *#DateTimeIndex and microsecond of current sample*
currSample = [dt,ms,PulseCnt,VolCnt,VH.ValveState] *#store time, flow data, ValveState*

clear PulseCnt, VolCnt

for TMP275 *in* TMP275List:
    currSample.append(TMP275.read16()) *#read and store all temperature readings*

if(VN!=0 *and* (Ven==True *or* dt.second==30)): *#if vibration burst sample is required*
    currStdDevs = BurstSampleLSM(LSM303, VN, engine, currVibTable)
    currSample.append(currStdDevs)*#add standard deviation values*

SampleList.append(currSample) *#add current sample to SampleList*
return

CheckResolution(TMP275List, sched): *#Check and reset TMP275 resolution*

sched.pause_job(*'PrimarySweepJob'*) *#stop PrimarySweep() from being called*
for TMP275 *in* TMP275List:
    currResolution = TMP275.get_resolution() *#get sensor resolution*
    if currResolution != 12−bit:
        TMP275.set_resolution_12() *#set sensor to maximum resolution*
sched.resume_job('PrimarySweepJob') *#PrimanrySweep() executes at* 1 Hz *again*
return

OpenValve(VH, sched, TMP275List): *#Open valve and check TMP275 resolution*

VH.Open_Valve() *#use ValveHandler to open solenoid valve*
CheckResolution(TMP275List, sched) *#reset any TMP275 resolutions after valve toggle*
return

CloseValve(VH, sched, TMP275List): *#Close valve and check TMP275 resolution*

VH.Close_Valve() *#use ValveHandler to close solenoid valve*
CheckResolution(TMP275List, sched) *#reset any TMP275 resolutions after valve toggle*
return

InsertAcquisition(engine, sched, currAcqTable, TMP275List): *#insert one hour of acquisition data into acquisition MySQL database*

global SampleList *#one hour of locally stored PrimarySweep() samples*
SampleListCopy = SampleList.copy() *#make copy of data to be stored*
SampleList.clear() *#clear global list so that PrimarySweep() can continue*

SampleDF = pandas.DataFrame(SampleListCopy) *#pandas DF prior to MySQL insert*
SampleDF.to_sql(currAcqTable, engine) *#insert 3600 PrimarySweep() samples into acquisition table in MySQL database*
CheckResolution(TMP275List, sched) *#check TMP275 resolution*
return

HighPriorityVibration(): *#vibration burst sample occurs once per second*

global Ven = True *#set global flag so that BurstSampleLSM() is always called in PrimarySweep()*
return

LowPriorityVibration(): *#vibration burst sample occurs once per minute*

global Ven = False *#set global flag so that BurstSampleLSM() is only called in Primary sweep when dt.second==30*
return

B.2.2 APScheduler Jobs

The following important APScheduler jobs were controlled by the blocking scheduler object. The functions called and the trigger conditions are shown in Table B.4.

Function Call	Trigger Details
PrimarySweep()	Interval, 1 Hz
InsertAcuisition()	Cron, minute = 50
OpenValve()	Cron, predefined event start times
CloseValve()	Cron, predefined event end times
HighPriorityVibration()	Cron, 5 min prior to event
LowPriorityVibration()	Cron, 5 min after event
CheckResolution()	Cron, minute = 55

Table B.4: APScheduler jobs and trigger conditions

B.2.3 Acquisition MySQL Database

Name	Type	Description	Additional
Datetime	DTI	Sweep Start Time	1 Hz
Microsecond	Int	Exact Time of Sweep	For Resampling
ValveState	Int	Status of *SV*	Scheduled Flow
PulseCnt	Int	*FFM* Pulse Count	Flow Rate
VolCnt	Int	*CFM* Pulse Count	Flow Volume
T_{N1}	Int	Near Temperature 1	
T_{N2}	Int	Near Temperature 2	
T_{N3}	Int	Near Temperature 3	
T_{F1}	Int	Far Temperature 1	
T_{F2}	Int	Far Temperature 2	
T_{F3}	Int	Far Temperature 3	
T_{In}	Int	Inlet Temperature	
T_{∞}	Int	Ambient Temperature	
$\sigma_{x'}$	Float	x' Standard Deviation	Not In Dataset 1
$\sigma_{y'}$	Float	y' Standard Deviation	Not In Dataset 1
$\sigma_{z'}$	Float	z' Standard Deviation	Not In Dataset 1

Table B.5: Acquisition Data Format. An overview of the data format of each sample in the Acquistion MySQL Databases is provided. The data type are DateTimeIndex (DTI), integers (Int) and floating point numbers (Float).

Acquisition MySQL databases contained data as shown in Table B.5 for each sample. It can be seen that effort was made to minimize the size of the stored data by using integer values where possible. The data was stored into a MySQL database at the 50^{th} minute of every hour during data acquisition and the local variables were cleared.

Dataset 1 did not contain the standard deviation values because the minimum accelerometer sampling requirements were calculated using Dataset 1 (which used the full Vibration MySQL database). Datasets 2 and 3 stored a single σ value each second in the Acquisition MySQL database because post processing was not required.

B.2.4 Dataset 1 Scheduling

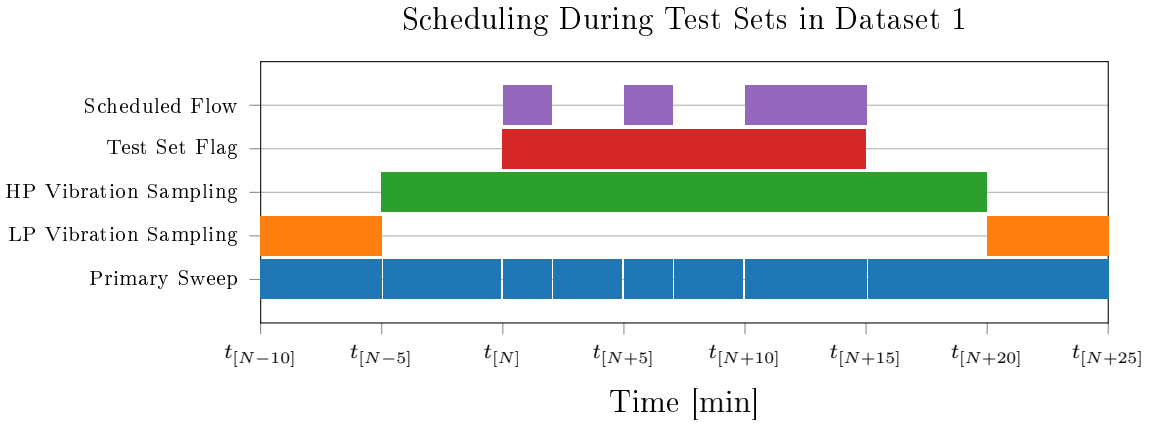

Figure B.8: Software scheduling for Dataset 1. The APScheduler 'Primary Sweep' *job* was paused near scheduled flow events as shown. 'Scheduled Flow' shows the automated control of *SV* to induce scheduled flow events. 'Test Set Flag' shows which samples were included in a respective test set when data analysis was performed. The entire duration of any vibration events which occurred during a test set were included in the analysis. The different use of High and Low Priority Vibration Sampling ('HP' and 'LP' Vibration Sampling) is shown. The total time which the 'Primary Sweep' *job* was paused is shown to show that the sampled data was very clean.

Figure B.8 shows the scheduling used to generate Dataset 1 near scheduled flow events. The 2 min, 2 min, and 5 min, long scheduled flow events are indicated on the Figure as 'Scheduled Flow'. It can be seen that the test set numbering system includes the total time encompassing the 3 flow events as shown by 'Test Set Flag'. 5 min prior to the start of a scheduled test set, 'High Priority Vibration Sampling' was enabled (meaning that a 500 sample burst accelerometer sweep was performed every second) until 5 min after the completion of the test set. 'Low Priority Vibration Sampling' was used for the rest of the sampling time, meaning that a single 500 sample burst accelerometer sweep was performed every minute. The 'Primary Sweep' *APScheduler job* was used to sample the 8 temperature sensors and record the measured flow rate once per second. The Acquisition job was only paused when the local Pandas DataFrame was inserted into the MySQL database at $t_{[N-10]}$ minute and after *SV* was opened and closed (at the start and end of 'Scheduled Flow') to verify that the temperature sensors are set to maximum resolution.

Appendix C

Results Appendix

C.1 Vibration Interference

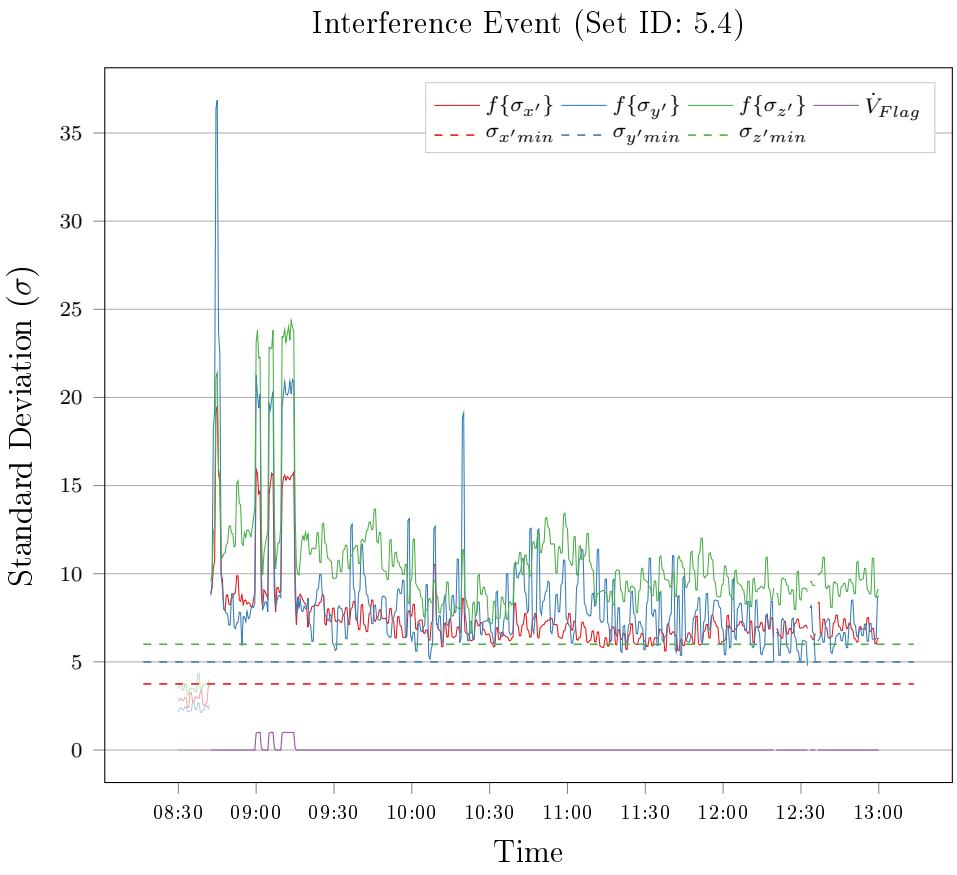

Figure C.1: Interference Event (Test Set 5.4) resampled to 30 s resolution to enable plotting. The σ magnitude and duration of the interference event which occurred during test set 5.4 in Dataset 1 can be seen. The external vibration was consistently higher than the shown threshold values between 08:42:29 and 12:19:34. Test set 5.4 was between 09:00:00 and 09:15:00, but none of the 3 flow events shown by $\dot{V}_{flag}$, were detected as usage events by the algorithm. The vibration event which contained the flow experiments was completely contained within the external vibration.

Figure C.1 shows the vibration interference which occurred during Test Set 5.4. It can

be seen that the magnitude of the standard deviations measured during this interference event is significantly greater than the respective threshold values. The threshold values were designed to be able to detect the lowest measured flow events which were present in Dataset 1, and increasing the threshold to exclude the shown interference event would mean that low flow rates would not be detected. The experimental unit was situated close to heavy machinery and the somewhat consistent magnitude of the σ values indicate that machinery may have been responsible for the interference event.

The flow events can be seen as denoted by $\dot{V}_{flag}$ in Figure C.1 and the standard deviation values can be seen to increase during measured water flow. Thermal event classification is performed using the temporal boundaries provided by vibration event detection. When the flow events are entirely contained within an interference event then the temporal boundaries provided reflect those of the interference event and not the flow event.

C.2 Usage Event Detection: Dataset 1

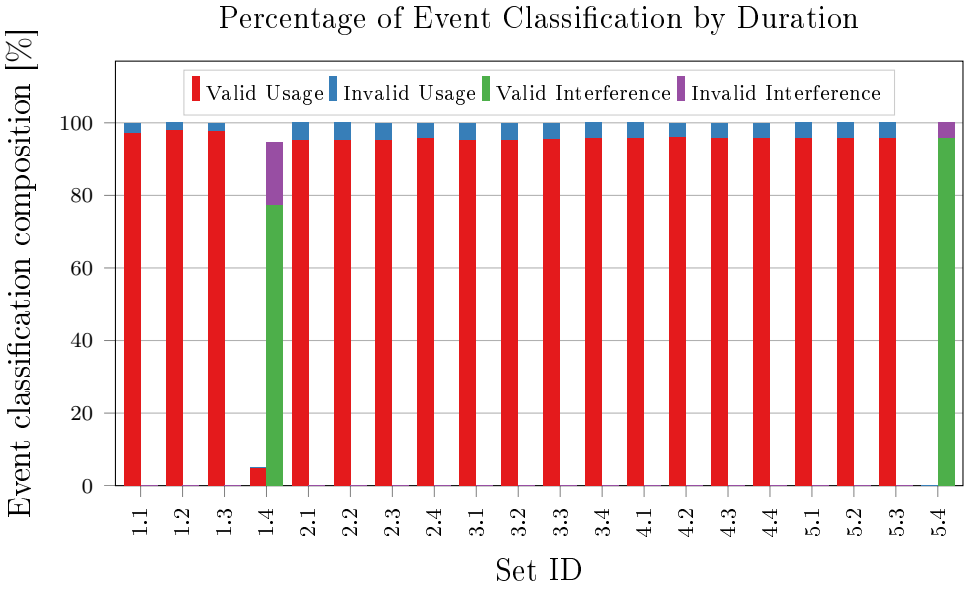

Figure C.2: Event classification validity by duration. The event classification for each vibration event which occurred during Scheduled test sets 1.1 to 5.4 was analysed. The bars show the classification of events by duration as usage or interference events. Valid classification means that the non-invasive classification matched the measured in-line flow meter data.

Figure C.2 shows the percentage classification per test set between usage (red and blue) and interference (green and purple) events for Dataset 1. It also shows which percentage of the sum of the respective classified events were valid within each test set with the remainder being invalid or incorrectly classified.

It can be seen from Figure C.2 that test sets 1.4 and 5.4 were the only test sets which contained vibration events which were caused by interference (shown by the presence of green and purple sections). It can also be seen that the majority of the interference events which occurred during these two test sets were correctly identified as interference events (meaning that the duration of the interference event was much longer than the duration of water flow). The remainder of the test sets did not have externally induced

Set ID	Usage Event [s]		Interference Event [s]	
	Valid	Invalid	Valid	Invalid
1.1	548	15	0	0
1.2	543	11	0	0
1.3	547	12	0	0
1.4	122	6	1907	426
2.1	547	27	0	0
2.2	547	27	0	0
2.3	547	26	0	0
2.4	548	23	0	0
3.1	547	26	0	0
3.2	547	26	0	0
3.3	547	25	0	0
3.4	547	24	0	0
4.1	549	24	0	0
4.2	550	22	0	0
4.3	549	23	0	0
4.4	549	23	0	0
5.1	549	24	0	0
5.2	549	24	0	0
5.3	549	24	0	0
5.4	0	0	12477	549
Int Events	0	0	35089	0
Total	9981	412	49473	975

Table C.1: Event classification displayed per test set and showing durations. The sum of the duration of each Usage event and Interference event which occurred during a test set ID is shown. Usage and interference events are analysed as being Valid or Invalid based on the status of the flow meter for each sample.

vibrations occurring during scheduled flow times and it can be seen that no usage events were incorrectly classified as interference events (meaning that no flow induced vibration events were missed, or no false negatives). It can also be seen for these test sets that the duration of the classified usage events was over 90 % correct which means that the temporal data provided by vibration event detection can be considered to be accurate. The accuracy of the edge detection is important when considering mean flow rates and volumetric usage estimation which is the information which the SGC requires.

Table C.1 shows the sum of the duration of categorised events which occurred during each test set. Table C.1 is useful to evaluate the performance of the usage event detection component of the non-invasive flow rate meter. Each vibration event was considered separately and was categorised as a usage event or interference event. Samples in a usage event are valid if water flow was measured during the sample, and invalid if water flow was not measured. Samples in an interference event are valid if no water flow was measured, and invalid if water flow was measured. The total valid classification of all vibration events in Dataset 1 comprised 97.7 % of the measured duration of all vibration events.

It can be seen from the 'Int Events' row of Table C.1, (which contains the sum of durations of all interference events which did not occur within a test set) that no water flow was

estimated during isolated externally caused vibration events (There were no false positive usage events estimated).

Table C.1 shows that test sets 1.4 and 5.4 were the only test sets which contained Invalid interference event estimations (where flow occurred during a vibration event, but the event was classified as an interference event instead of a usage event). This was caused by external vibration interference extended over the scheduled test times. Figure 5.3 shows a case where scheduled flow occurs during external interference.

C.3 Flow Rate Estimation

Flow No	Start Time	Duration [s]	$\bar{\dot{V}}_M$ [L min^{-1}]	$\bar{\dot{V}}_E$ [L min^{-1}]	Error [%]	Reliability
1	16:01:58	52	1.85	6.98	276.55	False
2	16:03:28	71	7.23	9.39	29.82	True
3	16:05:20	71	7.91	8.79	11.01	True
4	16:07:32	88	11.75	14.09	19.84	True
5	16:10:12	74	11.96	13.08	9.31	True
6	16:12:37	90	15.37	16.00	4.10	True
7	16:15:54	99	22.05	25.36	15.00	True
8	16:19:40	239	10.85	10.92	0.58	True
9	16:24:49	31	0.66	4.68	607.80	False
10	16:26:01	30	2.31	4.81	107.91	False
11	16:26:42	177	6.41	8.46	31.96	True

Table C.2: Dataset 2 flow estimation summary

The mean flow rates per flow event in Dataset 2 are shown in Table C.2. Usage event detection was not possible for Dataset 2 due to insufficient time between flow events. Vibration events were confirmed as flow events when flow pulses were recorded during within non-invasively determined temporal boundaries. Dataset 2 displayed larger $\bar{\dot{V}}_E$ errors that usage events in Datasets 1 and 3. Manual flow control was done (using BV) for Dataset 2. It was suspected that the BV created larger vibrations during flow events where the flow rate was adjusted resulting in larger overestimations.

It can be seen the 'Reliability' flag (using vibration data) to identify mean flow rates above $\bar{\dot{V}}_{(min)}$ was successful for Dataset 2. Dataset 2 generally consisted of shorter duration events and events of various flow rates. Each $\bar{\dot{V}}_M$ value in Table C.2 which was below 5 L min^{-1} was correctly marked as unreliable. The error margin of

C.4 Field Units

C.4.1 Individual Events

The individual composition of the Field Datasets relating to $\bar{\dot{V}}_{(min)}$ is assessed.

C.4.1.1 Flow Rate Analysis

Unit ID	Volumetric Estimation			Temporal Estimation		
	No [L]	Yes [L]	Percent [%]	No [Min]	Yes [Min]	Percent [%]
U02	252	5998	96.0	122	444	78.4
U01	180	3268	94.8	68	340	83.3
U33	1093	9875	90.0	521	1053	66.9
U07	264	1822	87.3	134	192	58.9
U29	444	2912	86.8	232	337	59.2
U13	351	2256	86.5	130	201	60.7
U28	706	4096	85.3	356	377	51.4
U03	2267	11979	84.1	1097	1204	52.3
U20	378	1586	80.8	179	250	58.3
U00	692	2784	80.1	325	420	56.4
U08	831	3304	79.9	409	279	40.6
U24	734	2496	77.3	345	328	48.7
U21	390	1302	77.0	226	142	38.6
U16	451	1393	75.5	204	170	45.5
U23	1513	4523	74.9	737	554	42.9
U05	703	2063	74.6	394	208	34.6
U12	1326	3314	71.4	634	402	38.8
U31	1530	2818	64.8	707	447	38.7
U19	3541	6498	64.7	1622	876	35.1
U04	1912	3093	61.8	1238	460	27.1
U14	1224	1949	61.4	686	280	29.0
U11	1042	1563	60.0	483	243	33.5
U22	1422	2048	59.0	758	229	23.2
U18	375	459	55.0	201	72	26.4
U25	2010	1959	49.4	1151	239	17.2
U27	3428	3194	48.2	1605	451	21.9
U15	975	870	47.2	396	100	20.2
U32	436	379	46.5	258	66	20.4
U17	351	256	42.2	161	37	18.7
U06	2778	1459	34.4	911	276	23.3
U26	4448	2170	32.8	1971	342	14.8
U30	2264	908	28.6	674	176	20.7
U10	3449	421	10.9	1881	79	4.0
U09	2497	294	10.5	1216	53	4.2
Grouped	46256	95308	**67.3**	22032	11327	**34.0**

Table C.3: Individual user flow rate analysis. The volumetric and temporal contribution of flow rates below and above $\bar{V}_{(min)}$ is shown for each individual user. The users are ranked in descending order of the percent of total monthly consumption attributed to higher flow rates.

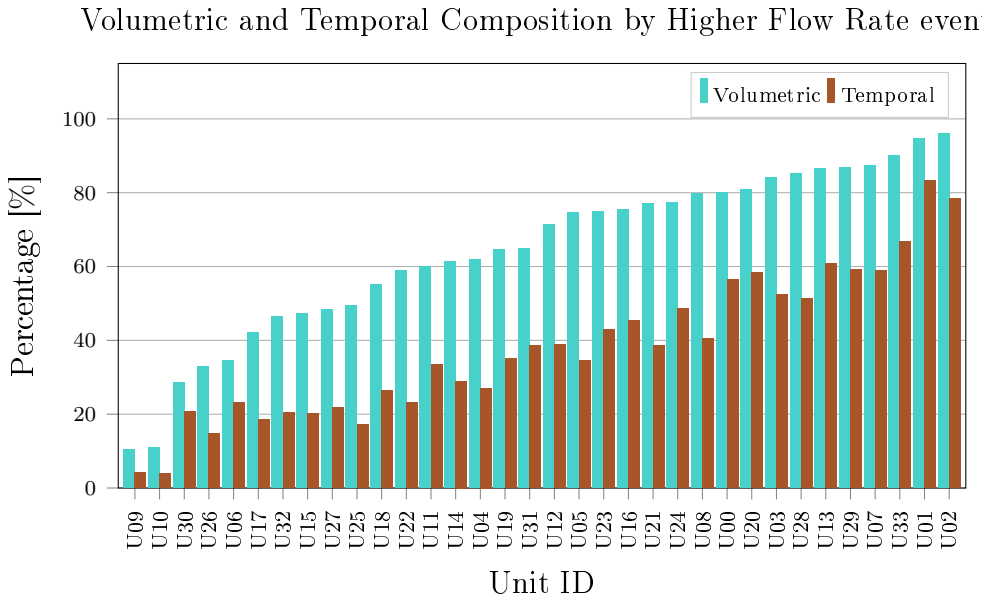

Figure C.3: Individual volumetric and temporal composition by higher flow rate is shown for the Field Dataset. The bars shown for each user indicate the percentage of the volumetric consumption and duration of measured flow which was contributed by flow rates greater than $\bar{\dot{V}}_{(min)}$. The units are shown in ascending order of volumetric consumption by flow rates which can be quantitatively estimated using the designed algorithm.

Table C.3 and Figure C.3 show the break down of flow rate analysis for each user. Each user's consumption was analysed and the displayed values are the contribution by flow rates which were measured to be greater than $\bar{\dot{V}}_{(min)}$. This means that 96 % of the total monthly consumption for Unit U02 could receive quantitative estimation (if no t_{cd} limitation existed) whereas Unit U09 only had 10.5 % of the total monthly consumption which could be eligible for quantitative estimation based on flow rate composition.

C.4.2 Simulated Performance

Individual analysis was performed for the Field Dataset with both algorithm limitations, $\bar{\dot{V}}_{(min)}$ and t_{cd}, applied to simulate the performance of the algorithm. Usage event detection was thus simulated and the results were analysed to determine how effective non-invasive flow measurement would have been for each user.

The constant approximation of $2\,\mathrm{L\,min^{-1}}$ for quantitative flow estimation can be seen to be a valid approximation from Figure 6.14. The height of the approximated and measured volumes, $V_{E(Approx)}$ (orange) and $V_{M(Ideal)}$ (green) respectively, can be seen to be similar. The exact user behaviour affects how accurate each estimation is depending on how close to the approximation value the user's low flow rates are.

The remainder of usage events (above $V_{M(Ideal)}$) occur during flow events which occur in too quick succession which results in the events being discarded as interference events due to the thermal criteria not being met. This volumetric discrepancy is not able to be measured using the system. Users with higher $V_{M(Ideal)}$ bars therefore have usage events which are generally more than 2 min apart. Users with consumption patterns like this are likely to be good candidates for non-invasive estimation.

Field unit 32 overestimated the total monthly volumetric consumption when low flow rate approximation was implemented. The reason for this is due to a low flow rate for the specific user (present for detectable low flow events) less than the $2\,\mathrm{L\,min^{-1}}$ constant approximation used. Analysis of the unit showed that the mean low flow rate was $1.79\,\mathrm{L\,min^{-1}}$. 244 min of low flow rate approximation was required for U32 during the 28 days of data which resulted in the total estimated consumption being too large. The discrepancy was 52 L or 6.38 % of the measured consumption of U32. Figure C.4 shows that U32 was a low volumetric user, and that the overestimation is an exception.

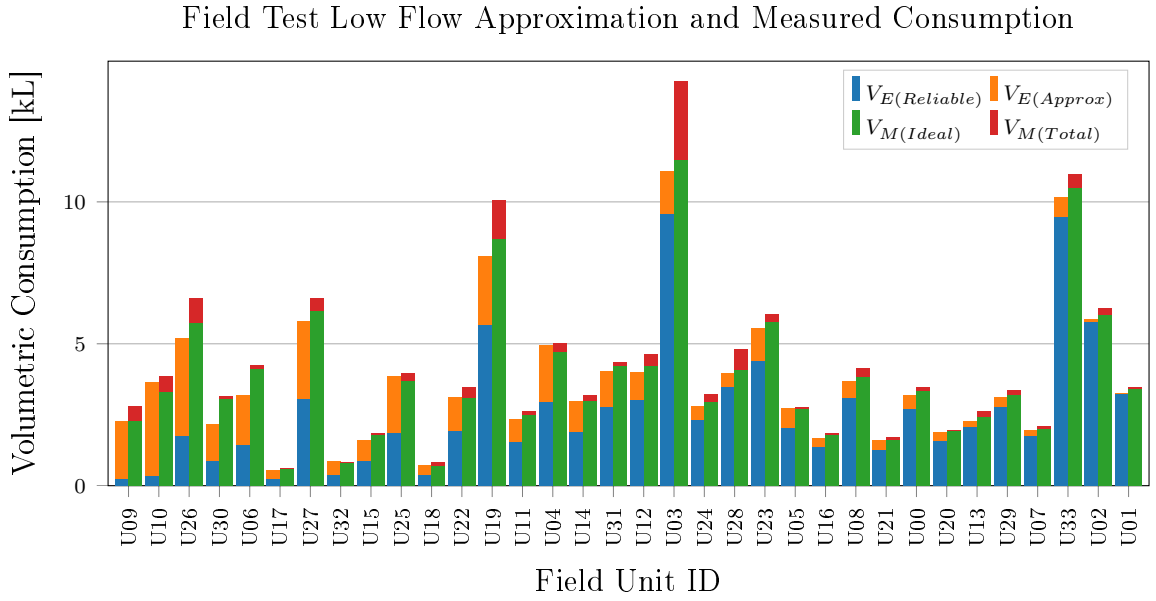

Figure C.4: The estimated and measured volumetric consumption is shown for the individual Field Units. The estimated volumes consist of the reliable estimation, $V_{E(Reliable)}$ (blue), and the estimation using low flow approximation, $V_{E(Approx)}$ (orange). The measured volumes during detectable events, $V_{M(Ideal)}$ (green), as well as the total monthly consumption, $V_{M(Total)}$ (red) for each Field unit. The Field units are sorted in ascending order by percentage $V_{E(Reliable)}$ of the total consumption.

It can be seen from Figure C.4 that the anonymous users varied drastically in their total consumption. Users with larger $V_{M(Ideal)}$ (green) bars had sufficient time between events to enable event detection for the greatest number of events which contributed to volumetric consumption. Users with larger $V_{E(Reliable)}$ bars additionally used predominantly higher flow rates. These users are the best suited to non-invasive water flow rate measurement.

Users with larger $V_{E(Approx)}$ (orange) bars required the most low flow rate approximation. This was because low flow rate events contributed to a larger portion of their total monthly usage. The expected effectiveness of the flow estimation system does not appear to be connected to the actual volume of water consumed but is more closely linked to the individual consumption patterns of users.

List of References

[1] C. of Cape Town, "Level 5 water restrictions -the city of cape town has implemented level 5 water restrictions, effective from 3 september 2017 until further notice." Cape Town, Western Cape, Sep. 2017.

[2] S. de la Rue du Can, V. E. Letschert, G. Leventis, T. Covary, and X. Xia, "Energy efficiency country study: Republic of south africa," Lawrence Berkeley National Laboratory, Tech. Rep., 08 2013.

[3] M. Roux, N. Naude, M. Booysen, and A. Barnard, "Electric water heaters in smartgrids: Individual savings versus network peak load management," in *SAUPEC 2017*, Stellenbosch, Western Cape, 01 2017.

[4] C. Ripunda and M. Booysen, "Understanding and affecting water consumer behavior using technological interventions at a primary school in stellenbosch," 2017, unpublished.

[5] K. Fielding, A. Spinks, S. Russell, and A. Mankad, "Water demand management study: Baseline survey of household water use (part b)," CSIRO, Tech. Rep. 93, 2012.

[6] Eskom, "Geyser fact sheet," 2013.

[7] K. Fielding, A. Spinks, S. Russell, and A. Mankad, "Water demand management: Interventions to reduce household water use," CSIRO, Tech. Rep. 94, 2012.

[8] Y. Cengel and J. Cimbala, *Fluid Mechanics: Fundamentals and Applications (2nd Edition in SI Units)*, 2nd ed. New York: McGraw-Hill, 2010.

[9] *SANS 10254: The installation, maintenance, replacement and repair of fixed electric storage water heating systems*, SABS Std., Rev. 4, 2012.

[10] *SANS 241-2: Drinking Water*, SABS Std., 2011.

[11] M. Pereira, "Flow meters: Part 1," *IEEE Instrumentation & Measurement Magazine*, vol. 12, no. 1, pp. 18–26, Feb. 2009.

[12] Tuvnel, "An introduction to Non-Invasive Ultrasonic flow monitoring," Oct. 2010.

[13] R. P. Evans, J. D. Blotter, and A. G. Stephens, "Flow Rate Measurements Using Flow-Induced Pipe Vibration," *Journal of Fluids Engineering*, vol. 126, no. 2, p. 280, 2004.

[14] D. Whitson, "an overview of Non-Invasive Flow measurement methods," Feb. 2009.

[15] M. T. Pittard, R. P. Evans, R. D. Maynes, and J. D. Blotter, "Experimental and numerical investigation of turbulent flow induced pipe vibration in fully developed flow," *Review of Scientific Instruments*, vol. 75, no. 7, p. 2393, 2004.

[16] Y. Kim, T. Schmid, Z. M. Charbiwala, J. Friedman, and M. B. Srivastava, "NAWMS: nonintrusive autonomous water monitoring system." Rayleigh, North Carolina: ACM Press, 2008, p. 309.

[17] R. Safari and B. Tavassoli, "Initial Test and Design of a Soft Sensor for Flow Estimation Using Vibration Measurements." Piscataway, NJ: IEEE, 2011.

[18] L. Xuejun, B. Guangfu, and B. Dhillon, "A New Method of Multi-sensor Vibration Signals Data Fusion Based on Correlation Function." IEEE, 2009, pp. 170–174.

[19] Geoscience and Remote Sensing Society and International Society for Photogrammetry and Remote Sensing, Eds., *2007 Urban Remote Sensing Joint Event: Paris, France, 11 - 13 April 2007 ; [URBAN 2007 - 4th IEEE GRSS/ISPRS Joint Workshop on Remote Sensing and Data Fusion over Urban Areas and URS 2007 - 6th International Symposium of Remote Sensing of Urban Areas].* Piscataway, NJ: IEEE, 2007.

[20] H. Jacobs, Y. Skibbe, M. Booysen, and C. Makwiza, "Correlating Sound and Flow Rate at a Tap," *Procedia Engineering*, vol. 119, pp. 864–873, 2015.

[21] H. Kakuta, K. Watanabe, and Y. Kurihara, "Development of Vibration Sensor with Wide Frequency Range Based on Condenser Microphone -Estimation System for Flow Rate in Water Pipes," *International Journal of Mechanical, Aerospace, Industrial, Mechatronic and Manufacturing Engineering*, vol. 6, no. 10, pp. 2267–21 272, 2012.

[22] S. Mylvaganam, "Some Applications of Acoustic Emission in Particle Science and Technology," *Particulate Science and Technology*, vol. 21, no. 3, pp. 293–301, Jul. 2003.

[23] M. Sanderson and H. Yeung, "Guidelines for the use of ultrasonic non-invasive metering techniques," *Flow Measurement and Instrumentation*, vol. 13, no. 4, pp. 125–142, Aug. 2002.

[24] P. D. Lysak, D. M. Jenkins, D. E. Capone, and W. L. Brown, "Analytical model of an ultrasonic cross-correlation flow meter, part 1: Stochastic modeling of turbulence," *Flow Measurement and Instrumentation*, vol. 19, no. 1, pp. 1–7, Mar. 2008.

[25] M. S. Beck, "Correlation in instruments: cross correlation flowmeters," *Journal of Physics E: Scientific Instruments*, vol. 14, no. 1, pp. 7–19, Jan. 1981.

[26] J. Coulthard, "Ultrasonic cross-correlation flowmeters," *Ultrasonics*, vol. 11, no. 2, pp. 83–88, Mar. 1973.

[27] J. H. Huijsing, A. L. C. v. Dorp, and P. J. G. Loos, "Thermal mass-flow meter," *Journal of Physics E: Scientific Instruments*, vol. 21, no. 10, pp. 994–997, Oct. 1988.

[28] P. J. C. Nel, "Rethinking electrical water heaters," Master's thesis, Stellenbosch: Stellenbosch University, 2015.

[29] R. Bernier and C. Brennen, "Use of the electromagnetic flowmeter in a two-phase flow," *International Journal of Multiphase Flow*, vol. 9, no. 3, pp. 251–257, Jun. 1983.

[30] J. A. Shercliff, *The theory of electromagnetic flow-measurement*, ser. Cambridge science classics. Cambridge [Cambridgeshire] ; New York, NY, USA: Cambridge University Press, 1987.

[31] Y. Kim, H. Park, and M. B. Srivastava, "A longitudinal study of vibration-based water flow sensing," *ACM Transactions on Sensor Networks*, vol. 9, no. 1, pp. 1–28, Nov. 2012.

[32] M. T. Heath, *Scientific computing: an introductory survey*, 2nd ed. Boston: McGraw-Hill, 2002.

[33] E. Jones, T. Oliphant, P. Peterson *et al.*, "SciPy: Open source scientific tools for Python," 2001–. [Online]. Available: http://www.scipy.org/

[34] A. C. Hindmarsh, "Brief description of odepack - a systematized collection of ode solvers double precision version," http://www.netlib.org/odepack/opkd-sum, 2001.

[35] *TMP275 Temperaure Sensor With I2C and SMBus Interface in Industry Standard LM75 Form Factor and Pinout*, Texas Instruments, 6 2006, revised November 2015.

[36] *Ultra compact high performance e-compass 3D accelerometer and 3D magnetometer module*, STMicroelectronics, 4 2011, rev. 1.

[37] J. G. Proakis and D. G. Manolakis, *Digital signal processing*, 4th ed., ser. Always learning. Harlow: Pearson, 2014.

[38] W. McKinney, "Data structures for statistical computing in python," in *Proceedings of the 9th Python in Science Conference*, S. van der Walt and J. Millman, Eds., 2010, pp. 51 – 56.

[39] *Technical Information: Bulletin 001*, Armacell, 9 2007.

[40] *510-12 Series Datasheet*, Wakefield-Vette.